DISSERTATION

SEEING THE RIVER THROUGH THE TREES:

USING COTTONWOOD DENDROCHRONOLOGY TO RECONSTRUCT RIVER DYNAMICS IN THE UPPER MISSOURI RIVER BASIN

Submitted by

Derek Michael Schook

Department of Geosciences

In partial fulfillment of the requirements

For the Degree of Doctor of Philosophy

Colorado State University

Fort Collins, Colorado

Spring 2017

Doctoral Committee:

Advisor: Sara Rathburn

Jonathan Friedman
Ellen Wohl
Tim Covino
Scott Denning

ABSTRACT

SEEING THE RIVER THROUGH THE TREES:

USING COTTONWOOD DENDROCHRONOLOGY TO RECONSTRUCT RIVER DYNAMICS IN THE UPPER MISSOURI RIVER BASIN

Understanding the past is critical to preparing for the future, especially regarding rivers where extreme events and gradual changes underlie modern forms and processes. Both biological and human communities rely on the abundant resources provided by rivers and floodplains, particularly in dry regions of the western U.S. where water limits growth. To expand temporal perspectives on river processes, I reconstructed flow, channel migration, and riparian forest growth patterns in the Upper Missouri River Basin. Flow reconstructions typically use tree rings from montane conifers. However, I used riparian plains cottonwoods (*Populus deltoides* ssp. *monilifera*) directly connected to the alluvial water table to reconstruct flow on the Yellowstone (n = 389 tree cores), Powder (n = 408), and Little Missouri Rivers (n = 643). A two-curve Regional Curve Standardization approach was used to remove age-related growth trends from tree rings at each site. The flow reconstructions explained 57-58% of the variance in historical discharge and extended back to 1742, 1729, and 1643, respectively. Low-frequency flow patterns revealed wet conditions from 1870 to 1980, a period that includes the majority of the historical record. Two 19th century droughts (1816-1823 and 1861-1865) and one pluvial (1826-1829) were more severe than any recorded, revealing that risks are underestimated when using the instrumental period alone. These are the first flow reconstructions for the

Lower Yellowstone and Powder Rivers, and they are the farthest downstream among Rocky Mountain rivers east of the Continental Divide.

Cottonwood-based flow reconstructions were possible because the trees used river-connected groundwater, and tree ring width strongly correlated with March-June flow magnitude at the Yellowstone River (r = 0.69). Beyond the site-level growth patterns typically used to reconstruct flow, I found that biological and spatial characteristics affected how individual trees responded to flow and climate. Older trees contained stronger signals of non-growing season flow, precipitation, and temperature, which challenges the common dendrochronological assumption of stable tree ring-climate relationships through time. Although trees both near and far from the channel were better correlated to spring flow than precipitation, more distant trees had a stronger relative connection to precipitation, suggesting that greater distance decreases the ability of river water to fulfill transpirative demands.

Like annual growth, cottonwood establishment is related to river flows, and tree age indicated fluvial processes including channel migration. I quantified nearly two centuries of channel migration on the Powder River by integrating measured channel cross-sections (1975-2014), air photos (1939-2013), and transects of aged cottonwoods (1830-2014). The combined data revealed that channel migration rates were lower (0.81 m/yr) in the recent and intensively studied cross-section period compared to the longer air photo (1.52 m/yr) and cottonwood (1.62 m/yr) periods. On the Powder River, extreme floods such as those in 1923 and 1978 increase subsequent channel migration rates and initiate decades of channel morphological adjustments. Across the study rivers, data indicate that fundamental fluvial processes have responded to climatic and watershed pressures. By identifying and quantifying past events,

diverse research approaches improve understanding of the river, floodplain, and riparian forest processes that are essential to the persistence of these valuable ecosystems.

ACKNOWLEDGEMENTS

I am greatly appreciative for my dissertation advisor Sara Rathburn for her guidance and support throughout my time under her mentorship. She provided a rich environment for me to develop as a scientist. She has created learning opportunities in the field from the Rockies to the Alps, indoors within the friendly confines of our lab group, and in various entertaining social settings. My complete gratitude also goes to Jonathan Friedman, whose devotion as an unofficial co-advisor has greatly enhanced my development as a scientist and my perspective on how best to integrate into the greater scientific community. Jonathan's ability to link ecological processes greatly improved the quality of the research presented herein. Both the quality of the science contained in this dissertation and my experience at CSU have been improved by generous contributions from committee members Ellen Wohl, Tim Covino, and Scott Denning. Thank you to Ellen Wohl, Sara Rathburn, and the Fluvial Geomorphology Lab for supporting a thought-provoking and fun research group. Additionally, thank you to David Cooper for his continued support and opportunities throughout my tenure at CSU.

Several people outside of the CSU community have helped along the way. Thank you to John Moody and Bob Meade for creating an impressive collaboration between the USGS scientists and the Powder River ranching community. Allowing me into this unique relationship enabled the Powder River research to take place. Thanks to Greg Pederson, John Moody, and Eleanor Griffin for being colleagues who provided critical reviews of my ideas and writing. Dave Meko and Ramzi Touchan of the University of Arizona were valuable resources that helped me break into the field of dendrochronology.

I could neither have collected nor processed the number of tree cores analyzed in this study without help from CSU undergraduate researchers. Thanks to Marshall Wolf and Brendan Elba for each spending a great summer with me, living in a trailer, down by the river. Thanks to Marshall, Brendan, and Fisher Ankney for meticulous work in the Dendro Laboratory processing tree cores. Thank you to the USGS Riparian Ecology research lab for use of their facilities during this research.

This dissertation was primarily funded by two sources. The first was the Integrated Water Atmosphere Ecosystems Education and Research (I-WATER) program, a National Science Foundation IGERT program (Grant No. DGE-0966364). The second major funder was the United States Geological Survey. Supplemental funding was acquired from the Geological Society of America, Colorado Scientific Society, Warner College of Natural Resources, and Department of Geosciences.

Finally, in this dissertation I repeatedly use the singular terms “I” and “my” when the plural terms “we” and “our” would be more accurate. Please accept this as a dissertation formality, not an indication that I produced this body of research alone. My colleagues and co-authors were, in fact, absolutely essential to the ideas and research that follows.

TABLE OF CONTENTS

LIST OF TABLES

LIST OF FIGURES

1. INTRODUCTION

1.1 Motivation

Rivers and their associated floodplains are among the most productive, biodiverse, and anthropogenically manipulated environments on the landscape [*Ward et al.*, 1999; *Tockner and Stanford*, 2002; *Naiman et al.*, 2010]. Dynamic river flows create biological, hydrological, and geomorphological processes that are essential to functioning floodplain ecosystems, but changes within the watershed can disrupt the balance among these processes [*Richter et al.*, 2003; *Poff et al.*, 2010]. In dry regions, rivers and their verdant floodplain forests cut through the landscape and contrast the surrounding sparsely vegetated uplands [*Patten*, 1998]. *Populus* species are widespread along Northern Hemisphere rivers [*Stettler and Canada*, 1996], and in the western USA, Fremont (*P. fremontii*) and plains cottonwoods (*P. deltoides*; hereafter "cottonwood") are the most common trees in floodplain forests [*Friedman et al.*, 2005b].

In the interior West, cottonwood habitat ranges from small ephemeral streams [*Snyder and Williams*, 2000; *Friedman and Lee*, 2002] to large perennial rivers [*Johnson*, 1994; *Cooper and Andersen*, 2012; *Dixon et al.*, 2012; *Johnson et al.*, 2012]. Cottonwood tree ring growth patterns are tightly linked to river flows [*Edmondson et al.*, 2014; *Meko et al.*, 2015; *Schook et al.*, 2016a, 2016b] because their roots access groundwater that is replenished by the river [*Scott et al.*, 1999; *Amlin and Rood*, 2003; *Rood et al.*, 2003]. Cottonwoods often grow in dry areas where access to the water table is essential, and trees can die if river-derived water becomes inaccessible [*Albertson and Weaver*, 1945; *Rood and Heinze-Milne*, 1989; *Scott et al.*, 1999]. Cottonwood recruitment generally requires flood events that raise the water table, wet floodplain soils, deposit sediment on the floodplain, and cause channel migration [*Scott et al.*,

1997; *Cooper et al.*, 2003a; *Rood et al.*, 2007]. Channel migration enables point bar deposition adjacent to the river, producing areas with bare mineral soil, full sun, and a shallow water table. These point bars are ideal habitat for cottonwood regeneration [*Mahoney and Rood*, 1998; *Benjankar et al.*, 2014]. Riparian trees establish sequentially on the point bar as it expands in size, forming bands of trees whose ages increase with distance from the channel [*Everitt*, 1968; *Hickin and Nanson*, 1975; *Merigliano et al.*, 2013].

Channel migration is a planform adjustment that occurs when the driving forces in river flows overcome the resisting forces associated with bank stability [*Knighton*, 1998]. Channel migration erodes banks, destroys floodplain surfaces, redistributes sediment, and promotes point bar creation. The rate of channel migration is variable across rivers and hydroclimatic regimes, but some migration is necessary to sustain floodplain ecosystems that evolved with fluvial disturbance regimes [*Naiman et al.*, 2010]. Damming rivers decreases peak flows, suppressing channel migration [*Brandt*, 2000; *Nilsson et al.*, 2005] and causing riparian forests to age and transition into dry upland communities [*Merritt and Cooper*, 2000; *Johnson et al.*, 2012]. However, channel migration can be affected by subtler changes as well, such as changes in land use or land cover [*Costa et al.*, 2003], irrigation [*Nadler and Schumm*, 1981; *Johnson*, 1994], and climate [*Favaro and Lamoureux*, 2015]. This makes free-flowing meandering rivers excellent locations to identify environmental changes [*Erskine et al.*, 1992; *Palmer et al.*, 2008].

River flow varies across daily, annual, decadal, and century scales. In the western USA, river-derived water is essential to urban and rural economies, although too much water can devastate both. Thus, an understanding of flow variability is essential. Streamgages are widely distributed to measure river flows, but most flow records only extend back to the early- to mid-

1900s [*Slack and Landwehr*, 1992]. This is a short duration considering the importance of extreme events and century-scale climatic change. To overcome this, tree ring-based flow reconstructions can extend flow records and reveal past flow variability to inform urban, land, and water management. Flow reconstructions use trees from water-limited growing environments, relying on the common positive response to precipitation by both river flow and tree radial growth [*Woodhouse et al.*, 2006, 2013; *Allen et al.*, 2013; *Cook et al.*, 2013]. However, most flow reconstructions use cores from upland trees that are not physically connected to the rivers, so these trees do not express flow changes due to altered runoff generation processes or flow regulation. Riparian trees, such as the cottonwoods that dominate western riparian forests, are directly connected to rivers and have recently been shown to improve flow reconstructions [*Meko et al.*, 2015; *Schook et al.*, 2016b].

1.2 Study Area

The Missouri River is the longest river in the USA and drains most of the eastern Rocky Mountains and western Great Plains. It is the only major river in the West lacking systematic hydroclimatic reconstructions [*Pederson et al.*, 2016]. Because of this, a large collaboration is underway to characterize flows across the basin to improve management of water supplies. In this dissertation, I discuss research from three rivers in the Upper Missouri River Basin: the Yellowstone, Powder, and Little Missouri (Fig. 2.1). The Yellowstone River is the largest tributary to the Missouri and provides the largest flood pulse in the region. The Yellowstone is the longest undammed river in the contiguous USA, and its annual hydrograph is dominated by snowmelt sourced from the Rocky Mountains. The river travels 1100 km to its confluence with the Missouri, and most of this length is in the semi-arid plains of Montana. The Powder River is

a tributary to the Yellowstone. It drains the Bighorn Mountains before meandering through the plains in eastern Wyoming and Montana. The Little Missouri River watershed is mostly in eastern Montana and western North Dakota and lies immediately east of the Yellowstone and Powder watersheds. The Little Missouri watershed is low-elevation, lacking mountains, and snowmelt occurs early in spring at the time of ice break-up. I used data from three streamgages and the riparian cottonwood forests along each of these rivers in the western Great Plains. The streamgages and riparian study sites are located within 300 km of each other and have similar local climate and topography, but the unique watersheds cause flows to differ substantially. All three rivers are relatively unaffected by major engineering works, leaving the flow regimes among the most unaltered in the West. Therefore, these rivers provide an ideal system to identify changes in the hydrologic, geomorphic, and ecological processes that are vital to river systems.

1.3 Study Approach

In Chapters 2-4, I describe three studies from the Upper Missouri River Basin to understand the hydrologic, geomorphic, and ecological processes along rivers. In Chapter 2, I present flow reconstructions for the Yellowstone, Powder, and Little Missouri Rivers using plains cottonwood tree rings [*Schook et al.*, 2016b]. I highlight the research potential of cottonwood dendrochronology by creating single-species reconstructions as accurate as those from other studies in the region that incorporated multiple species and multiple proxies. My reconstructions date back to at least 1742, adding centuries to the flow record to better characterize natural hydroclimatic variability. The results improve our understanding of the

severity and frequency of droughts and pluvials that preceded the measurement records, providing a fuller perspective on recent flows and what the future may bring.

In Chapter 3, I take a geomorphic perspective on river history by reconstructing Powder River channel migration rates [*Schook et al.,* in review]. To do this I integrate channel cross-section measurements, air photo analyses, and cottonwood transects. This approach combines physically measured, remotely sensed, and ecological lines of evidence to analyze channel migration over nested spatial and temporal scales. In order to extend the analysis before the earliest air photo (1939), I take advantage of the tendency for cottonwoods that establish on point bars to have ages representative of the underlying land surface [*Everitt*, 1968; *Merigliano et al.*, 2013]. These channel migration analyses suggest that although the Powder remains free-flowing, minor changes in land use, climate, and water management have substantially altered channel migration processes.

In Chapter 4, I deconstruct the site-level tree ring variations explored in Chapter 2 for the three rivers to analyze tree ring growth patterns in individual cottonwoods. I explore how biological and spatial factors affect tree ring growth in relation to seasonal flows, precipitation, and temperatures. After analyzing all years, I analyze dry years and reveal that tree ring relationships with flow and climate change based on water availability. Because different trees within a forest have variable relationships to flow and climate, the findings presented suggest that strategic grouping of tree cores during analysis can improve flow reconstructions. As a whole, Chapters 2-4 present three distinctly separate research approaches that complement each other to build a multi-century, interdisciplinary perspective of river, floodplain, and riparian forest processes.

2. FLOW RECONSTRUCTIONS IN THE UPPER MISSOURI RIVER BASIN USING RIPARIAN TREE RINGS

2.1 Introduction

Quantifying the long-term variability in river flows is essential for managing water supplies and floodplain ecosystems [*Richter et al.*, 2003; *Nicault et al.*, 2014], but available flow records are short. In the United States most streamgage records extend back to the early-to-mid-20th century [*Slack and Landwehr*, 1992], a limited period considering the importance of infrequent events and century-scale climate changes [*Stahle et al.*, 2000; *Benito et al.*, 2004; *Meko et al.*, 2012]. Dendrochronology is a well-established method for extending flow records. In water-limited growing environments, the positive response to precipitation by both river discharge and tree growth permits flow reconstructions [*Woodhouse et al.*, 2006; *Pederson et al.*, 2011; *Cook et al.*, 2013; *Belmecheri et al.*, 2016]. However, flow reconstructions generally use montane conifers that have no direct connection to rivers. These reconstructions are susceptible to errors resulting from 1) factors affecting flow that occur downstream from the mountains [*Meko et al.*, 2012], and 2) changes through time in the relationship between montane precipitation and downstream flow, such as those occurring from water management, land use, and climate change [*Malevich et al.*, 2013]. The first problem limits the accuracy of flow reconstructions in lowland rivers far downstream from montane conifers. To deal with the second problem, researchers have estimated naturalized flows (*i.e.* flows that would have occurred in the absence of water management) for use in flow reconstruction models [*Woodhouse et al.*, 2006; *Meko et al.*, 2012; *Salas et al.*, 2015]. Errors in naturalized flow estimation are propagated through the flow reconstruction.

Both problems could be alleviated by using rings from riparian trees near the streamgage targeted for flow reconstruction. These trees may be directly influenced by the measured flows and do not require estimation of naturalized flow. Although riparian tree rings have been widely used for floodplain geomorphological investigations [*Sigafoos*, 1964; *Friedman et al.*, 2005a; *Merigliano et al.*, 2013; *Radoane et al.*, 2015], their use in flow reconstructions has been limited [*Cleaveland*, 2000; *Meko et al.*, 2015]. Riparian trees can be short-lived and their growth is unlikely to be correlated with flow if floodplain moisture is abundant. However, I build on recent findings that riparian plains cottonwoods (*Populus deltoides* ssp. *monilifera*) in the semiarid northern Great Plains, USA, can live up to 370 years and have growth highly correlated with river flow [*Edmondson et al.*, 2014; *Meko et al.*, 2015].

Understanding low-frequency (defined here as century-scale) flow variation is essential for both quantifying long-term shifts in mean flows associated with climate change and for comparing the severity of droughts and pluvials across century time scales. The ability of tree rings to reveal low-frequency climate information has been challenged [*Bunde et al.*, 2013; *Franke et al.*, 2013], but recent research builds a strong case for the persistence of low-frequency signals within tree rings [*Ault et al.*, 2013, 2014; *Markonis and Koutsoyiannis*, 2016]. The most common dendrochronological techniques produce reconstructions portraying centuries of discharge as variations around an unchanging mean, an unlikely scenario given our understanding of climate events such as the Little Ice Age and Medieval Warm Period [*Bradley and Jonest*, 1993; *Cook et al.*, 2004]. This problem results from detrending procedures that account for the effect of tree age on growth by removing low-frequency trends from each tree core. Recently, the Regional Curve Standardization (RCS) detrending method has been adopted

because of its ability to remove the effect of tree age while preserving low-frequency variation [*D'Arrigo et al.*, 2006; *Briffa et al.*, 2013; *Meko et al.*, 2015]. RCS requires large numbers of samples to accurately estimate the regional growth curve. RCS is improved when datasets include a wide range of tree ages, which permits separation of the effects of tree age and environment on tree growth. Such datasets are often available in riparian cottonwood forests [*Merigliano et al.*, 2013].

The Missouri River is the principal river of the Great Plains and has served as a locus of human populations since before European settlement [*Fenn*, 2014]. The Yellowstone River is its largest tributary and provides the major flood pulse in the Upper Missouri River Basin. Despite the regional importance of the Missouri River, discharge measurements only extend back a century, and flow reconstructions have been limited to small headwater reaches [*Graumlich et al.*, 2003; *Watson et al.*, 2009]. The Missouri is the last major watershed in the western USA to lack basin-wide flow reconstructions, so most water management decisions are informed by only a short historical record.

I reconstructed river discharge using riparian cottonwoods at three lowland streamgages in the Upper Missouri River Basin on the Yellowstone, Powder, and Little Missouri Rivers. Plains cottonwoods dominate riparian forests across the region, and their inclusion in flow reconstructions has the potential to greatly enhance the accuracy and spatial coverage of multi-century flow reconstructions. My goals were to 1) extend the discharge records on three important yet understudied Great Plains rivers, 2) examine the explanatory power of reconstructions that use only riparian tree rings, and 3) identify pronounced wet and dry periods to inform water supply and management.

2.2 Study Sites

2.2.1 Physical setting

I reconstructed river discharge near the outlets of the Yellowstone, Powder, and Little Missouri Rivers in the Upper Missouri River Basin (Fig. 2.1). The three study streamgages are within 300 km of each other and are at locations with similar elevation, geology, and climate, but the contributing watersheds differ substantially in size and elevation. The Yellowstone River is the longest free-flowing river in the contiguous USA, travelling 1100 km in a 181,500 km^2 watershed that drains the central Rocky Mountains and western Great Plains in Wyoming, Montana, and North Dakota. The Powder River occupies a 34,700 km^2 watershed, drains the east side of Wyoming's Bighorn Mountains and travels 600 km before joining the Yellowstone in eastern Montana. The Little Missouri River drains 24,600 km^2 of low-elevation plains directly east of the Yellowstone watershed and extends 900 km to the Missouri River.

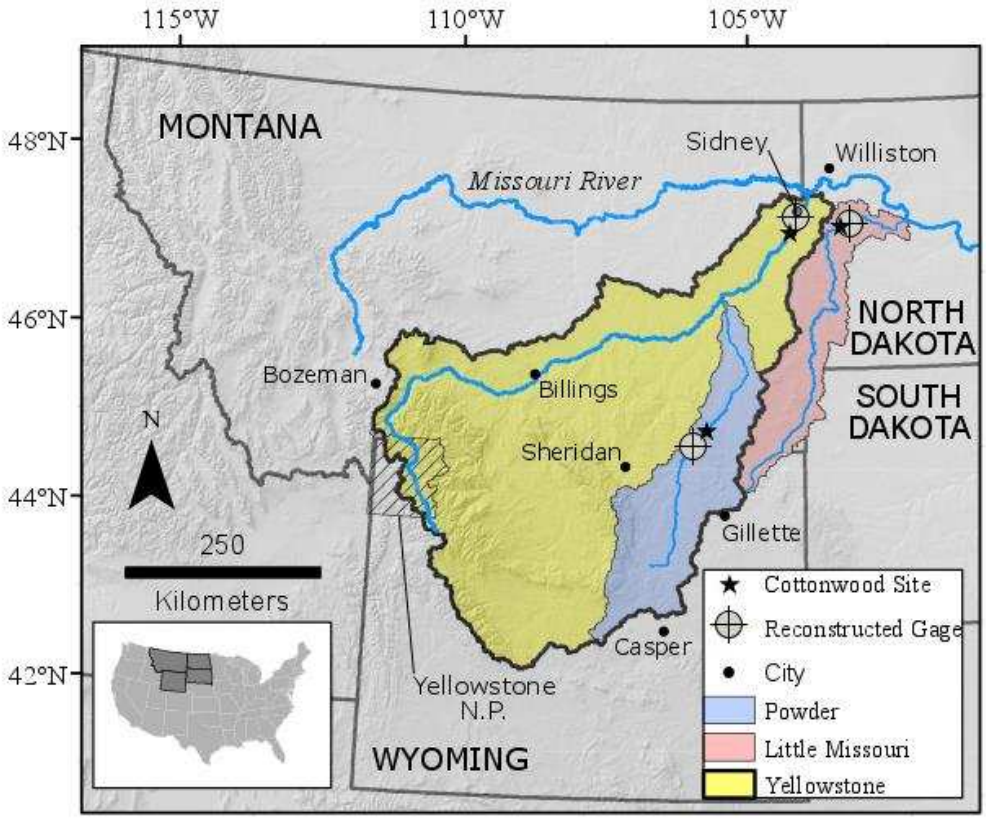

Figure 2.1. The Yellowstone, Powder, and Little Missouri watersheds within the Upper Missouri River Basin. Cottonwood sampling sites are entirely within the river corridors. Streamgage sites for flow reconstructions are the Yellowstone River near Sidney, MT (#06329500), the Powder River at Moorhead, MT (#06324500), and the Little Missouri River near Watford City, ND (#06337000).

At the Yellowstone, Powder, and Little Missouri cottonwood sampling sites, the 1911-2010 mean July high temperatures were 30.6, 31.8, and 29.8° C (*river order is preserved throughout the paper*), while mean January lows were -16.5, -13.7, and -16.9°C [*Daly et al.*, 2008] (Table 2.1). Mean annual precipitation was 346, 329, and 377 mm, and the greatest local precipitation occurred in June. High-elevation snowpack in the Yellowstone and Powder watersheds melts in May through July. Low-elevation snow in all three watersheds melts in March and April, when river flow can be affected by ice jam floods. Yellowstone River peak

annual discharge at Sidney, MT occurred reliably in June (76% of years in the historical record) and the slightly lower elevation Powder River at Moorhead, MT had peak discharge in May or June in 60% of years. This reflects the importance of high-elevation snowmelt in both rivers. In contrast, the Little Missouri at Watford City, ND peaked in March or April in 54% of years, reflecting the relative dominance of low-elevation snowpack (Fig. 2.2). Lowland summer precipitation affects flows in all three basins, especially the Little Missouri.

Table 2.1. Summary statistics for flow, weather, and cottonwood chronologies from the three study sites.

Metric	***Yellowstone***	***Powder***	***Little Missouri***
Average July high temperature (°C)	30.6	31.8	29.8
Average January low temperature (°C)	-16.5	-13.7	-16.9
Precipitation (mm/yr)	346	329	377
Gaged discharge period	1911-2014	1931-2014	1929-2014[1]
Area above streamgage (km^2)	177,300	20,800	21,500
Streamgage elevation (m)	573	1021	588
Mean annual flow (m^3/s) [1]	329	12.5	15.9
Tree ring period	1729-2012	1740-2013	1643-2010
Number of trees	210	222	336
Number of cores	389	408	643
Interseries correlation	0.58	0.60	0.68
Mean sensitivity	0.34	0.32	0.35
Mean series length (yr)	89	83	112

[1] Mean annual flow is for 1930-2010. Streamgage record extended from 1935 to 1929 by [*Meko et al.*, 2015].

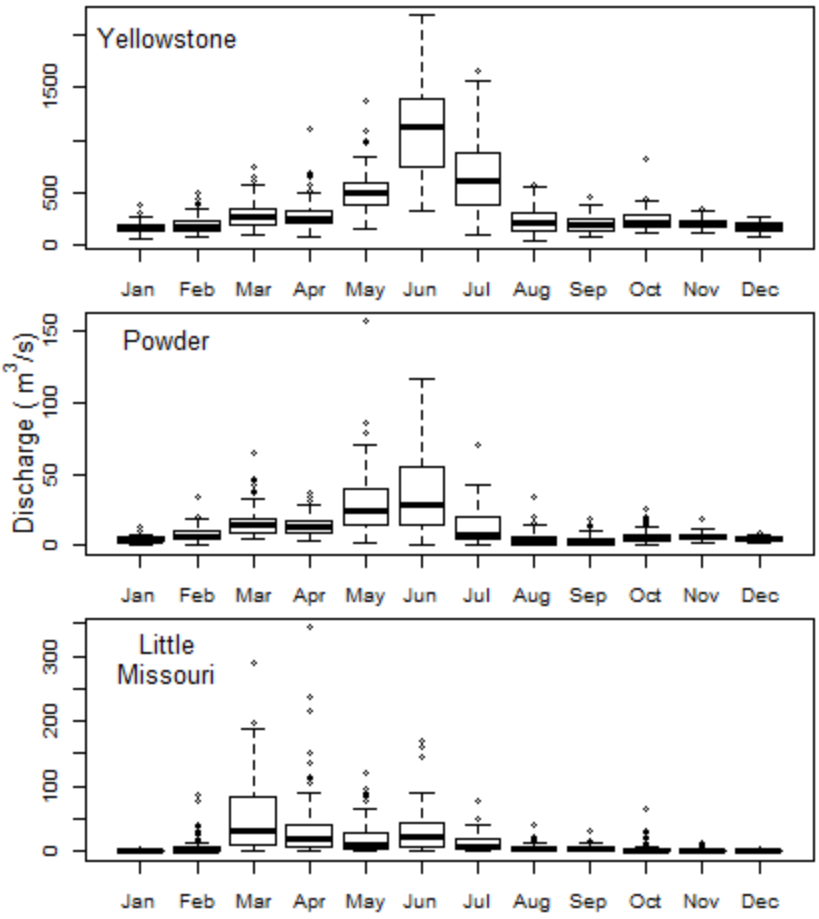

Figure 2.2. Mean monthly discharge over the period of record for the Yellowstone (1911-2014), Powder (1931-2014), and Little Missouri (1929-2014) Rivers. The Yellowstone and Powder have montane snowmelt runoff regimes, while the Little Missouri discharge is less predictable and often has a bimodal peak resulting from late-winter snowmelt and late spring or summer rain.

Although all three rivers maintain relatively natural patterns of seasonal flow (Fig. 2.2), they have experienced different degrees of flow regulation through time [*U.S. Bureau of Rec.*, 2013]. No mainstem reservoirs exist on the study rivers, but large tributary reservoirs have been built in the Yellowstone and Powder watersheds. The Bighorn River, the Yellowstone's largest tributary, has a highly regulated flow regime. Bighorn River peak annual discharge decreased by 62% after the completion of its two main dams in 1952 and 1967 (flow records for

1935-1951 vs. 1968-2014). Approximately 23% of annual flow is depleted from both the Yellowstone and Powder watersheds [*Chase*, 2013], 95% of which is used for irrigation [*U.S. Army Corps of Engineers and Yellowstone River Conservation District Council*, 2015], while the Little Missouri depletions are much less.

2.2.2 Ecological setting

Plains cottonwoods dominate the remaining floodplain forest across the Upper Missouri River Basin. Because of the semiarid climate and high water requirement for cottonwoods, I expected cottonwood growth to be limited by water availability and annual ring width to be strongly correlated with flow [*Rood et al.*, 2011; *Edmondson et al.*, 2014; *Meko et al.*, 2015]. In this region, plains cottonwood establishment typically occurs on point bars [*Everitt*, 1968; *Mahoney and Rood*, 1998]. Progressive lateral migration of the river can lead to the formation of even-aged bands of trees increasing in age with distance from the channel [*Merigliano et al.*, 2013]. As a result, migrating rivers can support a broad range of tree ages useful for RCS flow reconstructions.

2.3 Data and Methods

2.3.1 Flow and climate data

I reconstructed Yellowstone River flows near the river's mouth at USGS streamgage #06329500 near Sidney, MT. Mean annual flow (MAF) was 329 m^3/s over the 1911-2014 flow record. The Powder River streamgage is #06324500 located at Moorhead, MT, and MAF was 12.5 m^3/s for the 1931-2014 flow record. The Little Missouri streamgage is #06337000 near Watford City, ND, and MAF was 15.9 m^3/s for the extended 1929-2014 flow record (Table 2.1) [*Meko et al.*, 2015]. I conducted Mann-Kendall tests using the rkt library in R [*Marchetto*, 2015]

to identify monotonic trends in flow over the 1931-2010 period that was common to tree ring, discharge, and climate data.

Monthly temperature and precipitation data were downloaded from PRISM for points at the center of each cottonwood sampling site [*Daly et al.*, 2008]. Yellowstone River data are for the Elk Island Wildlife Management Area south of Sidney, MT at 104.35° W 47.44° N. Powder River data are between Moorhead and Broadus, MT at 105.70° W 45.24° N. Little Missouri River data are from the North Unit of Theodore Roosevelt National Park at 103.4° W 47.6° N. I characterized watershed-scale temperature and precipitation patterns using PRISM data from WestMap [*http://www.cefa.dri.edu/Westmap*]. Mann-Kendall tests were conducted for temperature and precipitation for each watershed for 1931-2010, but PRISM-based trend analyses should be cautiously interpreted because the contributing weather stations may have changed through time.

2.3.2 Tree ring data

In 2013-14 floodplain cottonwoods were cored from a 25-km reach of the Yellowstone River upstream of Sidney, MT (389 cores from 220 trees) and an 85-km reach of the Powder River upstream of Broadus, MT (408 cores from 222 trees; Fig. 2.1; Table 2.1). These cores complemented an existing dataset from an 18-km reach of the Little Missouri River in the North Unit of Theodore Roosevelt National Park, ND (643 cores from 336 trees) [*Edmondson et al.*, 2014]. At all three sites, the closest tree to randomly or systematically selected points was cored in order to minimize bias in tree selection [*Briffa and Melvin*, 2011; *Brienen et al.*, 2012]. Additional cores were taken opportunistically from old trees (43 trees at Yellowstone, 48 at Powder, and 1 at Little Missouri) to increase sample size in the early years of the chronologies.

This sampling strategy produced a large number of cores from a broad range of tree ages and floodplain habitats. At least two cores were collected from each tree at 1.3 m above the ground using Haglöf increment borers ranging from 4.3 to 12 mm in diameter and up to 1 m long. Cores were mounted and sanded using progressively finer grades between 120 and 600 grit. Cross-dating was performed visually under a dissecting microscope using skeleton plots (Stokes and Smiley 1996) and quality controlled using the program COFECHA [*Holmes*, 1983; *Grissino-Mayer*, 2001].

2.3.3 Flow reconstructions

I used the RCS approach to preserve low frequency variation [*Briffa et al.*, 1992]. This technique detrends using one-to-several growth curves for a site, an approach that minimizes distortion of the low-frequency signal but necessitates a large sample size and a range of tree ages. All trees in the sample had at least one core containing pith or rings curved tightly enough to permit calculation of the number of missing rings to pith. I calculated the number of missing rings by dividing the radius of curvature of the innermost ring boundary by the average width of the four innermost rings [*Meko et al.*, 2015]. Assigning a pith date permitted alignment of cores by age, which improves the precision of RCS growth curves.

Sample design is an important consideration in dendrochronology, as tree selection can introduce bias into reconstructions. Some RCS climate reconstructions based on cores from living trees show a Modern Sample Bias (MSB) [*Briffa and Melvin*, 2011]. This results from the common practice of sampling the largest living trees. Because fast growing trees tend to die earlier [*Black et al.*, 2008], the oldest sampled trees are often slow growers. Young slow-growing trees are still small, so the youngest selected trees are mostly fast growers. This two-

part bias produces an apparent low-frequency trend of increasing growth [*Brienen et al.*, 2012]. My random sample technique selected the closest tree to a predetermined point on the floodplain and resulted in inclusion of trees of all sizes, avoiding MSB at the young end of the age spectrum. It was not possible to avoid the bias caused by slower growing trees surviving longer, so it is likely that the old trees in my sample grew slower than average. To correct for this, an RCS technique applying multiple growth curves was used [*Melvin and Briffa*, 2014b]. I used CRUST software to create signal-free 2-curve RCS reconstructions [*Melvin and Briffa*, 2014a, 2014b]. I applied up to nine growth curves to the data which reduced sample size per curve and the magnitude of the low-frequency trends, but did not reverse or eliminate the patterns found (Appendix Fig. 7.2). I explored variance stabilization and prewhitening the chronologies, but effects were negligible so they were not reported. Flow reconstruction models for all three rivers were selected using the all-subsets multiple linear regression technique with Mallow's Cp as the selection criterion [*Watson et al.*, 2009; *Schook et al.*, 2016a]. The RCS cottonwood chronologies from each site were the only three candidate independent predictors in flow reconstructions.

To confirm low-frequency trends using an alternative analysis that avoided all complications associated with detrending, I developed old-tree chronologies based on raw ring width for the oldest trees at each site. Annual ring width was negligibly affected by tree age after 60 years (Appendix Fig. 7.1), so I used ring width for old-trees starting in their 60^{th} year. Each core used to construct the chronology lasted through the duration of the chronology, so individual trees entering and exiting the chronology could not have influenced the results. To maintain a reasonable sample size, start date for the old-tree chronologies varied among sites:

Yellowstone = 1870 (n = 34 cores), Powder = 1890 (n=23), and Little Missouri = 1810 (n = 35). Any trend in growth in these old-tree chronologies indicated changed growing conditions that could be a function of climate or water management, but could not be a result of MSB or detrending.

I used the program seascorr to explore monthly correlations for tree rings with flow, local precipitation, and local temperature [*Meko et al.*, 2011]. Because the sensitivity of cottonwood growth to flow can decrease with increasing discharge, I tested correlations with both flow and $\log_{10}$ flow [*Meko et al.*, 2015]. One-to-twelve month periods were explored for correlation with annual ring width.

2.3.4 Climate indices

Although discharge and tree growth are influenced by weather at the local to watershed scales these conditions can be influenced by global atmospheric-oceanic teleconnections. The Pacific Decadal Oscillation (PDO) has positive (negative) phases corresponding to dry (wet) conditions in the northern Rocky Mountains [*Brown and Comrie*, 2004; *Pederson et al.*, 2013]. El Nino-Southern Oscillation (ENSO) also affects precipitation, with El Nino (La Nina) events correlating to dry (wet) conditions in the region [*Dettinger et al.*, 1998]. In the Atlantic, the North Atlantic Oscillation (NAO) [*Hurrell*, 1996] and the Atlantic Multidecadal Oscillation (AMO) [*Enfield et al.*, 2001] have also been shown to affect climate in North America [*McCabe et al.*, 2004]. I related water year (October-September) and early-season measured and reconstructed flows to monthly climate indices averaged over three periods: the October-September water year, March-June of the current year, and November-

March of the previous winter. This separation yielded 12 comparisons for each river and climate index. Correlations cover the period of flow record for each river.

2.4 Results and Discussion

2.4.1 Chronology development

Cottonwoods reached ages over 270 years at all three sites. The tree cores showed distinct, reliable annual rings whose widths had strong interannual variability and consistency among trees. Even though tree cores were collected from large areas of heterogeneous floodplain, series intercorrelations were high (0.58-0.68) and mean interannual sensitivities (0.32-0.35) were appropriate for reconstructions [*Grissino-Mayer*, 2001]. Missing rings accounted for only 9 out of 130,830 (0.007%) rings, revealing a near absence of the common dendrochronological difficulty of missing rings [*Cook and Kairiukstis*, 2013]. The chronologies at the Yellowstone, Powder, and Little Missouri Rivers extended back to 1729, 1740 and 1643, respectively. Due to a progressively decreasing sample size back in time, the widely adopted Expressed Population Signal threshold of 0.85 [*Wigley et al.*, 1984] identified the chronologies to be reliable back to 1805, 1830, and 1762, respectively.

2.4.2 Relationship between ring width and environment

Interannual variation in cottonwood growth was closely related to flow and climate. Ring width was strongly positively correlated to flow ($p < 0.01$), positively correlated to precipitation ($p < 0.01$), and negatively correlated to temperature ($p \leq 0.02$) over periods ranging from 1 to 12 successive months (Table 2.2; Appendix Figs. 7.3-7.4); I focus on 4- and 12-month periods because of their high correlations and the significance of annual flow. This confirmed that cottonwood growth in the semi-arid study region is water-limited [*Edmondson et al.*, 2014;

Meko et al., 2015]. River discharge explained more variance in cottonwood growth than did local precipitation at the Yellowstone and Powder Rivers, reflecting the strong contribution of remote montane snowmelt to lowland river flow and tree growth. In contrast, local precipitation and flow were more similarly correlated to cottonwood growth at the Little Missouri, reflecting the relative homogeneity of the low-elevation watershed.

Table 2.2. The highest-correlated sequence of 4- and 12-month periods for environmental predictors and tree ring indices (Pearson's ***r*** values). The final month in each sequence is reported. All *p*-values ≤ 0.02.

Environmental	*Yellowstone*		*Powder*		*Little Missouri*	
Predictor	**4 mo**	**12 mo**	**4 mo**	**12 mo**	**4 mo**	**12 mo**
Discharge	Jun	Jul	Jun	Jul	Jul	Jul
	0.69	0.69	0.73	0.72	0.53	0.53
Log Discharge	Jun	Aug	Jun	Sep	Jul	Sep
	0.69	0.69	0.76	0.74	0.65	0.64
Precipitation	Jul	Jun	Jul	Jul	Jul	Jun
	0.28	0.33	0.50	0.57	0.57	0.67
Temperature	Apr	Jul	Sep	Sep	Jun	Jun
	-0.45	-0.53	-0.40	-0.45	-0.50	-0.41

2.4.3 Flow reconstructions

The highest correlations between growth and mean flow occurred over four months in the spring and early-summer: March-June at the Yellowstone and Powder, and April-July at the Little Missouri (Table 2.3). This finding is consistent with cottonwood branch growth cessation in mid-summer [Friedman et al., 2011]. From a predictor pool of the three cottonwood chronologies, the selected flow reconstruction model for the Yellowstone River retained Yellowstone and Powder trees ($r^2_{Adj.}$ = 0.58), the Powder model retained only Powder trees ($R^2_{Adj.}$ = 0.57), and the Little Missouri model retained Little Missouri and Powder trees ($r^2_{Adj.}$ = 0.57; Fig 3; SI2). The relationship between river flow and tree ring width was nonlinear, and

models of log-transformed flows explained more variance in cottonwood growth than did models of untransformed flows at all sites (Table 2.3) [Meko et al., 2015]. The log relationship between growth and flow suggests that as flow decreases, moisture increasingly limits growth. Discharge and precipitation from the late summer and fall of the previous year were weakly correlated to current-year growth. As a result, increasing the discharge duration from 4 months to 6, 8 or 12 months generally did not strengthen the relationship between growth and flow. For these reasons, my flow reconstructions are for March-June on the Yellowstone and Powder Rivers, and for April-July on the Little Missouri. Model residuals were approximately normally distributed and homoscedastic, and the Durbin-Watson test revealed that they were not significantly autocorrelated.

Table 2.3. Comparisons of the best untransformed 12-month and logged 4-month discharge (Q) reconstructions created using all combinations of the predictor cottonwood chronologies ($r^2_{Adj.}$). Model calibration period starts when flow measurements began on each river and continues through 2010. The best model for each river and flow type is denoted with an asterisk (*). Acronyms represent the tree ring series from each site: YL = Yellowstone, PW= Powder, and LM = Little Missouri.

	Yellowstone		*Powder*		*Little Missouri*	
Model Predictors	**Q12**	**log(Q4)**	**Q12**	**log(Q4)**	**Q12**	**log(Q4)**
YL	0.50	0.50	0.21	0.28	0.33	0.34
PW	0.43	0.47	0.51*	0.57*	0.29	0.43
LM	0.22	0.21	0.08	0.11	0.27	0.41
YL, PW	0.55*	0.58*	0.51	0.56	0.36	0.45
YL, LM	0.49	0.50	0.20	0.27	036	0.45
PW, LM	0.47	0.50	0.51	0.56	0.38	0.57*
YL, PW, LM	0.55	0.57	0.50	0.56	0.40*	0.56

Previous Yellowstone River reconstructions were for a headwater streamgage that drains only 4% of the basin [*Graumlich et al.*, 2003; *Gray and McCabe*, 2010]. My work represents the first flow reconstruction for the Lower Yellowstone River, the principal tributary of the Missouri River. The multiple regression flow model for the Lower Yellowstone accurately identified most of the high and low flow years during the post-1911 historical record. Modeled flows successfully identified some of the wettest years in the historical record, including 1924, 1944, 1965, and 1978 (Fig. 2.3). The reconstruction identified the wettest years (in order) before gaging to be 1828, 1826, 1829, and 1888 (Fig. 2.4). The model identified many of the lowest measured flow years as well, including accurately identifying 2004 as the lowest flow year. The lowest flow years in the entire reconstruction were 1818, 1865, 1819, 1817, and 2004. Low flow occurred more frequently before the historical record, while high flows were more common during the historical record.

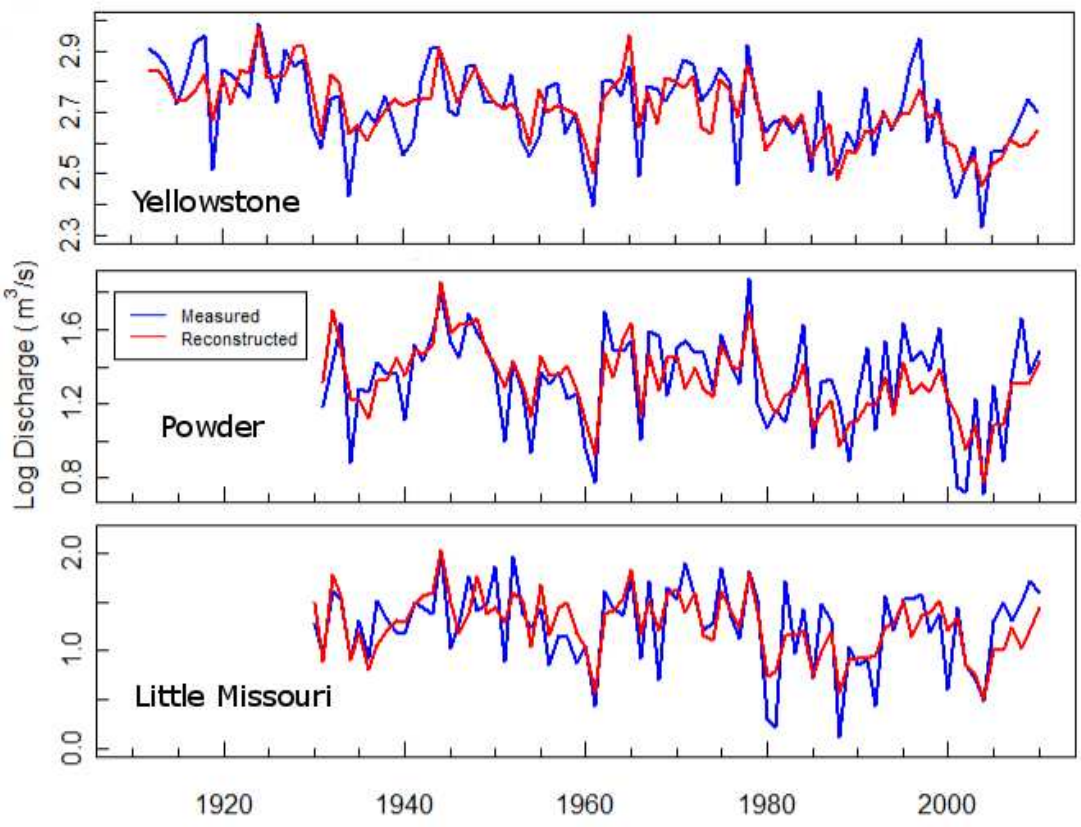

Figure 2.3. Measured (blue) and reconstructed (red) discharge for the periods of record overlap at the Yellowstone (1911-2010; r^2=0.58), Powder (1931-2010; r^2=0.57), and Little Missouri Rivers (1930-2010; r^2=0.57). Discharge is log of 4-month discharge for March-June (Yellowstone and Powder) or April-July (Little Missouri). Note that y-axes differ.

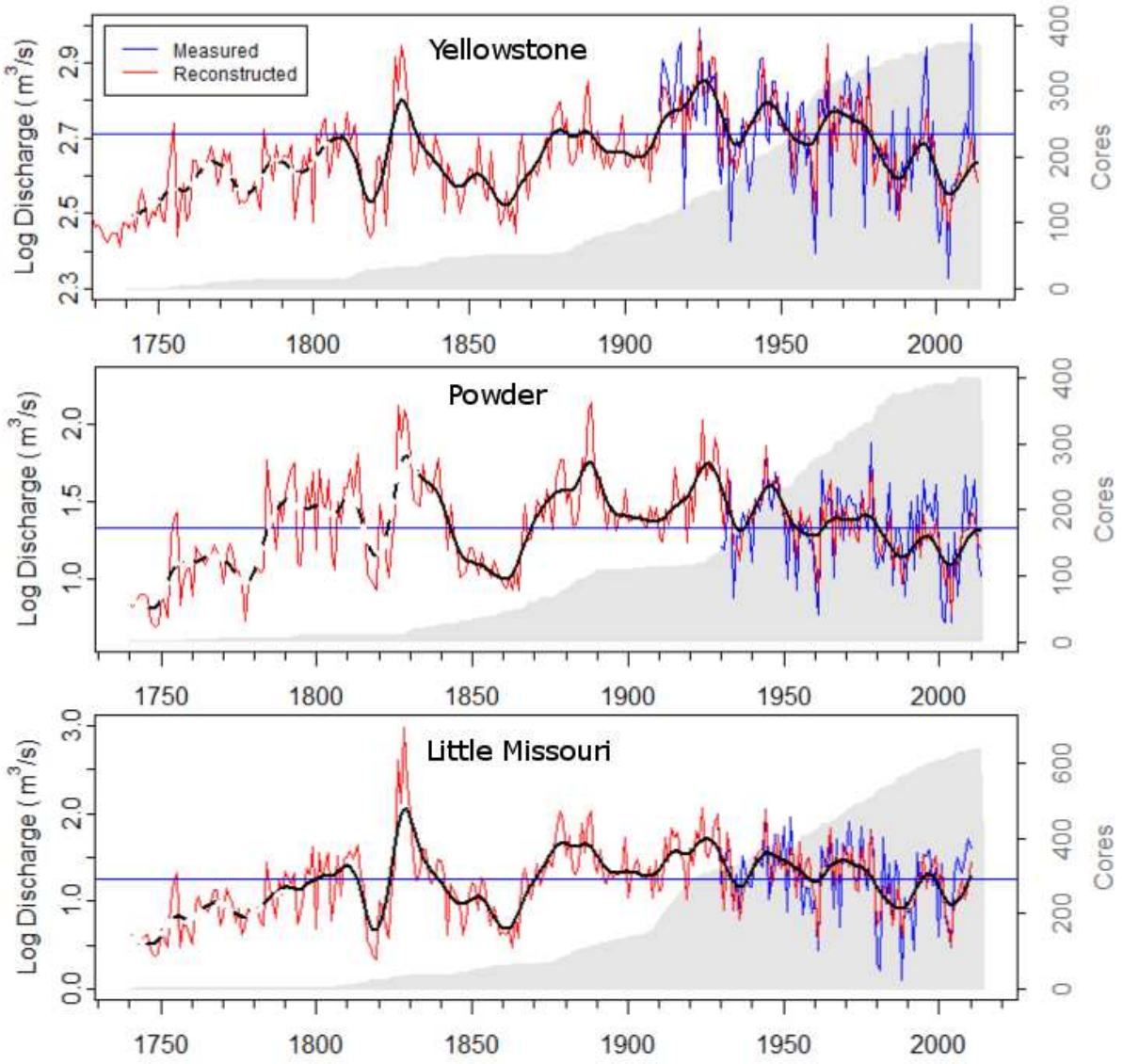

Figure 2.4. Reconstructed discharge for log-transformed 4-month spring discharge at the Yellowstone, Powder, and Little Missouri Rivers. Blue line is measured discharge, red line is reconstructed discharge, and black line is 15-yr smoothing spline. Spline is dashed where the Expressed Population Signal < 0.85 and confidence in the reconstruction is lower. Shaded area is the number of cores in each year. Note that y-axes differ.

This is also the first flow reconstruction for the Powder River, a basin important for energy production and agriculture. The Powder flow model accurately identified 7 of the lowest 10 measured flows in the post-1931 historical record, the driest being 2004, 1961, and 2002 (Fig. 2.3). Reconstructed discharge identified the five highest flow years before the gaged

record as 1826 and 1828, 1887-1888, and 1924. Because Powder River peak flows correlated with March-June flows (r = 0.52), reconstructions of wet periods can be corroborated by observations of historic floods in 1887 and 1924. An indirect estimate of peak discharge for the water year 1924 flood (which occurred in October 1923) estimated it to be three times larger than the 1978 flood of historical record [*http://waterdata.usgs.gov/nwis*]. The reconstruction identified 1887 and 1888 to have the highest flows of the entire reconstructed period. Supporting this finding, one homesteader reported that the 1924 flood was smaller than that of 1887 [*Powder River County Examiner*, 1923]. On the decadal scale, an 1850s-1860s drought lasted longer than any in the historical record, and it was followed by a prolonged 1870s-1920s period of high flows (Fig. 2.4).

High and low flow years were relatively consistent across the Yellowstone, Powder, and Little Missouri Rivers. All three reconstructions identified 1924 and 1944 as very wet, the latter year being confirmed by gaged flows (Fig. 2.3). The very low flows reconstructed for 1961 and 2004 were similarly confirmed by streamgage data. Before gaging began, 1823 and 1919 were two isolated dry years across all sites. Similar multi-year flows occurred across the study sites also. Droughts occurred in 1816-1823, 1860-1865 and 1934-38, while pluvials occurred in 1826-1830, 1877-1881, and 1975-1979. The droughts beginning in 1816 and 1860 were more severe than any in the historical record, and their occurrence is supported by Lakota Winter Counts [*Therrell and Trotter*, 2011], a regional Palmer Drought Severity Index (PDSI) reconstruction [*Cook et al.*, 2008], and a flow reconstruction for the Upper Yellowstone River based on indices of Pacific Ocean climatic variability and Douglas fir (*Pseudotsuga menzeisii*) tree rings [*Graumlich et al.*, 2003].

The 1816-1823 to 1826-1830 drought to pluvial climate shift was the most extreme of the last 200 years. This shift may have partially resulted from climate forcing from the largest volcanic eruption in the last 500 years, Mt. Tambora in 1815 [*Shindell et al.*, 2003]. My flow reconstruction necessarily attributes the rapid tree growth in the 1820s to high flow, but severe droughts can kill a large proportion of riparian trees [*Albertson and Weaver*, 1945], and competitive release following widespread tree mortality can increase subsequent growth rates [*Scott et al.*, 1999] even without an increase in flow. However, both a local upland ponderosa pine (*Pinus ponderosa*) chronology [*Sieg et al.*, 1996] and a PDSI reconstruction [*Cook et al.*, 2008] confirm the late 1820s pluvial, providing independent lines of evidence to support this climate shift. In addition, the largest recorded flood along the nearby Red River in Winnipeg, Manitoba, Canada, occurred in 1826 [*Rannie*, 1999].

Not all reconstructed flow years were consistent across the study sites. For example, data indicate that 1854 lacked low flows only on the Little Missouri, 1913 had high flows only on the Yellowstone, and 1873 had low flows relative to adjacent years only on the Powder. Extreme high flows on the Powder in 1887 and 1888 surpassed the modestly high flows at the other two sites. Finally, both modeled and measured flows were high in 2001 on the Little Missouri, but they were low on the Yellowstone and Powder. These examples highlight that spatially distinct weather patterns and hydrological processes can lead to unique hydrologic conditions in neighboring watersheds.

The alternative flow reconstructions using only one cottonwood chronology showed the local chronology to be a similar or better predictor than the chronologies from the other two rivers in all three cases (Table 2.3). Multivariate model selection favored the Powder

chronology over the other two, retaining it in the best model for each site. Although the Powder is a tributary to the Yellowstone, mean annual flow at the reconstructed streamgage is only 4% of the Yellowstone's annual flow, so the direct influence of the Powder on the Yellowstone is small. The strength of using data from the Powder River cottonwoods as a flow predictor at all three sites may reflect the central position of the watershed in terms of geography, physiography, elevation, and land cover. It is also possible that the larger geographic extent of the Powder River tree core collection area (85 river km) resulted in a chronology that incorporated the largest range of local characteristics, rendering it the least susceptible to site-level influences unrelated to flow.

Reconstruction models created from multiple sites and species can increase model fit because different chronologies represent different locations and processes within a watershed. However, my single-species flow reconstructions using chronologies from only three sites explained 57-58% of the variance in measured discharge. These correlations are among the highest for northern Rocky Mountain river flow reconstructions, including the Upper Yellowstone River (r^2 = 0.53) [*Graumlich et al.*, 2003], Logan River (r^2 = 0.48) [*Allen et al.*, 2013], Snake River (r^2 = 0.56-0.63) [*Wise*, 2010b], and the Wind River headwaters (r^2 = 0.40-0.64) [*Watson et al.*, 2009]. The other reconstructions all used either multiple species or tree rings combined with another proxy dataset. Similarly, the previous Little Missouri flow reconstruction combined tree-rings from cottonwoods and upland conifers [*Meko et al.*, 2015]. I was able to match the variance explained in that reconstruction by using plains cottonwoods from two rivers, the Little Missouri and Powder. Future efforts can advance the techniques used to combine riparian and upland tree rings within a single reconstruction. A challenge in

integrating trees from uplands and riparian areas is that riparian trees respond to actual flows, while upland trees cannot reflect manipulations to the natural flow regime. Thus, the two datasets may be incongruous wherever flow manipulation occurs.

2.4.4 Climate indices and flow

Water year and 4-month measured discharges were correlated to oceanic-atmospheric teleconnections (PDO, ENSO, NAO, and AMO). For the 4-month period of reconstructed flows, Yellowstone River discharge was weakly but significantly correlated with spring AMO (r = -0.32, p < 0.01), winter ENSO (r = -0.24, p = 0.01), and winter PDO (r = -0.27, p = 0.01). Powder River discharge was not significantly correlated to any index (p > 0.10). The strongest correlation at the Little Missouri River was with water year PDO (r = -0.26, p = 0.02; Fig 6a). Water year correlations were similar to 4-month correlations. Most climate indices were similarly correlated with measured and reconstructed flows. The most notable difference was that the Yellowstone River measured 4-month flow was more correlated to ENSO compared to the reconstructed flow (Fig. 2.5). Because the effects of ENSO decrease east of the Rocky Mountains [*St. George*, 2014], the lowland cottonwoods used in my reconstruction appear to be less connected with ENSO compared to the snowmelt driven river flow. The negative correlation coefficients indicate that positive climate phases correspond to decreased discharge. This is consistent with observations that the negative phases of PDO and ENSO are associated with wet conditions in the study region [*Dettinger et al.*, 1998; *Brown and Comrie*, 2004; *Pederson et al.*, 2013]. The documented effects of climate teleconnections vary across the northern Rocky Mountains and western Great Plains [*Barlow et al.*, 2001; *Wise*, 2010a], but PDO generally has been shown to be the most significant teleconnection of those investigated

[*Rood et al.*, 2005; *Pederson et al.*, 2010; *St. Jacques et al.*, 2010]. Two of the study rivers have headwaters in the Rocky Mountains, but I found only modest correlations to PDO. Possible explanations include that the watersheds are located at the periphery of strong influences from ENSO and PDO [*Dettinger et al.*, 1998; *Barlow et al.*, 2001] and that the effect of PDO is less in the Great Plains, where the streamgages are located, than in the Rocky Mountains [*St. George*, 2014]. The study sites are over 1400 km from any ocean, and this separation contributes the mixed and low correlations between flow and climate teleconnections.

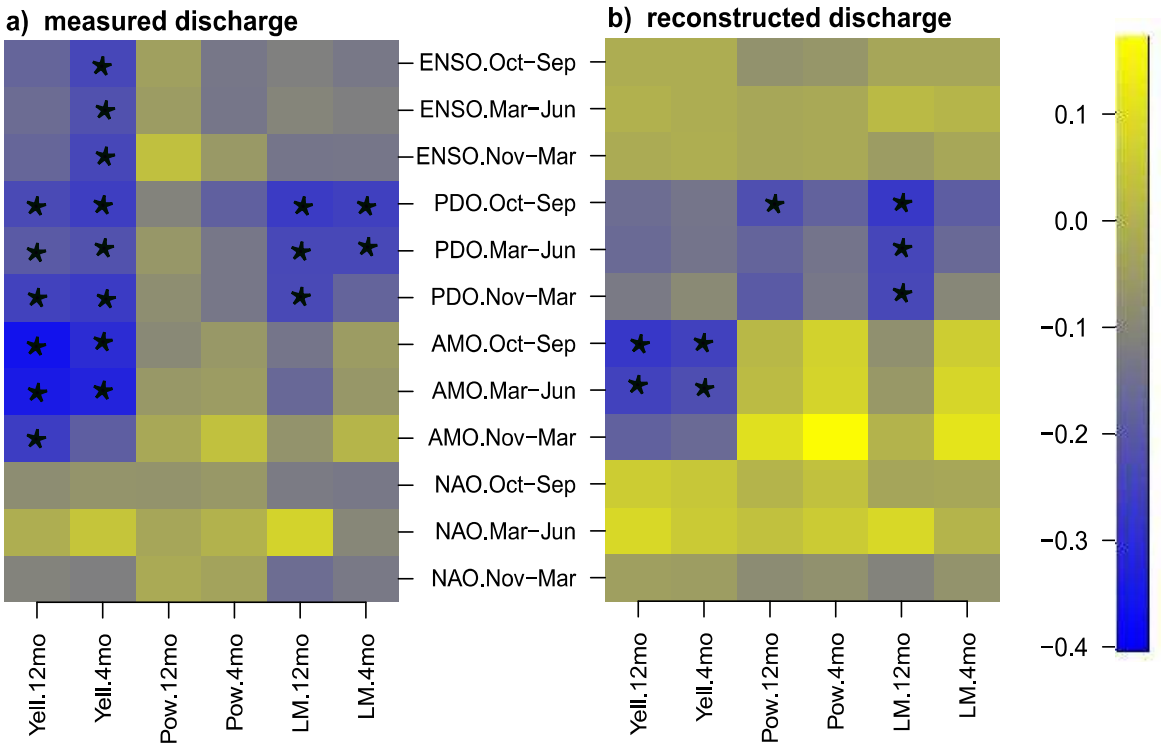

Figure 2.5. Correlations between river flow and climate indices. Flows (columns) are for the Yellowstone, Powder, and Little Missouri Rivers and are for the annual and 4-month periods. Climate indices (rows) are monthly values averaged over winter, spring, and water year periods. Stars indicate $p \leq 0.05$.

2.4.5 Low-Frequency trends, flow timing, and climate change

Even when different flow reconstructions share the same decadal patterns, the relative severity of droughts and pluvials varies if low-frequency patterns in the reconstructions differ [*Briffa et al.*, 2013; *Meko et al.*, 2015]. The reconstructions retained low-frequency changes, revealing high flows from 1870-1980 across the three study sites and indicating that two 1800s droughts were more severe than the 1930s drought (Fig. 2.4). Applying traditional spline detrending to the Little Missouri River cores eliminated the low-frequency trend found in a previous RCS reconstruction and portrayed the three droughts as similar in severity [*Meko et al.*, 2015] . The low-frequency trend identified was also dampened in a PDSI reconstruction that applied traditional standardization to most chronologies in a large multi-species tree ring dataset [*Cook et al.*, 2008]. On the other hand, high flows from 1870-1980 have been observed in other traditionally detrended tree ring reconstructions. These include reconstructions of precipitation from conifers [*Stockton and Meko*, 1983], flow in the Souris River in central North Dakota from bur oak (*Quercus macrocarpa*) [*Vanstone*, 2012], Upper Yellowstone Basin precipitation from conifers [*Gray and McCabe*, 2010], and Upper Yellowstone River flow from Douglas fir and Pacific Ocean climatic indices [*Graumlich et al.*, 2003]. In summary, there is disagreement among authors about the overall pattern of low-frequency variation in precipitation and streamflow over the last two centuries, but the issue remains highly pertinent to water management.

I developed an old-tree chronology for each site that verified the low-frequency trends in the tree ring chronologies and flow reconstructions. These old-tree chronologies had no between-year sample bias because the participating cores were unchanging through time and

the growth metric was ring width instead of a calculated index. Small deviations occurred between the old-tree chronologies (Fig. 2.6b) and the chronologies based on RCS detrending of all trees (Fig. 2.6a). More important, however, the old-tree chronologies from all three sites verified the period of relatively high flows from 1870-1980 found in the RCS chronologies and the flow reconstructions (Fig. 2.4).

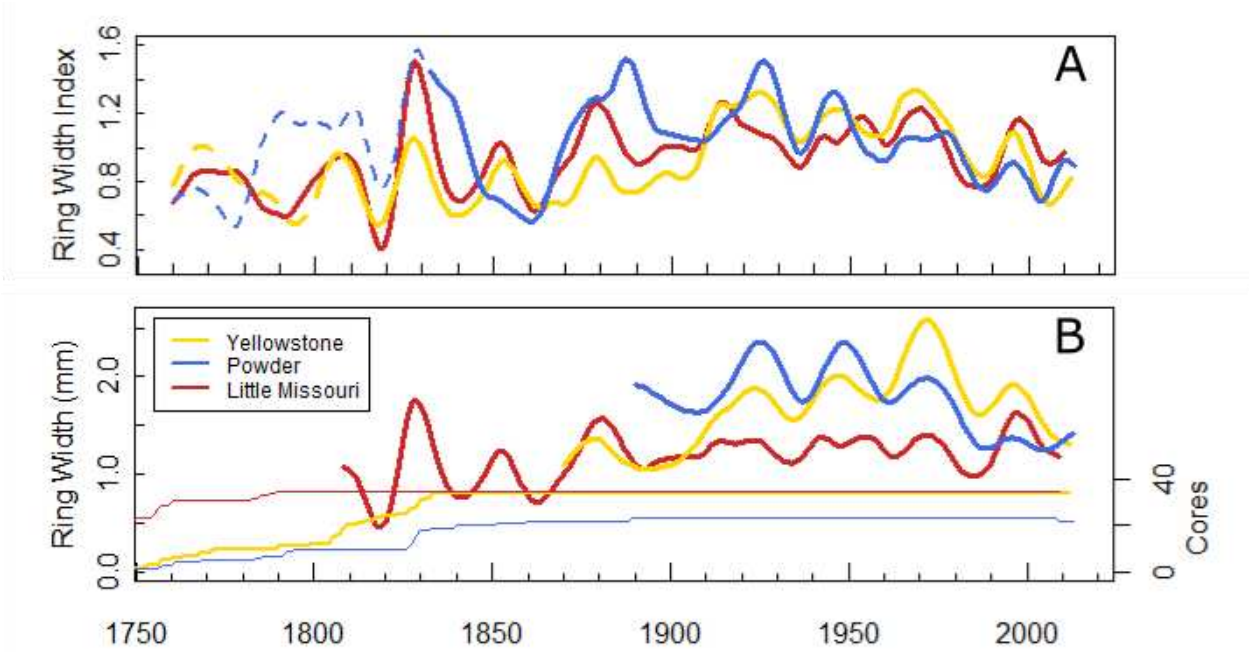

Figure 2.6. (A) 15-year smoothed values for the RCS cottonwood chronologies created from trees of all ages. Dashed lines indicate EPS < 0.85. (B) The old-tree chronologies: 15-year smoothed chronologies constructed from mean annual ring width (i.e., without detrending) for only the oldest trees at each site. Chronologies in (B) are displayed for the period when sample size did not change and all trees were ≥ 60 years old.

Trend analysis revealed that ring widths significantly declined at the Yellowstone and Powder Rivers from 1931-2010 ($p < 0.001$), the period common to all flow and tree ring records (Table 2.4). The decreased growth period follows the construction of large reservoirs on the Bighorn River that decreased the proportion of flows occurring during the early-summer

reconstruction period ($p \leq 0.03$; Table 2.4; Appendix Table 7.2) [*Chase*, 2013]. In contrast, in the Little Missouri watershed no large reservoirs have been constructed, no change has occurred in the proportion of annual flow occurring in the early summer ($p = 0.59$), and ring widths have not declined ($p = 0.49$; Table 2.4).

Table 2.4. Trend analyses for the common 1931-2010 period for climate, tree ring, and flow metrics. Tau (τ) statistics and *p*-values are shown for Mann-Kendall tests; one asterisk (*) denotes significance at $p < 0.10$ and two asterisks (**) denote significance at $p < 0.05$. The 4-month periods are for the reconstructed early-summer months, residuals are the difference between measured and modeled flows, and "proportion 4 mo" is the proportion of annual flows occurring during the reconstructed 4-month period. Trends for temperature and precipitation are derived from PRISM data and should be cautiously interpreted.

	Yellowstone		***Powder***		***Little Missouri***	
Metric	**τ**	***p*-value**	**τ**	***p*-value**	**τ**	***p*-value**
temperature	0.13	0.08*	0.09	0.25	0.09	0.25
precipitation	0.13	0.09*	0.11	0.16	0.13	0.09*
ring width index	-0.29	< 0.001**	-0.32	< 0.001**	-0.05	0.49
modeled 4 mo	-0.33	< 0.001**	-0.32	< 0.001**	-0.20	0.01**
measured 4 mo	-0.14	0.08*	-0.10	0.19	-0.06	0.40
measured 12 mo	-0.06	0.46	-0.08	0.28	-0.07	0.35
residual 4 mo	0.14	0.06*	0.18	0.02**	0.11	0.16
proportion 4 mo	-0.22	0.003**	-0.17	0.03**	-0.04	0.59

The decline in the proportion of flows occurring in early summer at the Yellowstone and Powder may not, however, be sufficient to explain all of the decrease in tree growth at these sites. Declines in early summer flows were not statistically significant (at $\alpha = 0.05$) over the 1931-2010 period, and they were less than declines in ring width. As a result, there was an increasing trend in model residuals for both rivers, although this trend was significant only for the Powder (Table 2.4). Trends in model residuals may indicate a shift in the predictor-response relationship [*D'Arrigo et al.*, 2008] that would disrupt tree ring reconstructions [*Büntgen et al.*,

2008]. So far, this effect is relatively small (Fig. 2.3). Factors other than early summer flows that may be contributing to growth declines at the Powder and Yellowstone Rivers include decreased vertical infiltration of water on the floodplain caused by reduced flood peaks [*Reily and Johnson*, 1982], increased evapotranspiration related to higher temperatures, and increased competition for water resulting from introduction of non-native pasture grasses and the tree Russian olive (*Elaeagnus angustifolia*). Factors suppressing growth appear to have countered any fertilization effects of agricultural nitrogen fertilizers and increasing CO_2 in the atmosphere, a result that is consistent with a greenhouse study of plains cottonwood showing negative effects from increased aridity outweighing positive effects from increased CO_2 [*Perry et al.*, 2013].

2.4.6 Cottonwood growth and seasonal flow timing

The seasonality of river discharge is important to tree physiological processes. As a result, shifts in flow related to climate change or water management may affect tree growth even when mean annual flow does not change. Warming temperatures could cause earlier snowmelt, resulting in less flow during the early-summer growing season. Reservoir storage and irrigation return flows can decrease growth by delaying flow until after the growing season has ended. Photosynthetic energy assimilated later is available for the following year, but my results indicate that the previous year's late-summer through fall flows were less correlated to tree ring width than were flows from the current year's spring and early-summer. High summer temperatures, low water availability, and high susceptibility to vessel cavitation in cottonwoods can cause protracted stomatal closure, which reduces photosynthesis later in the growing season [*Reily and Johnson*, 1982; *Dickmann et al.*, 1992]. Additionally, much of the

carbohydrate produced in late summer is used for growth of roots and flower buds [*Ceulemans and Isebrands*, 1996]. Therefore, even without decreased annual flow, storage of spring flows for later release may decrease cottonwood ring widths. These processes may help explain the decrease in cottonwood growth rates downstream of large dams even without annual flow depletions [*Schook et al.*, 2016a].

2.4.7 Implications for water management

Nearly all cities in the sparsely populated Upper Missouri River Basin are located along rivers, and understanding the history of regional floods and droughts will better inform us about an uncertain water future in an agriculturally important area. Droughts in this semi-arid region endanger agrarian livelihoods and threaten the entire regional economy. Understanding the severity of past droughts, such as those from 1816-1823 and 1861-1865, can improve coordinated management of water supplies. Missouri River reservoir storage effectively buffers against isolated dry years, but my reconstructions reveal multi-year droughts more extreme than those in the instrumental record. An improved understanding of extreme events informs reservoir management that is operated with the goals of preserving late season water availability, river navigation, hydropower generation, and endangered species. The non-linear relationship between tree-growth and river discharge means that the magnitude of reconstructed wet periods is less precise than for dry periods, but reconstructions nonetheless indicate that pluvials in the 19th century exceeded those in the instrumental record. A recent example highlighting the threat of extreme events occurred in 2011. Historically, Missouri River reservoir management has used estimates of the 1881 flood to guide flood control storage, but 2011 runoff exceeded that of 1881 by 20% and pushed storage capacity to 98% of total [*U.S.*

Army Corps of Engineers, 2013]. My flow reconstructions on Missouri River tributaries suggest that 1826-1830 flows would have exceeded reservoir storage capacity, endangering infrastructure and municipalities. There is no reason to believe that extreme events such as those that occurred before the instrumental record cannot return.

2.5 Chapter Synthesis

My cottonwood-based flow reconstructions are the first to extend discharge records for the Lower Yellowstone and Powder Rivers, two major tributaries in the Upper Missouri River Basin. At all three reconstructed rivers, cottonwood growth was most strongly correlated with log-transformed discharge from March-June or April-July. The reconstructions explained at least 57% of the variance in historical flows and extended back to 1742, 1729 and 1643 at the Yellowstone, Powder, and Little Missouri Rivers, respectively. The RCS-detrended chronologies preserved low-frequency variation in the tree ring data and produced reconstructions featuring a prolonged wet period from 1870-1980 at all three sites. The flow reconstructions revealed droughts and wet periods in the 1800s more extreme than any occurring in the historical record. Declines in growth at the Yellowstone and Powder Rivers beginning in the mid-to-late 1900s resulted partly from flow regulation, which delayed much of the runoff until after the early-summer period when most tree ring growth occurs. These flow reconstructions, constructed from only three cottonwood predictor chronologies, explained at least as much variance as nearby reconstructions for headwater streamgages that incorporated several tree ring series, multiple species, and multiple climate proxies. Future flow reconstructions that combine riparian tree rings with additional datasets could produce even more powerful flow reconstructions to guide river management. This study can be used to inform water

management and serve as a launching point for future flow reconstructions in the Upper Missouri River Basin, the last major river basin in the western USA lacking widespread flow reconstructions.

3. DECLINING CHANNEL MIGRATION RATES ON A FREE-FLOWING MEANDERING RIVER

3.1 Introduction

Dynamic flows create the mosaic of floodplain landforms that make river environments disproportionately valuable for biodiversity and ecosystem processes. Flooding, sediment redistribution, and recycling of land are required for the persistence of these disturbance-adapted ecosystems [*Gurnell et al.*, 2012, 2016; *Meitzen et al.*, 2013]. River flows not only have the energy required to transport in-channel sediment, but they also destroy and create land through lateral channel migration [*Hickin and Nanson*, 1975; *Wohl et al.*, 2015]. Channels can migrate from 0 to > 100 m/yr along different reaches, rivers, and hydroclimatic periods [*Hooke*, 1980; *Lawler*, 1993; *Hudson and Kesel*, 2000]. The removal or alteration of disturbance regimes can cause floodplains to transition into upland communities that lose some of their biodiversity [*Merritt and Cooper*, 2000; *Johnson et al.*, 2012]. Even minor changes to water and sediment regimes may have significant effects, which makes free-flowing meandering rivers excellent indicators of environmental change [*Erskine et al.*, 1992; *Palmer et al.*, 2008].

Several conditions can alter the water and sediment fluxes responsible for channel migration [*Wohl et al.*, 2015]. Damming a river imposes an acute pressure that alters fluvial processes and landforms [*Brandt*, 2000; *Nilsson et al.*, 2005], but changes also result from more subtle perturbations caused by land cover changes [*Costa et al.*, 2003], irrigation extraction [*Johnson*, 1994], and climate [*Favaro and Lamoureux*, 2015]. Climate change has modified the timing and magnitude of flood peaks, especially in snowmelt-driven rivers [*Stewart et al.*, 2005; *Clow*, 2010]. Land use and land cover changes can increase [*Costa et al.*, 2003] or decrease [*Li et*

al., 2009] flood magnitudes. Channel migration may be directly suppressed through bank stabilization [*Florsheim et al.*, 2008] or indirectly through species invasion [*Cadol et al.*, 2011], flow regulation and water extraction [*Fremier et al.*, 2014].

Channel migration is governed by interactions between driving and resisting forces that are sufficiently complex to prevent accurate prediction of a meander's geomorphic response to flow [*Nanson and Hickin*, 1983; *Nanson*, 1986; *Güneralp et al.*, 2012]. Channel gradient, meander curvature, bank resistance, and flow history all affect the sensitivity of river meanders, and the complexity of these interactions prevents identification of migration thresholds [*Nanson and Hickin*, 1983; *Hooke*, 2007]. The fluvial geomorphic concept of complex response applies to channel migration because flow and geomorphic history affect channel response to subsequent flows [*Schumm*, 1973; *Moody et al.*, 1999]. For example, bank erosion may be affected by deposits from previous floods [*Nanson and Hickin*, 1983; *Nanson*, 1986], and extreme floods may incite channel responses that last several decades. Because of our inability to fully characterize individual meanders, assessing meander migration at the reach scale may be most useful for characterizing channel migration. Additionally, because of the time lags affecting channel responses to dynamic flows and major floods, channel migration should be considered over a range of timescales.

Diverse research approaches have been used to study channel migration. Field and mapping approaches include repeat planimetric and cross-sectional surveys, photogrammetry, terrestrial laser scanning, and structure from motion software [*Lawler*, 1993; *Milan et al.*, 2007; *Fonstad et al.*, 2013]. These datasets are usually collected over short time scales (years) that cannot be used to characterize the century-to-millennial time scales over which channels

migrate and floodplains are renewed [*Hughes*, 1997]. Approaches used to address multi-century timescales include radio carbon dating [*Nanson*, 1986; *Erskine et al.*, 2012] and optically stimulated luminescence [*Hobo et al.*, 2014], but both techniques generally suffer from low temporal resolution and spatial coverage. Intermediate length (10^1 – 10^2 years) datasets may be best for characterizing channel migration. These include multi-decade channel cross-section measurements, which have revealed mechanisms of floodplain formation [*Pizzuto*, 1994; *Moody and Meade*, 2008] and meander evolution [*Hooke*, 2007]. Mapped river channels from historical land surveys and aerial photographs provide datasets with longer time scales. Although some river maps in Europe date to the early 18th century [*Miřijovský et al.*, 2015], most long-term quantitative analyses use air photos collected since the 1930s. Floodplain trees can establish predictably in response to channel migration [*Merigliano et al.*, 2013], thereby offering an approach longer than covered by channel cross-sections and air photos. Among these floodplain trees are cottonwoods (*Populus spp*.), which can provide a living record of centuries of channel changes [*Hickin and Nanson*, 1975; *Edmondson et al.*, 2014]. Cottonwoods are widely distributed and the most common floodplain tree in the western USA [*Friedman et al.*, 2005b]. Their propensity to establish soon after a point bar surface is created means that channel migration can be traced using their ages [*Everitt*, 1968; *Cooper et al.*, 2003a; *Friedman et al.*, 2005b; *Stella et al.*, 2011; *Merigliano et al.*, 2013; *Wilcox and Shafroth*, 2013].

I combine repeated channel cross-sections, historical aerial photographs, and cottonwood age transects to analyze complementary approaches that document channel migration across spatial and temporal scales. This research builds on four decades of ongoing cross-section measurements from the Powder River, Montana, USA [*Moody and Meade*, 1990].

The lack of direct flow regulation on the Powder River makes it an ideal system to quantify the effects of flow on channel migration. This contrasts with most rivers in the American West, which have experienced substantial flow alterations caused by water management. My objectives were to 1) determine if channel migration rates have changed through time, given that the Powder River is free-flowing, and 2) identify if extreme floods cause prolonged effects that influence channel migration for decades thereafter. To investigate, I first quantify Powder River channel migration rates using three approaches, and second I investigate the processes controlling spatiotemporal patterns of channel migration rates through time.

3.2 Study Site

3.2.1 Hydrology

The Powder River is one of the few remaining medium-to-large sized rivers in the United States that is relatively unaffected by major engineering structures that would inhibit fluvial processes such as channel migration [*Gay et al.*, 1998]. The river is 600 km long and drains 34,700 km^2 of the eastern Bighorn Mountains in Wyoming and the western Great Plains in Wyoming and Montana. At USGS streamgage #06324500, located 20 km upstream from the study reach, 1930-2010 mean annual flow was 12.5 m^3/s and peak annual flow was 158.9 m^3/s [*Schook et al.*, 2016b]. There is one large off-channel storage reservoir, Lake DeSmet, but only 6% of its storage is consumed by irrigation, which translates to 0.8% of Powder River mean annual flow at the study gage [*HKM Engineering Inc.*, 2003]. The Powder River has experienced relatively small changes in flow over the instrumental record. However, water resources development has been estimated to remove 23% of annual flows [*Chase*, 2013], but there has been no significant trend toward lower mean annual flow during 1931-2010 [*Schook et al.*,

2016b]. Water resources developments in the basin are thought to negligibly impact peak annual flows [*Chase*, 2013], which have the greatest erosive power.

Powder River floods are produced in four main ways [*Moody et al.*, 2002; *Moody and Meade*, 2014]. First, low-elevation ice jam floods occur between late-February and early-April when the southern, upstream reaches of the river thaw before downstream reaches. These floods are spatially limited. Second, Bighorn Mountains high elevation snowmelt in May-June creates the peak annual flow in 60% of years [*Schook et al.*, 2016b]. These snowmelt floods may be augmented by spring rain. This occurred in 1978 to produce the largest peak discharge (930 m^3/s) in the continuous gage record. Third, flash floods from convective rainstorms occasionally produce short-duration high flows in spring, summer and fall. Fourth, frontal storms may cause autumn floods. The largest documented flood was in 1923 and preceded the gage record. It peaked at an estimated 3,000 m^3/s and was caused by a slow moving September cold front that stalled over the region for several days [*Grover*, 1925].

3.2.2 Vegetation

Plains cottonwood (*Populus deltoides*) is the most common riparian tree across the western USA [*Friedman et al.*, 2005b], including along the lower Powder River. Additional woody vegetation includes native sandbar willow (*Salix exigua*), and exotics Russian olive (*Elaeagnus angustifolium*) and tamarisk (*Tamarix ramossisima*). Cottonwood seedlings require abundant moisture and light, which is available on point bars after floodwaters subside. Cottonwood establishment pathways often produce tree ages similar to those of underlying point bars [*Everitt*, 1968; *Merigliano et al.*, 2013], although tree establishment may lag surface creation [*Scott et al.*, 1997; *Miller and Friedman*, 2009]. Establishment near the channel leaves

trees vulnerable to subsequent flood disturbance, but their survival is increased when the river migrates during point bar growth [*Auble and Scott*, 1998]. River migration creates scroll bars, each populated by bands of cottonwoods orthogonal to lateral channel migration with generally increasing ages farther from the channel. Although vegetative reproduction by root sprouting is common in some *Populus* species [*Rood et al.*, 2007], it is uncommon in *P. deltoides* which produces relatively even-aged stands of trees along the Powder River.

3.2.3 Study reach

In 1975, Moody and Meade [1990] established permanent channel cross-sections along the Powder River between Moorhead and Broadus, MT, just north of the Wyoming-Montana border. These cross-sections were designated by "PR" followed by the 1978 river distance (km) measured downstream from Crazy Woman Creek in Wyoming [*Moody and Meade*, 1990; *Moody et al.*, 2002]. My study reach is a subset of the Moody and Meade [1990] study area between PR130 and PR194, a valley distance of 37 km and river distance of 75 km in 2013 (Fig. 3.1). Floodplain turnover and all migration rates were calculated for this reach.

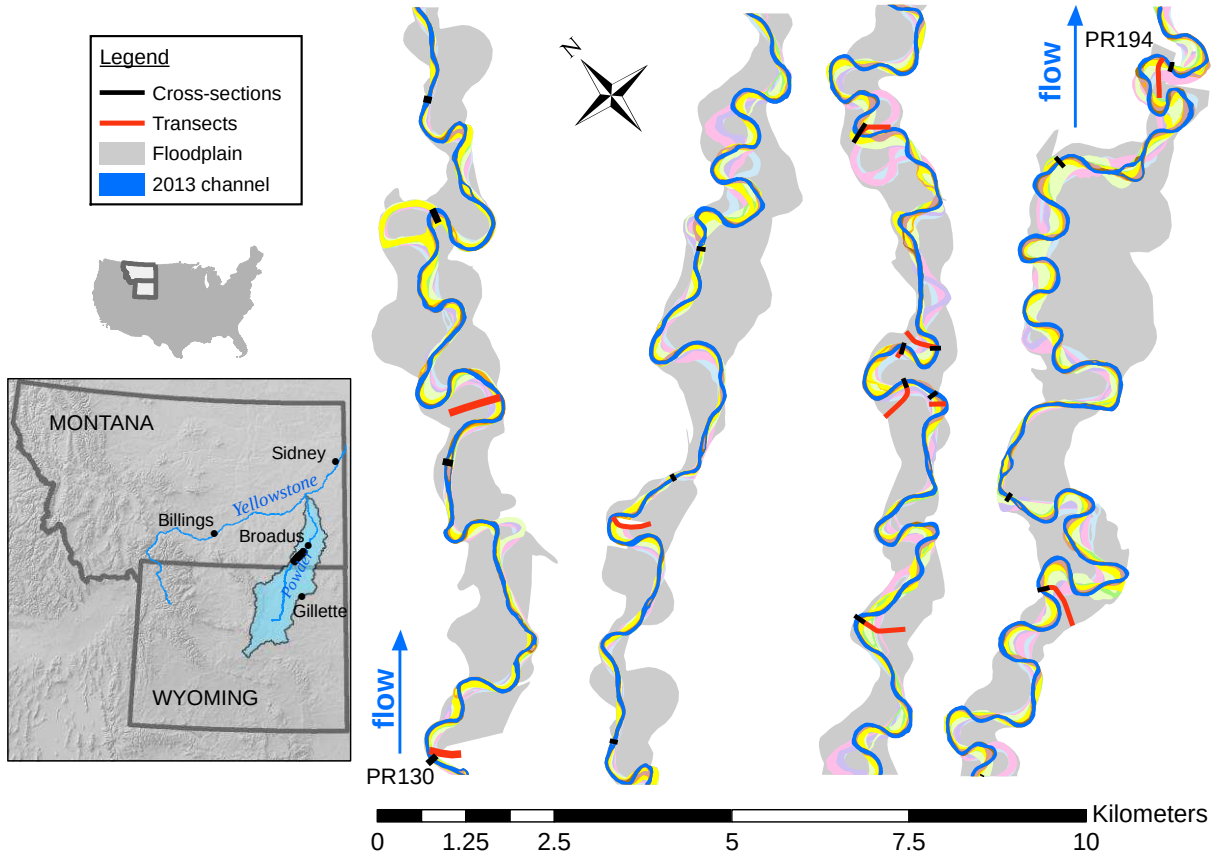

Figure 3.1. The Powder River study reach in southeast Montana (black line in inset). The topographic cross-sections (black) and cottonwood transects (red) within the study reach are shown. Orientation of the four river panels is from left to right, and flow is from bottom to top. The 2013 channel (blue) overlays former channel locations, whose colors correspond to those in Figure 3.2.

3.3 Methods

3.3.1 The Three Approaches

Overview

I used repeated channel cross-sections (XSs; spanning 1975-2014), historical aerial photographs (APs; 1939-2013), and cottonwood age transects (TSs; 1830-2014) as three approaches covering different spatial and temporal scales (Fig. 3.2). XS surveys were repeated at approximately annual intervals from 1975-1998 and less regularly from 1999-2014 [*Moody*

and Meade, 1990]. APs had continuous spatial coverage throughout the reach, enabling standardization of the place-based XS and TS measurements to represent a reach average. The ten APs spanned irregular time intervals, and consecutive photos were used to identify an average migration rate between each photo year. I established 13 cottonwood TSs at actively migrating river meanders as identified in the AP record. TSs were the least precise dataset but covered the largest spatial and temporal scales. Air photo coverage limited the upstream extent of the study reach. Two of the 13 cottonwood transects and 4 of the 20 cross-sections were located up to 10 km up valley from the study reach, and their migration rates were applied to the study reach as described below. Channel migration rates varied spatially from essentially no migration along some straight reaches to maximum migration rates at some meander bends.

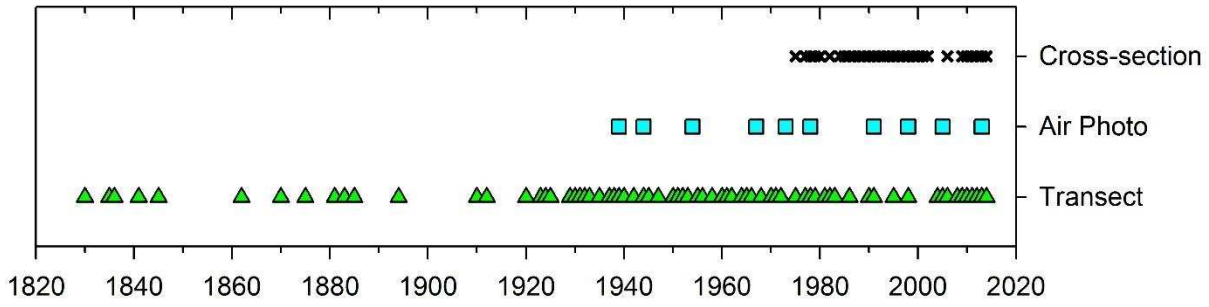

Figure 3.2. All years used in analysis of channel migration rates from channel cross-sections (1975-2014), air photos (1939-2013), and cottonwood transects (1830-2014).

Cross-sections (XSs)

XSs were established to monitor channel changes and sediment budgets beginning in 1975 [*Martinson and Meade*, 1983; *Moody and Meade*, 1990; *Moody et al.*, 2002]. They were placed at regularly spaced intervals to represented a quasi-random sample that included

straight reaches, cross-overs, cutoffs, and different locations around meander bends [*Moody and Meade*, 1990]. XSs were surveyed along a tag line stretched between permanent reference points on each bank using a stadia rod and level (Appendix Table 7.3) [*Moody and Meade*, 1990; *Moody et al.*, 2002]. I analyzed 20 of the XSs located between PR116 and PR194 and calculated migration rates using the channel centerline. XSs were originally oriented perpendicular to the channel, but channel migration altered orientations. I explored adjusting the XS data so that distances were perpendicular to the channel to reveal lateral migration. However, 18 of the 20 XSs remained within 11° of perpendicular to the channel, such that distance adjustments would be < 2% and were therefore neglected.

Air Photos (APs)

APs were used from ten years between 1939 and 2013, averaging eight years between photos (Table 3.1). Channel boundaries were visually identified in APs, and channel centerline was determined to calculate migration rates. APs through 1978 were georeferenced with channel boundaries identified by Martinson and Meade [1983]. I acquired 1978-2013 APs from public sources (Appendix Table 7.4). Georeferenced photos were reprojected into NAD83 UTM Zone 13N. Images not georeferenced were georectified to the 2013 NAIP imagery in ArcMap using a second-degree polynomial created from 12-18 control points (RMSE ≤ 1.6 m) [*Hughes et al.*, 2006].

Table 3.1. Reach average migration rates calculated from air photos for each photo interval.

Period	Time interval (yr)	Initial reach average migration (m/yr)	Underestimate due to interval (%)[1]	Final migration (m/yr)
1939 to 1944	5	5.10	29.26	**6.59**
1944 to1954	10	3.61	34.11	**4.84**
1954 to 1967	13	2.72	35.28	**3.68**
1967 to 1973	6	4.81	30.84	**6.29**
1973 to 1978	5	3.17	29.26	**4.10**
1978 to 1991	13	1.60	35.28	**2.16**
1991 to 1998	7	0.98	31.99	**1.29**
1998 to 2005	7	1.09	31.99	**1.44**
2005 to 2013	8	0.58	32.86	**0.77**

[1] This adjustment accounts for the proportion of lateral migration missed when viewing migration over different time intervals.

To assess the consistency of two research teams delineating the channel in APs for 1939-1978 [*Martinson and Meade*, 1983] and 1978-2013, I acquired the 1978 APs and repeated channel delineation. Consistency was strong. Channel length, slope, and sinuosity all differed by 0.11%. Channel width differed to a greater degree (4.2%), but this was much less than the 22.3% average between all nine sets of consecutive photos. In an uncertainty analysis, I found a median difference of 4.52 m (interquartile range of 2.52 - 10.00 m) between the two 1978 channel centerlines. The 1978 APs were taken two months after a 50-year flood that caused channel migration and avulsion, destroyed vegetation, and deposited fresh sediment on the floodplain. These factors made the 1978 channel boundary harder to identify compared to the others I analyzed. Thus, I conclude that the delineations produced by the different researchers were compatible. My 1978 delineation was used in all analyses.

For each AP year, I found channel centerline length over the river valley. I calculated average channel width by dividing channel area by its centerline length. I calculated slope by

dividing channel length by the difference in water surface elevations between PR130 and PR194 in 1978 [*Moody and Meade*, 1990], a difference likely representative of the AP period because it changed by < 0.40 m over the 37.1 km study reach throughout XS surveys. Sinuosity was calculated by dividing channel length by valley length.

Cottonwood Transects (TSs)

208 cottonwoods were sampled and aged. After a randomly chosen start location 1-40 m from the active channel boundary, the closest tree was cored at 40 m intervals to the end of the scroll bar sequence. Two cores were collected at 1.3 m above ground using 4.5 – 12 mm diameter Haglöf increment borers. Cores were mounted and sanded to progressively finer grades between 120 and 600 grit. I used skeleton plots [*Stokes and Smiley*, 1996] and the program Cofecha [*Holmes*, 1983; *Grissino-Mayer*, 2001] for cross-dating and aging. Using the core closest to pith (biological center) from each tree, I estimated the number of additional years to pith by dividing the radius of curvature of the innermost ring boundary by the average width of the four innermost complete rings [*Meko et al.*, 2015]. TSs were oriented perpendicular to the former channel (Fig. 3.3). I selected meander bends with high migration rates over the AP period because these locations had the most abundant and widest areas of cottonwood forest that established on extending point bars. The systematic sampling scheme provided a representative distribution of tree ages across all sampled meanders.

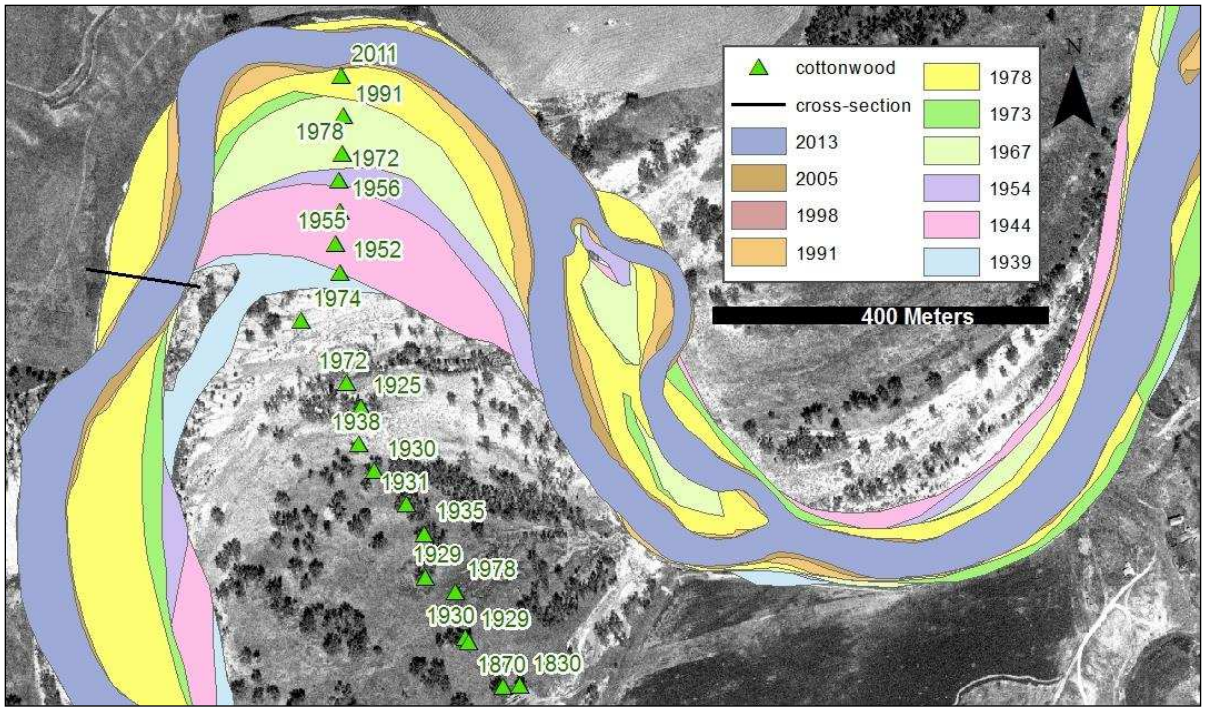

Figure 3.3. An example sequence of two Powder River meanders. Polygons represent the channel location from all air photos, spanning from 1939 (bottom light blue channel) to 2013 (top purple channel). A transect showing cottonwoods (green triangles) with their ages extends from the modern channel, and a cross-section is displayed as a black line. Background is the 1978 air photo, taken two months after a 50-year flood.

TS migration rates were dependent on tree establishment timing and locations, which generally occurred soon after bare sediment was deposited on point bars near the river. In order to precisely date establishment year, trees must be aged at their germination point [*Scott et al.*, 1997; *Holloway et al.*, 2016]. This would have involved digging out each tree and taking multiple cores or slabs to find the germination point, but there was over 1.5 m of aggradation on portions of the Powder River floodplain over just 18 years [*Moody et al.*, 1999], making such excavations very time consuming. Instead of excavating trees, I used above ground cores to age them, and thus all ages are for the collection height of 1.3 m above ground. This strategy increased the number of trees that could be sampled by at least a factor of ten, but the ages

identified were usually lagged from the year of true establishment. To quantify uncertainty associated with the lag, I isolated the 83 trees that were growing in locations that were channel at some point within the AP record (e.g., the top seven trees in Fig. 3.3). The surface beneath each tree was assumed to have been formed in the middle year between the last AP in which it was channel and the first AP in which it was floodplain. Subtracting tree age from this surface age quantified the lag. Lags in tree age vs. floodplain age could have arisen from beaver cutting and regrowth, ice-jam flood damage and regrowth, or germination on older floodplain surfaces caused by high flood stages.

Tree ages that represent point bar floodplain formation from lateral migration should increase or stay the same as distance from the channel increases. For determining channel migration rates, I adjusted the age of each tree dated younger than the previous tree on a TS by assigning it the same age as the previous tree. This adjustment relied on the TS locations being on laterally-extending meander bends. AP sequences demonstrated this to be true at all sampled meanders.

3.3.2 Channel migration analysis

The river channel was identified by the active channel boundary corresponding to the lowest extent of perennial woody vegetation [*Osterkamp and Hedman*, 1982]. On XS profiles, I identified the channel boundary as a break in slope above steeper bank. In years with APs and XSs, I cross-referenced the datasets to confirm that the XS banks were near the lower boundary of perennial vegetation. Similarly, I used the XS locations to support AP channel boundary identification when a break in slope was obvious in the XS. Thus, channel boundaries were identified using methods promoting consistency between approaches.

After the left and right banks were identified in APs, I used the Stream Restoration Toolbox to calculate channel centerlines [*Lauer*, 2012]. Using the centerline kept the river as a contiguous unit throughout the reach, instead of alternating sides as is necessary to measure cutbank or point bar migration. I also used the Stream Restoration Toolbox to calculate the lateral migration distance between centerlines at 25 m increments throughout the study reach. For XS migration rates, I also found lateral changes in centerline location, which was also the midpoint between left and right banks. In a supporting analysis I analyzed cutbank migration for the 14 XSs where a cutbank was clearly identifiable. This allowed analysis of channel migration by lateral extension of the cutbank, whereas centerline migration was a function of both cutbank erosion and point bar deposition.

Because XSs and TSs locations were not random, the spatially-continuous APs were used to standardize them to enable direct comparison of the three approaches and to apply the data to the entire study reach. First, I created polygons between all pairs of channel centerlines and found the cumulative area between them. Dividing area by mean channel centerline in the two AP years yielded a reach-averaged lateral migration distance between the years. I then plotted all migration distances by time interval and calculated the linear relationship for the data. The slope of this regression line represented the reach-average annual migration rate for 1939-2013. I standardized XS and TS migration rates to the whole reach by calculating the average migration rates *of the APs* at locations of each XS and TS (i.e., I compared integrated APs to subsets of APs; Appendix Fig. 7.7). AP migration was faster at the XS (1.11x) and TS (2.20x) locations compared to the reach average. Therefore, all XS and TS migration distances were divided by these ratios to standardize XS and TS data to the whole reach.

I present channel migration rates through time calculated from all three datasets. AP data represent migration rate during the nine between-photo periods. XS's data represent channel migration distance between consecutive years. TS data represent channel migration calculated from tree ages, but determining annual migration rates was more complicated. First, I weighted TS data to account for the TS's not all having trees extending back to the earliest year. To do this, the total number of trees aging to each year was divided by the number of transects with trees aging through that year, which essentially created a synthetic Powder River transect. All values were multiplied by 40 m because this was the sample interval and thus the lateral distance each tree represented. Finally, distances were divided by the AP-calculated standardization ratio (2.20) to yield annual migration rates representative of the study reach.

To investigate which aspects of the flow regime cause channel migration, I compared flow exceedance probabilities for each period between consecutive XS and AP measurements [*Miller and Friedman*, 2009]. Daily flows between each pair of APs were ordered and the flow corresponding to each of the following exceedance probabilities was calculated: 0.001, 0.002…0.009 and 0.01, 0.02…1. The same procedure was carried out for flows between each pair of XS measurements taken in consecutive years (n = 23 years for centerline, n = 22 years for cutbank). This procedure generated an exceedance probability between measurements to compare to migration distance. A series of regressions were run linking the flow for a given exceedance probability to the migration distance within each period. This procedure permitted exploration of the strength of the correlation between flows and channel migration to identify which flows were most strongly tied to channel migration.

The frequently repeated and long duration XS surveys provided a unique opportunity to analyze channel migration as a function of interval between measurements. This exercise addressed a common methodological issue in channel migration analyses occurring when either 1) data are collected at irregular intervals, or 2) measurements taken at longer intervals are scaled to annual rates. Issues arise because dividing multi-year measurements by the time between them ignores back-and-forth channel migration [*O'Connor et al.*, 2003; *Konrad*, 2012]. More of back-and-forth migration is missed as time interval increases, which produces an increasing underestimate of annual migration rate as interval increases. To address this, I used the XSs to calculate migration distance as a function of the interval between measurements. I compared channel centerline migration for all possible pairs of years within each XS. This provided a 4856-point dataset to calculate channel migration over various measurement intervals.

The 1-year channel migration distance calculated from all 337 measurements (i.e., all consecutive year measurements within each XS) was 1.34 m. This became the reference XS annual migration rate. I calculated migration distance for all intervals from 2 to 39 years and found that longer intervals increasingly underestimated annual migration rate (Fig. 3.4; Appendix Table 7.6). For example, measurements taken at 2-year intervals had a 1.15 m/yr migration rate, while the 35-year interval migration rate was 0.69 m/yr. I used these data to correct AP channel migration rates, as APs were taken at 5-13 year intervals. The correction factor was:

corrected migration rate (m/yr) = (*measured distance* – 0.375 + 0.377**interval*)/*interval*

where the empirical values were calculated using the regression line through all comparisons up to a 20-year interval (Table 3.1, Fig. 3.4).

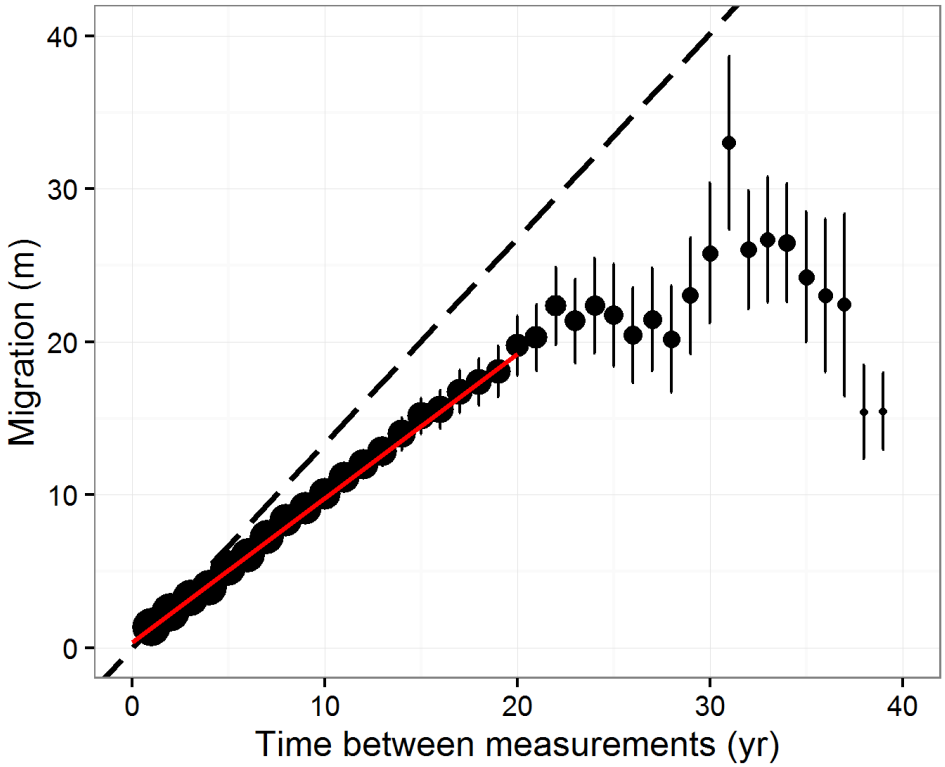

Figure 3.4. Channel migration distance (m) as a function of the number of years between measurements, calculated from all pairwise comparisons within cross-sections. Point size is scaled to sample size, ranging from 337 samples at a 1-year interval to 5 samples at 38- and 39-year intervals. Error bars are standard error of the mean. Dashed back line is the expected migration distance extended from the 1-year interval rate. Red line is the linear model (y = 0.375 + 0.961*x) using all pairwise comparisons ≤ 20 years. This function was used to calculate annual migration rates from air photos, which were taken at 5-13 year intervals.

Floodplains can be identified geomorphically, hydrologically, or from a combined approach. The Powder River floodplain boundary was difficult to delineate geomorphically because of floodplain forest conversion to agriculture, regrading of land surfaces, and

inconspicuous boundaries between terraces and modern floodplain. Therefore, I used a field-based delineation of the 50-year floodplain for the study reach (37.1 valley km, 36.44 km^2). After the 50-year flood in 1978, Meade and Moody [2013] delineated the extent of inundation throughout the study reach by 1) field mapping of deposited sediment and flood debris, 2) topographic map analysis to interpolate field data, and 3) conversations with resident ranchers. I georeferenced and digitized the 1978 flood map and used it to define the floodplain and calculate its area. Due to dikes, the floodplain area identified is likely 10-15% smaller than its pre-settlement extent [*B. Meade*, *pers. comm, 27 April 2016*]. To investigate floodplain turnover rate, I calculated the cumulative floodplain area occupied by the channel through time by overlaying all channel locations from 1939 (time = 0 yr) through 2013 (time = 74 yr). Cumulative areas occupied were divided by floodplain area to identify floodplain occupancy, which is the proportion of the floodplain occupied by the river channel through time [*Konrad*, 2012].

3.4 Results

3.4.1 Channel migration

Cross-method comparisons

Cross-method compatibility was evaluated by comparing channel migration rates from concurrent periods between methods. First, I compared centerline migration in the XS record (1975-2014) to that from APs at the XS locations (i.e., not the spatially-integrated APs, but APs at the 20 XS locations) from their most overlapping period (1978-2013). Channel migration rates were similar: 0.63 ± 0.33 and 0.81 ± 0.04 m/yr for APs and XSs, respectively (95% confidence intervals included; Appendix Fig. 7.8; Table 3.2). The difference in rates is not statistically significant ($z = 1.06$, $p = 0.36$) and is small compared to the 66-m mean channel

width during the AP period. The slightly higher XS-inferred migration rate may have been inflated by XS surveys not being evenly distributed through time, as relatively few measurements after 1998 underrepresented this slower-moving period. Additionally, more measurements after 1998 would have increased the sample size for longer time intervals (Appendix Table 7.6), increasing their contribution to the regression equation and moving the slope of the linear model even closer to that measured in APs.

Table 3.2. Values and 95% confidence intervals of the slope (migration rate) and intercept from linear models of channel migration from different datasets and periods. AP = air photo, XS = cross-section, TS = transect.

Dataset	Complete or subset of data	Standardized to whole reach?	Period	Migration rate (m/yr)	Migration rate 95% CI (m/yr)
AP – continuous	complete	NA	1939-2013	1.52	1.28 – 1.77
AP at XSs	subset	no	1939-2013	1.68	1.44 – 1.92
AP at XSs	subset	no	1939-1973	2.46	1.51-3.41
AP at XSs	subset	no	1978-2013	0.63	0.30 - 0.96
AP at TSs	subset	no	1939-2013	3.34	3.06-3.63
XS – centerline	complete	yes	1975-2014	0.81	0.76 – 0.85
XS – cutbank	complete	yes	1975-2014	0.88	0.82 – 0.94
TS	complete	yes	1830-2014	1.62	1.56-1.68
TS	subset	yes	1939-2013	1.72	1.56-1.88

In a second cross-method comparison, I matched the complete AP record by isolating the 101 cottonwoods whose ages indicated establishment between 1939 and 2013. The regression slope describing channel migration from these trees was 1.72 ± 0.16 m/yr, similar to the 1.52 ± 0.24 m/yr rate from the APs measured only at TS locations. Thus, for both between-method comparisons, both methods yielded similar channel migration rates and supported between-method comparisons.

In contrast, direct comparison of migration rates for individual calendar years of overlapping data showed APs migration rates greater than those from XSs and TSs. AP migration rates were 57% and 59% greater than those from XSs and TSs, respectively. Similar overestimates of XS and TS migration rates, coupled with high confidence in the precise XS measurements, suggests that AP migration rates were biased high.

Rates through time

The AP, XS, and TS datasets all show that Powder River channel migration has slowed over the last century (Fig. 3.5). The TS data had maximum migration following the 1923 flood, peaking around 5 m/yr in the 1920s and 1930s. Given the extreme magnitude of the 1923 flood (3,000 m^3/s), the known planform effects of the large 1978 flood (960 m^3/s) [*Moody and Meade*, 1990; *Gay et al.*, 1998], and a newspaper report from the time [*Powder River County Examiner*, 1923], I assume that the flood widened the channel and deposited sediment on the floodplain. These processes would facilitate subsequent channel narrowing and cottonwood establishment. The apparent increase in TS-inferred migration rate since the year 2000 is a spurious result caused by herbivory that suppressed cottonwood growth.

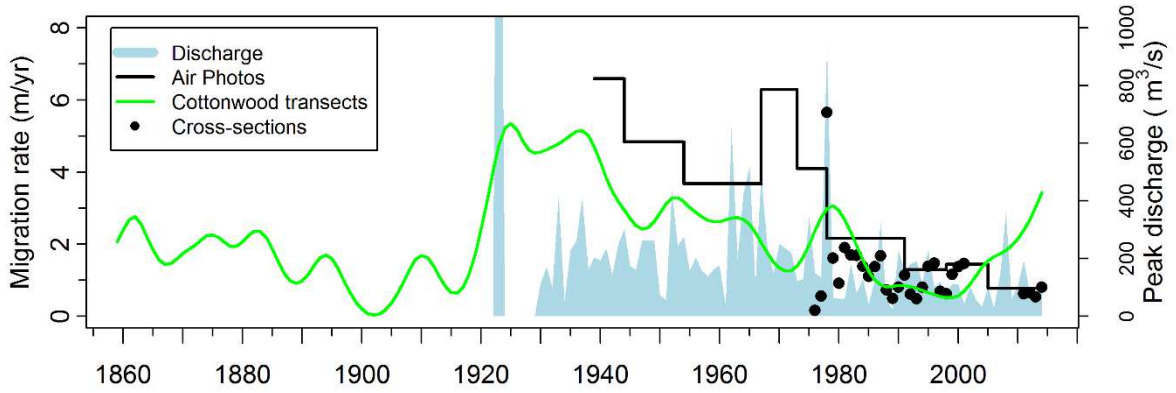

Figure 3.5. Channel migration rates through time for the Powder River study reach. Continuous discharge measurements (blue) began in 1930, but the 1923 peak flow is documented as 3,000 m^3/s (value surpasses axis extent). Circles are for channel centerline migration rate from all cross-sections measured in consecutive years. The air photo line (black) is the centerline migration rate between consecutive photos. The cottonwood transect migration line (green) is a point bar migration spline calculated from tree ages, which is smoothed to better depict uncertainty associated with lags between floodplain surface ages and tree ages (Appendix Table 7.7). The number of trees establishing was inversely weighted by the number of transects with trees as old or older than a given year because some transects only included relatively young surfaces. Results were truncated at 1860 because of decreasing number of transects having data farther back in time.

AP and XS analyses also revealed decreasing migration rates through time (Fig. 3.5). The maximum migration rate between APs was 6.59 m/yr for 1939-1944, the period closest to the 1923 flood. Similar migration rates were found for 1967-1973, a period in the middle of the record. This fast channel centerline migration period was largely caused by channel narrowing from 117 to 77 m that occurred after four ≥ 14-year floods from 1962-1967. Over the entire AP period, the general trend was a decline in channel migration rate through time. AP-inferred channel migration was < 1.5 m/yr in all three inter-photo periods after 1991, culminating at 0.77 m/yr from 2005-2013 (Table 3.1; Fig. 3.5).

A general decline in migration rate also occurred in XS measurements. 1978 migration was highest, and each of the three most-recent years (2012-2014) had among the slowest

migration (Fig. 3.5). As a whole, AP and TS data indicate that the XS measurements from the past four decades do not represent longer-term averages.

Calculations of annual channel migration rate depend on measurement interval. The XS measurements revealed increasing migration up to an interval of 23 years between measurements, where total migration distance unexpectedly plateaued and annual migration rate decreased (Fig. 3.4). One possible explanation is the inability of this analysis to disassociate longer intervals from their chronological occurrence. While the 1-year measurements were scattered through the XS record, all 39-year intervals necessarily characterized changes from 1975-2014. XS and AP data revealed little channel migration after 1998, but all XS intervals spanning ≥ 23 years necessarily include a measurement in or after 1998, which may contribute to the decreasing migration rates at longer intervals.

Over the 1939-2014 AP period, channel migration destroyed 24.8% of the 50-year floodplain, leaving 75.2% of the land surface intact. I fit an exponential decay function to the data to identify a floodplain half-life (i.e., the period when half of the floodplain is lost to the river) and to assess the null model that all areas of the floodplain have an equal chance of being destroyed in each year. The calculated half-life was 178 years, but the data had a biased fit to the model. The cumulative area occupied by the channel increased rapidly in the first 39 years of the AP record before leveling off over the next 35 years (Fig. 3.6). The reduction in turnover rate leaves the AP period poorly equipped to extrapolate the multi-century-scale process of floodplain turnover.

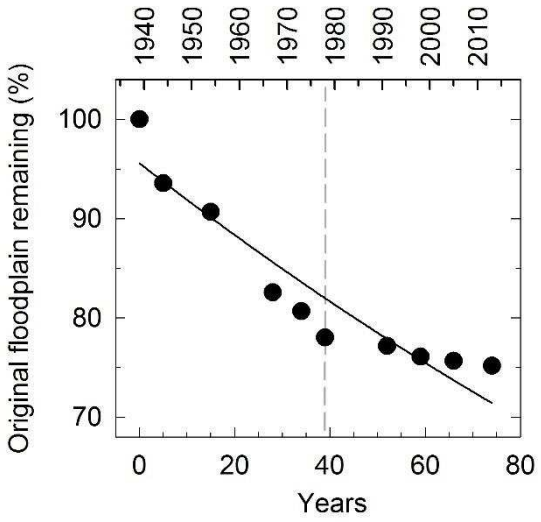

Figure 3.6. Percent of 1939 floodplain remaining in each photo year through 2013. The black line is an exponential decay function ($y = 95.59*e^{-0.0039*x}$) that suggests the floodplain half-life is 178 years, but the fit illustrates that Powder River floodplain turnover did not conform to the exponential model over the air photo period. Gray dashed line is the 1978 flood.

Channel migration rate was most highly correlated to flows with low exceedance probabilities (i.e., high flows), and relationships slightly differed for XSs and APs. For XSs, migration rate was best correlated to the discharge having 0.005 exceedance, or the second highest flow day of a year. Cutbank migration was more strongly predicted by this discharge compared to centerline migration (r = 0.98 vs. 0.87; Fig. 3.7). The XS calculations for flows of low exceedance probability were dominated by 1978, and this large flood strongly influenced the correlations.

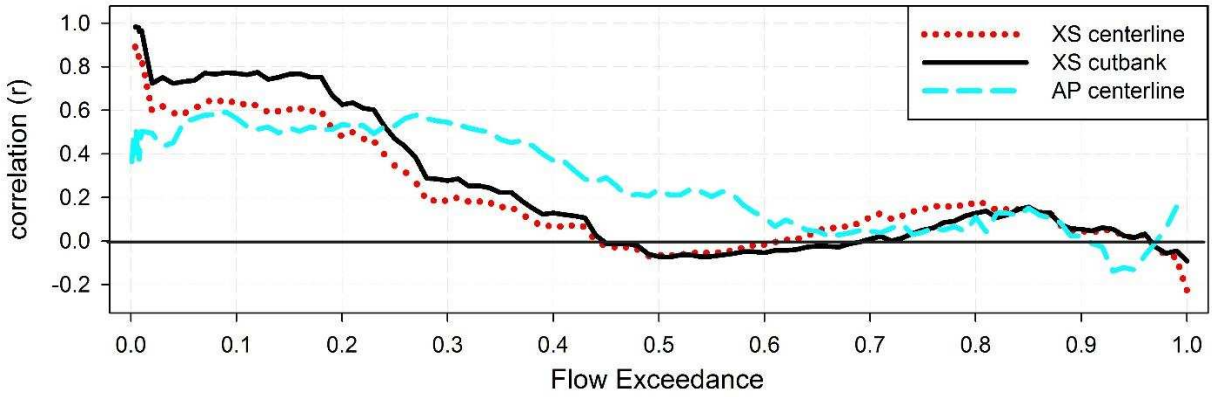

Figure 3.7. Correlation between channel migration and flow exceedance probabilities within each measurement period. Cross-section data are shown for both cutbank (black solid line) and centerline (red dotted line) migration. Air photo (turquoise dashed line) data describe centerline migration between photos.

AP analysis characterized centerline migration over a longer period and had weaker correlations to discharge compared to XSs (Fig. 3.7). Correlation peaked at $r = 0.59$ for a flow exceedance of 0.09, which corresponded to the 33rd highest flow day in a year. This analysis showed that above-average flows were more closely related to channel migration compared to below-average flows, but it did not identify the highest < .01 proportion of flows as most influential, unlike the XS analysis and Miller and Friedman's [2009] AP analysis of the Little Missouri River.

Because the extreme 1923 flood could have affected channel migration patterns for decades thereafter, I introduced time as a secondary variable to combine with measured flow. I conducted a multiple regression using both time since 1923 and inter-photo flows, finding that the model correlation increased from 0.59 to 0.75 ($r^2_{Adj.}$ = 0.26 to 0.41). The longer time interval and more even distribution of flood peaks in the AP record compared to the XS record reduced the influence of the 1978 flood, which was the largest flood in both records. Any correlations

below 0.4 were considered weak, and there were no cases of below-average flows with more than weak correlations to channel migration.

3.4.2 Assessing methodological uncertainties

Linear models were created to describe channel migration rates because they provided easily interpretable comparisons across methods and periods. Prominently, the slope of each model represented migration rates (Fig. 3.8). Consistent with other analyses, the analysis identified the recent XS dataset to have the slowest migration rate (0.81 ± 0.05 m/yr, 95% confidence interval included) when considering the entire duration for each record. In contrast, the AP (1.52 ± 0.24 m/yr) and TS (1.62 ± 0.06 m/yr; Fig. 3.8; Table 3.2) migration rates were faster and not significantly different from each other ($z = 1.18$, $p = 0.24$).

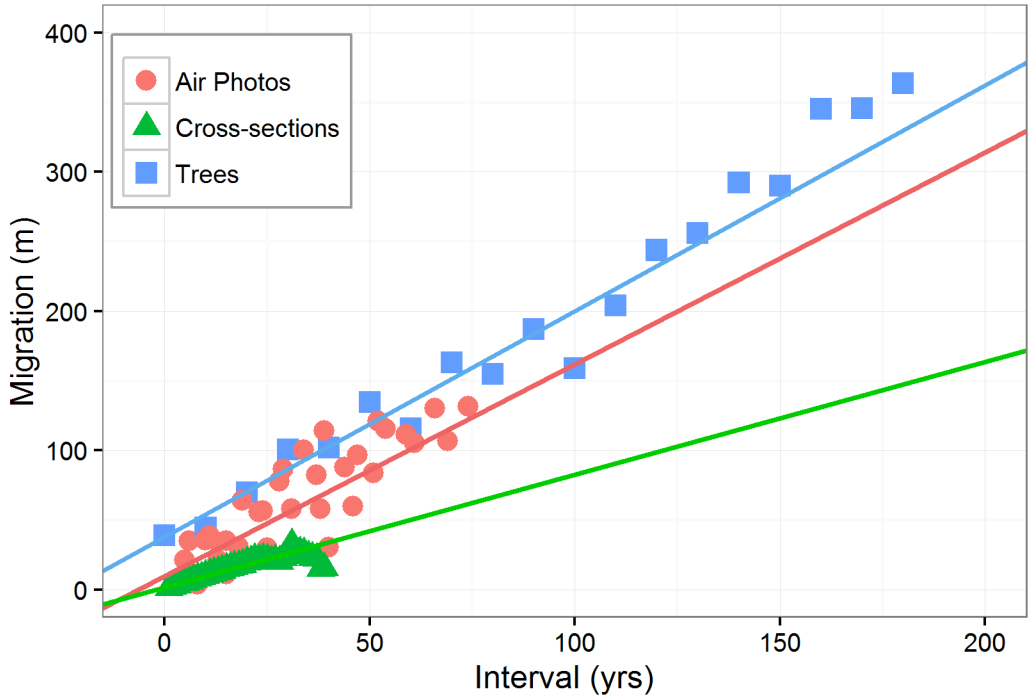

Figure 3.8. Channel migration rates over the measurement periods for cottonwood transects (1830-2014), air photos (1939-2013), and cross-sections (1975-2014). Each point displays the average migration distance for all measurements for a given time interval between them (x-axis). Lines are the linear models for each dataset. Slopes of lines using data from trees and air photos are not statistically different but they are both greater than that from channel cross-sections. Time interval for trees is the difference between ages, which are rounded to decade-intervals for display. Note that the best-fit line for cottonwood trees deviates from the graphed points at longer intervals because the line was calculated from each pair of trees (i.e., not the decadal groups that are displayed), and sample size was small at large intervals.

For each dataset, the y-intercepts of regression models were positive, suggesting that migration occurred without any time passing. This impossibility reflects methodological uncertainties. For XSs, the best-fit line is greater than zero partly because back-and-forth migration is missed as measurement interval increases. This reduced the migration distance at longer intervals and increased the y-intercept. For APs, the positive y-intercept could have resulted from imprecise photo georectification, difficulty identifying the channel banks in photos, and variable intervals between photosets. The TS intercept was influenced by cottonwood recruitment processes. Instead of trees establishing immediately and reliably in

narrow bands after decimeter-to-meter-scale annual migration, successful recruitment may only occur every several years [*Scott et al.*, 1997; *Friedman and Lee*, 2002]. Cottonwood recruitment is dependent on ideal conditions related to light availability, soil moisture, rate of water table decline, and subsequent floods [*Mahoney and Rood*, 1998; *Benjankar et al.*, 2014]. Therefore, pulses of recruitment occur, which can lead to even-aged bands tens of meters wide that are generally oriented perpendicular to the channel [*Merigliano et al.*, 2013]. This pattern was evident at the Powder River where consecutive trees on a TS belonged to the same cohort.

3.4.3 Channel profile and planform evolution

Flows on the Powder River changed between the pre- and post-1978 flood years (1930-1977 vs. 1979-2015). Although mean annual discharge has decreased by only 9% (12.9 vs. 11.7 m^3/s), the median peak annual flow decreased by 48% (201 vs. 104 m^3/s). Additionally, the planform geometry of the Powder River changed over the AP record. Between 1939 and 2013, a gradual increase in sinuosity from 1.55 to 2.01 corresponded to a decrease in slope and width (Fig. 3.9, Appendix Table 7.8). The length of the channel increased from 57 to 75 km, and slope declined proportionally from 0.0012 to 0.0009. Channel length, slope, and sinuosity maintained a consistent trajectory throughout the photo record except for a minor reversal after the 1978 flood. Peak discharge of the 1978 flood was 1.43 times greater than any other during the AP record and 2.60 times greater than any after. The flood temporarily shortened and widened the channel, which is consistent with previous research of large floods with high sediment loads in Great Plains rivers [*Schumm and Lichty*, 1963; *Nadler and Schumm*, 1981; *Moody et al.*, 1999].

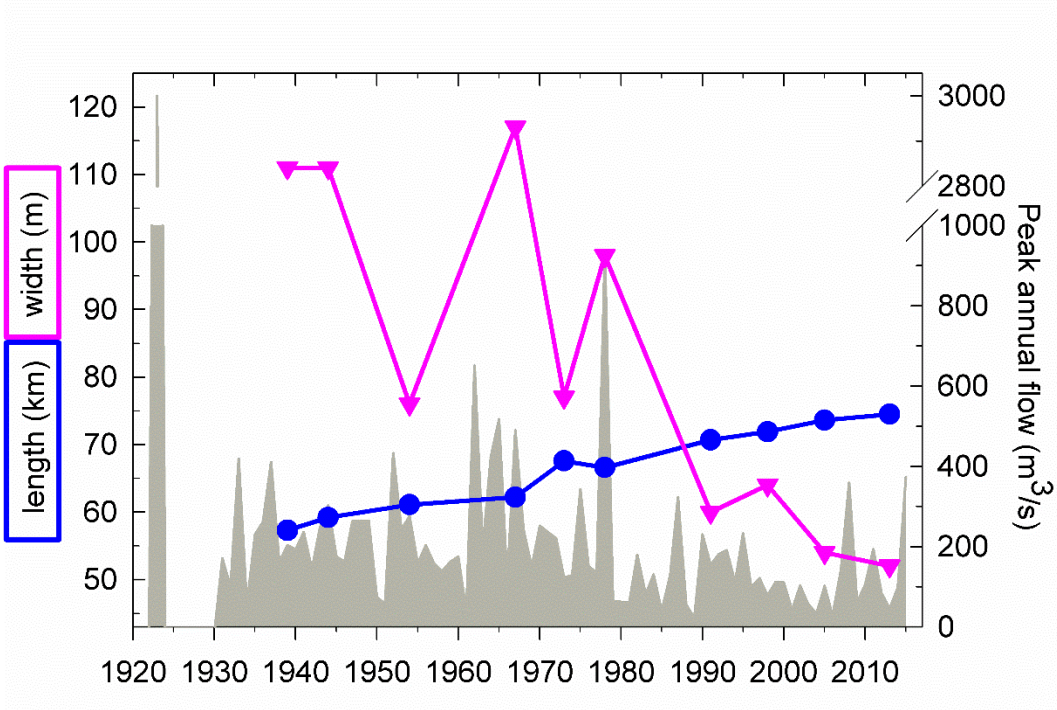

Figure 3.9. Channel length (pink, triangles) and width (blue, circles) throughout the air photo record. Peak annual flow (gray) is included. Channel sinuosity increased and slope decreased in proportion with channel length.

3.4.4 Cottonwood population dynamics

Powder River cottonwoods provided nearly a two-century perspective on channel migration. Tree ages were used as proxies for the age of the underlying surfaces that were formed by channel migration. Tree ages ranged from 0 (tree present, but lower than sampling height) to 184 years. Tree ages increased with distance from the channel (r^2 = 0.83 after square root transformation to stabilize variance; Fig. 3.10). Age distribution suggested that establishment conditions differed after the two largest floods of the last century, in 1923 and 1978. While tree establishment remained high for two decades after the 1923 flood, the pulse of establishment after the 1978 flood was limited to the four years after the flood (Fig. 3.11).

Few trees dated to soon before each flood, likely because the floods killed or sheared the young trees growing near the channel.

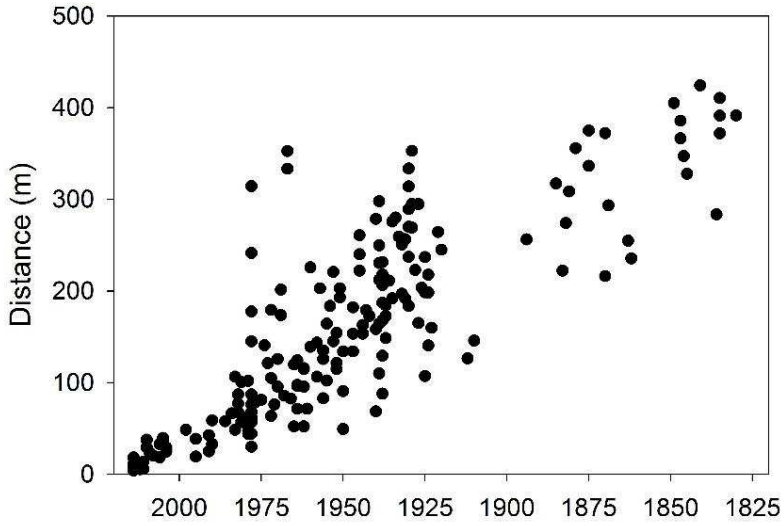

Figure 3.10. Distance from the channel as a function of first year of tree growth. Wider point distributions after 1923 and 1978 represent widespread post-flood recruitment. r^2 = 0.83 for a linear model after performing a square root transformation on the x-axis to stabilize variance.

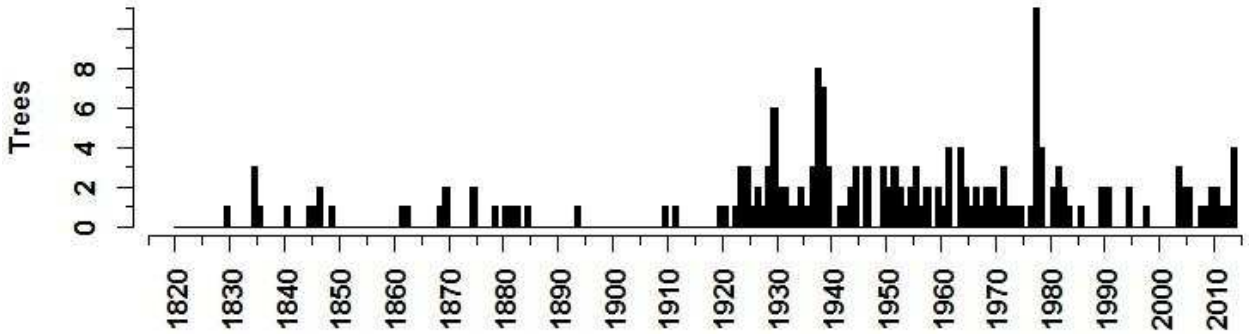

Figure 3.11. Unadjusted establishment dates for all trees sampled on the cottonwood transects. Groups of trees established after the 1923 and 1978 floods.

Eighty-three of the 189 sampled cottonwoods were located within the zone that transitioned from channel to floodplain during the AP record (Fig. 3.3). If tree age was the same as that of the underlying surface, all trees would have aged to between the two bounding photo years. However, median tree age lagged 8.5 years behind the middle year between the photos, with the interquartile range being a 5-13 year lag (Fig. 3.12). The small median lag and narrow range support the hypothesis that tree establishment was generally limited to point bars. These results closely resemble the 7.3-year lag for cottonwood at the nearby Little Missouri River (J. Friedman, *unpub. data*) and the 5-year lag between germination point and ground surface at the Missouri River [*Scott et al.*, 1997]. Possible mechanisms for the time delay at the Powder River include: not every year are conditions favorable to seedling germination and growth [*Benjankar et al.*, 2014]; resprouted trunks were aged if young trees were knocked down by floods, ice jams, or beavers; and browsing by deer and livestock delayed a tree's permanent arrival to sampling height. A range of lags was found because each tree has a unique history, and the complete dataset provided a broader perspective on cottonwood recruitment in relation to channel migration.

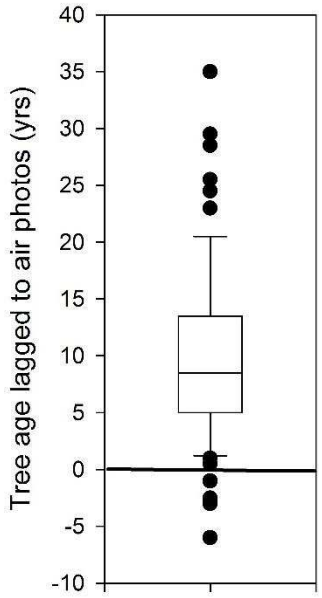

Figure 3.12. Tree ages (n = 83 trees) displayed as a lag from the middle year between the two bounding air photos (i.e., the last photo where the tree's location was within the channel and the first photo where the location was floodplain). Black line at time = 0 is where tree age equals the middle year between photos, and positive numbers mean trees were younger.

3.5 Discussion

I integrated three research approaches to document variable channel migration rates on the Powder River since 1830. Combining multiple datasets overcame two problems common to fluvial geomorphic research. The first is that it is difficult to characterize the processes driving channel migration because of the long and variable spatial and temporal scales at which migration occurs. The XS, AP, and TS data spanned spatial and temporal scales to provide nested views of migration. Combining approaches enabled assessment of each, thus providing a fuller perspective than possible with independent datasets. For example, the high frequency of XS measurements enabled quantification of the migration missed for multi-year measurement intervals, such as is common in AP records. Second, I also overcame the common problem of applying data collected from discrete locations to a larger reach. This problem arises when

sampling locations are chosen non-randomly, such as may occur because of site access. To account for this, the spatially continuous APs were used to identify the relative magnitude of channel migration over the AP period for three locations: at XSs, at TSs, and averaged over the entire reach. These data enabled standardization of channel migration to the entire reach from all datasets.

The Powder River's trend of decreasing migration and width through time is consistent with other rivers in the region [*Nadler and Schumm*, 1981; *Miller and Friedman*, 2009; *Merigliano et al.*, 2013]. The river transitioned from relatively wide and straight to narrow and sinuous. This pattern has occurred to a more extreme degree in smaller and more arid watersheds [*Wolman and Gerson*, 1978], which are not snowmelt-dominated systems. Research in Kansas describes the small Cimarron River starting as a single-thread meandering river with vegetated banks [*Schumm and Lichty*, 1963]. The sequence of floods, growing season precipitation, vegetation colonization, channel narrowing, and floodplain formation caused it to transition to multi-threaded before returning to a single-threaded sinuous form. On the Powder River, interacting pressures also appear to have affected channel migration over decadal-to-century scales. The entire AP record on the Powder River demonstrates a transition to a more vegetated narrower channel (Fig. 3.13). This may be a response to the largest flood in 1923, which likely straightened and widened the river [*Powder River County Examiner*, 1923], providing abundant bare sediment on the floodplain for plants to colonize. Smaller (1-in-14 to 1-in-33 year floods) in the early 1960s may have prolonged the straighter channel planform.

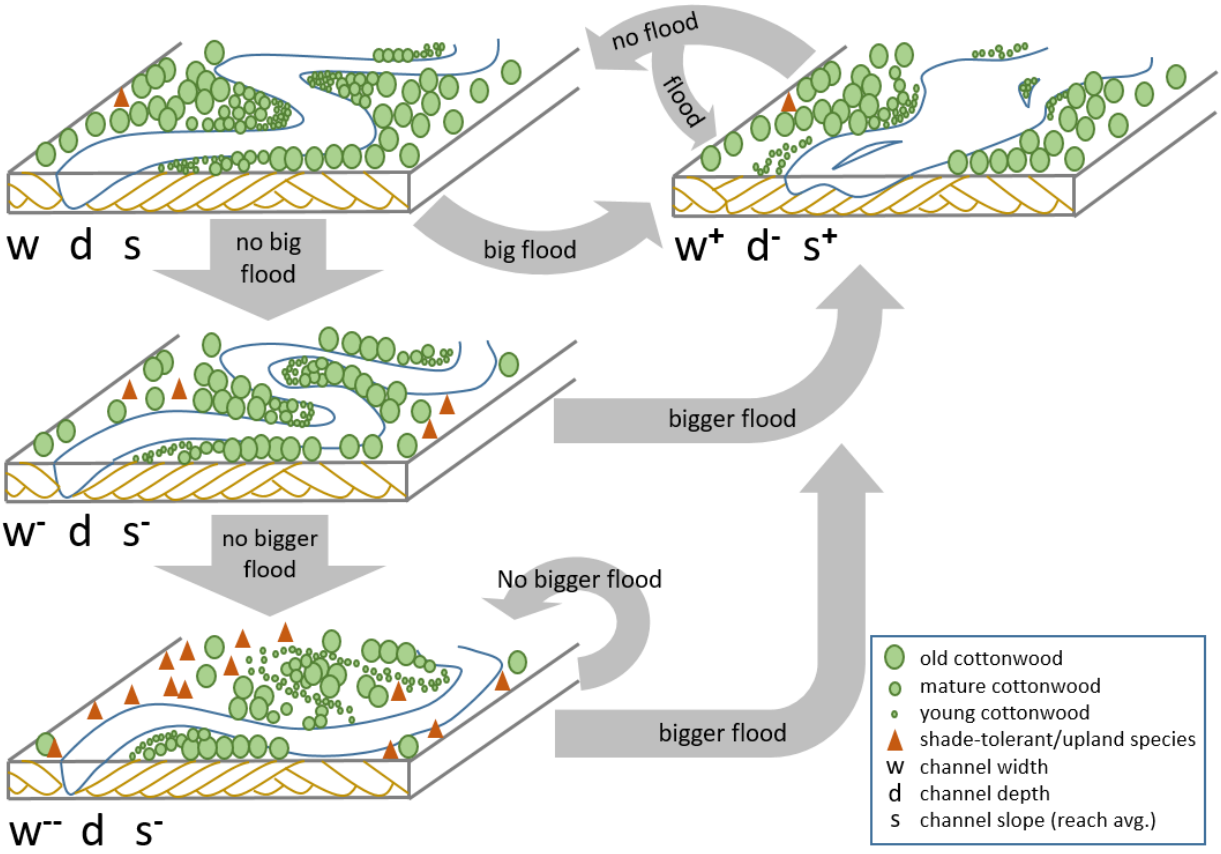

Figure 3.13. Conceptual model of the evolution of the Powder River. Changes in channel width (w), depth (d), and slope (s) are relative increases (+) or decreases (-) from that of the baseline sinuous river. Big floods play a critical role in changing river planform, re-working floodplain surfaces, and promoting heterogeneous floodplain forests. Without big floods to rejuvenate the fluvial system, channel migration slows, channel complexity decreases, cottonwood recruitment decreases, and shade-tolerant and upland species replace cottonwood forests.

Less channel migration in a free-flowing river indicates that changes in climate, land use, or water management have affected the balance between driving and resisting forces. A climate shift has decreased snowpack in the Northern Rocky Mountains [*Pederson et al.*, 2010], and caused earlier snowmelt discharges [*Stewart et al.*, 2005]. Peak flow has also decreased at the nearby Redwater and Little Missouri Rivers, whose watersheds are low in elevation and are

unaffected by mountain snowmelt [*Griffin et al.*, in revision, *Merigliano et al.*, 2013]. Both of these rivers have experienced little flow regulation, and changes in flows have been linked to increases in temperature and evapotranspiration. Powder River flows reflect characteristics of mountain and plains rivers because the flow regime is snowmelt-dominated but most of the watershed is in the Great Plains. Besides climate changes, channel narrowing and decreased migration can be caused by damming [*Shafroth et al.*, 2002], exotic plant invasion [*Birken and Cooper*, 2006], re-growth of native forest [*Erskine et al.*, 2012], and gravel mining [*Dufour et al.*, 2015]. However, none of these mechanisms appears to dominate on the free-flowing Powder River. Although invasive Russian olive trees have expanded in the reach since the 1940s, tree density is higher in the downstream portion of the reach where the channel migration is greater.

People of European descent began to colonize the Powder River watershed in the late 19th century, and changing land uses could have affected planform geometry and channel migration. Powder River headwaters are in the Bighorn Mountains, which have experienced periods of heavy livestock use (peaking in the 1890s), tie drives (1890s – 1910s), clearcutting (peaking in 1960s), and forest fire (peaking in 1920s, although data are for post-1910) [*Winters et al.*, 2004]. Each of these processes could increase sediment load to the Powder River, pushing the river toward the wider and less-sinuous geometry characteristic of the earlier parts of the AP period. Land uses within the Powder River floodplain have evolved through time as well. Homesteaders colonized the Powder River floodplain at the start of the 20th century. Results suggested very little channel migration in the 20th century before the 1923 flood, but

the arrival of the homesteaders and their cottonwood-foraging livestock could have coupled with the destructive flood to leave few surviving young trees.

Because geomorphic processes can respond to extreme floods over decades, river measurements reflect flow history. The chronology of channel migration through time I documented was heavily influenced by large floods in 1923, 1962-1967, and 1978, and cottonwood establishment dates reflected this. The 1978 flood has been recognized as the catalyst for many Powder River changes over the past four decades [*Gay et al.*, 1998; *Moody et al.*, 1999; *Moody and Meade*, 2008, 2014; *Meade et al.*, 2013]. The flood widened the channel, which facilitated bench formation, vertical and lateral accretion, and channel narrowing [*Pizzuto*, 1994; *Moody et al.*, 1999]. These processes deepened the channel and raised the floodplain, which increased the flow magnitude required for overbank flows by a factor of 3.7 between 1978 and 1996 [*Moody et al.*, 1999]. The 1923 flood was three times larger than that of 1978 and may have catalyzed responses that persisted throughout the AP period. It is unclear exactly how the channel migration patterns documented in the 1939-2013 AP record were affected by one extreme flood in 1923 or a general tendency toward decreasing peak flows. What is clear is that XS, TS, and AP records show patterns consistent with those from rivers responding to large floods, and these pulse disturbances can affect channel migration for decades thereafter. It is possible that the entire evolution in channel planform in the AP record has been driven by the 1923 flood.

Although the concept of a floodplain half-life has been effectively used as a null model to describe floodplain turnover [*Gottesfeld and Gottesfeld*, 1990; *O'Connor et al.*, 2003], two assumptions within the exponential decay model are that all locations are equally likely to be

destroyed in a given year and floodplain destruction rate is constant through time. However, rates differ under variable runoff and climate periods, and meandering rivers move away from point bars, preferentially destroying old floodplain [*Hickin and Nanson*, 1975]. Empirical and modelling efforts have shown fluctuations in channel width that cause preferential destruction of young floodplain [*Nakamura and Kikuchi*, 1996; *Miller and Friedman*, 2009; *Konrad*, 2012], and numerical modeling has shown the active meander belt to occupy a limited width close to the modern channel within the floodplain [*Xu et al.*, 2011]. Some areas of floodplain may be protected from erosion by large clasts, log jams, cohesive sediment or valley position [*O'Connor et al.*, 2003; *Wohl*, 2013]. I determined a floodplain half-life that was calculated from planform evolution over the AP record. However, this value is inherently unstable because of hydroclimatic changes, human impacts, and floods with prolonged effects. Changing pressures and lagged effects are widespread across rivers, so floodplain turnover rates calculated for any river should be cautiously interpreted.

Channel centerline migration is a function of erosion and deposition, but these processes are driven by different flows. Although erosion is commonly caused by high flows, deposition has been shown to be inversely correlated to the magnitude of low flows on the Little Missouri River [*Miller and Friedman*, 2009]. The XS and AP analyses used centerline migration because AP centerlines were continuous throughout the reach. However, because centerline was calculated from both banks, its location was dictated by erosion and deposition. I extracted the subset of XSs having a clear cutbank to quantify differences between migration from centerlines and cutbanks, and cutbank migration was more strongly correlated to high flows. The second highest between-photo migration rate unexpectedly occurred in 1967-1973,

a period when channel width reduced by 34% following four of the five largest floods in the gage record. Preferential narrowing from one bank was likely responsible for much of the documented channel migration. The cottonwoods did not concurrently reflect this high migration period, but instead their ages peaked a decade later (Fig. 3.5). A possible explanation for the offset is the delay I documented between AP-determined surface creation and TS-determined tree ages. Alternatively, the TS-inferred migration peak in the late 1970s may have mostly resulted from the 1978 flood, which likely promoted cottonwood germination and knocked down trees whose resprouts were aged.

Calculating annual migration rates from data collected over longer intervals is susceptible to systematic errors, and researchers have acknowledged potential underestimates of annual channel migration rates when using APs with multi-year intervals [*O'Connor et al.*, 2003; *Miller and Friedman*, 2009]. I examined biases imparted when unequal and multi-year intervals are analyzed by using the exceptionally long XS dataset to quantify reductions in annual migration rate over various intervals. Annual migration rates were underestimated between 17-46% for intervals ranging from 3-29 years, intervals that have been used in previous air photo channel analyses [*Cadol et al.*, 2011; *Dean et al.*, 2011; *Miřijovský et al.*, 2015]. The empirical values I identified result from site- and time-specific conditions, however, and values will vary across time and rivers.

Directly comparing channel migration rates for a given year between methods showed APs to indicate faster migration than XSs and TSs. Each method contains uncertainties that obscure identification of the true migration rate, uncertainties that the three-method approach helped to detect. For example, under the scenario in which no migration occurs, APs are likely

to indicate some migration due to errors in georectification and the researcher's ability to consistently identify channel boundaries in photos with variable spectral qualities, river discharges, and vegetation patterns. These errors should be inconsequential at large spatial scales when the actual migration distance exceeds error magnitude, because the errors would be equally likely to over- and under-predict migration distance. Researchers have attempted to deal with some of these errors (CITE), and proper quantification of them should improve migration calculations and increase cross-method compatibility. AP analyses remain useful independent of complementary XS or TS datasets, but the accuracy of their migration rates should be further explored. Recent advancements in frequently collected high resolution satellite imagery should allow similar approaches to be applied to larger scales to more broadly characterize channel migration and better assess various measurements.

Riparian tree establishment is a combined response to climate, river flows, and the surfaces created from interactions between flows and vegetation [*Wilcox and Shafroth*, 2013]. I sampled cottonwoods from healthy, multi-aged forest stands on the Powder River that were located on meander bends that migrated at 3.34 m/yr from 1939-2013 (this rate is pre-standardization to the reach). Although not sampled, straight reaches and meanders with slower migration appeared to have fewer and older trees. Cottonwoods can establish from channel narrowing, meandering, and flood deposition within a site [*Cooper et al.*, 2003a], but the relative influence of these processes varies predictably across settings [*Scott et al.*, 1996]. For example, most cottonwood recruitment on the Missouri River floodplain constrained by the Missouri Breaks, Montana, was associated with overbank deposition from large floods [*Scott et al.*, 1997]. However, farther downstream and in other Great Plains rivers, cottonwoods

established from channel narrowing caused by flow regulation [*Friedman et al.*, 1998; *Dixon et al.*, 2012]. Spatial patterns of sampled tree ages at the Powder River suggested establishment through channel migration and narrowing. The high tree recruitment in the 1920s and 1930s occurred during a period of moderate floods on a channel that had been straightened and widened by the 1923 flood [*Powder River County Examiner*, 1923]. This combination of geomorphic and hydrologic conditions facilitated channel migration and tree establishment, which would in turn stabilize point bars, narrow and deepen the channel, and focus flow energy on erodible cutbanks.

Cottonwood ages indicate that a period of low channel migration was followed by high migration after the 1923 flood. However, the 1923 flood could have killed young cottonwoods [*Friedman and Lee*, 2002] that established in the early 1900s, precluding surface dating with them. Alternatively, young trees may have been knocked down in the flood before resprouting [*Sigafoos*, 1964], a phenomenon observed in the field. The resprout scenario was not widely captured in the sample, however, because only six trees dated to within the two years after the 1923 flood. The flood likely aggraded the channel and lowered the flow magnitude required for floodplain inundation, as occurred after the 1978 flood [*Moody et al.*, 1999]. Additionally, an even larger flood may have occurred in 1887 [*Powder River County Examiner*, 1923]. Although I did not detect a pulse in cottonwood establishment after the 1887 flood, a Powder River flow reconstruction identified 1887 as the third wettest year since 1830 [*Schook et al.*, 2016b] and a Yellowstone River flow reconstruction identified it as the 6th largest flow year since 1706 [*Graumlich et al.*, 2003].

These research findings can inform land and waters management. First, in demonstrating that Powder River cottonwoods establish from channel migration and point bar formation, results suggest a loss of native floodplain forests if dynamic flooding flows do not continue. Across the West, a general transition from floodplain cottonwood forests to invasive, shade-tolerant, and upland species is occurring [*Merritt and Cooper*, 2000; *Friedman et al.*, 2005b; *Andersen et al.*, 2007; *Merritt and Poff*, 2010], and flow regime preservation on free-flowing rivers has the greatest chance to resist region-wide habitat loss. I found an 8.5 year lag between floodplain formation and cottonwood establishment on Powder River point bars from 1939-2013, but evolving conditions will modify this relationship. Along one sampled TS (at PR163), the first 70 m from the river had few cottonwoods and none that escaped browse level, even though 50 m of the length had been floodplain since at least 1991. A possible mechanism explaining the decreased cottonwood recruitment is that slow channel migration enabled establishment of a relatively small number of cottonwoods, whose growth has been suppressed by browsing from deer, beaver, sheep, and cattle. Similar suppression has occurred in Wyoming's Yellowstone National Park, where extreme floods with major cottonwood recruitment are required for seedlings to escape bison and elk herbivory [*Rose and Cooper*, 2016].

Many rivers are dammed, and managers often remove the highest flows because they threaten property and replenish reserves. However, a consequence of this action is a decrease in channel migration, floodplain sedimentation, and replacement of old cottonwoods. If not wisely managed, climatic and anthropogenic flow modifications may induce cascading effects

including riverine habitat loss due to vegetation encroachment, replacement of cottonwood forests, and decreases in habitat complexity and biodiversity.

3.6 Chapter Synthesis

All data suggest that Powder River channel migration has decreased, and the recent history (1978-2014) is not representative of fluvial geomorphic processes from the past two centuries. Even though the Powder River is predominantly a snowmelt-dominated river where variability of interannual floods is relatively low, the largest two floods were caused by a frontal storm and a rain-on-snow event. Both floods induced years-to-decades of channel responses. The periods of highest channel migration were in the two decades following the 1923 flood and in the decade following floods in the early 1960s. The relatively small peak annual flows from the past three decades correspond to a gradual reduction in channel migration rate since the 1920s, which has led to migration occurring half as fast during the XS period compared to the longer AP and TS periods.

This study can inform the selection and interpretation of research methods in fluvial geomorphology. Findings from the Powder River can aid in interpretation of channel migration across geographic and hydroclimatic settings. Direct comparison of the three approaches revealed that even four decades of highly repeated and highly precise cross-sectional surveys may not fully characterize the century-scales over which channel migration occurs. Additionally, aerial photos are often used alone to describe channel migration rates, but they may bias true annual migration rates because of errors in georectification, difficulty in consistent identification of channel boundaries, and the inability of multi-year intervals to detect back-and-forth channel migration. Annual migration rates are commonly the standard when

assessing geomorphic processes, but converting measurements taken at multi-year intervals to an annual rate should be conducted with consideration of the spatial and temporal scales at which the process varies. Ultimately, fluvial geomorphic processes are affected by multi-layered, complex, and delayed responses induced by flows, climate, and land uses. Therefore, channel migration results from interacting processes across a wide range of scales within the watershed, and integrating multiple research approaches can build a stronger understanding of the processes causing migration.

4. SPATIAL AND BIOLOGICAL VARIATION IN PLAINS COTTONWOOD (*POPULUS DELTOIDES* SUBSP. *MONILIFERA*) TREE RING RELATIONSHIPS TO RIVER FLOW AND CLIMATE

4.1 Introduction

Trees catalog environmental conditions in annual growth rings that can persist for centuries. Deciphering variations in these rings has produced much of the modern understanding of climate changes [*Fritts*, 1976; *Jones et al.*, 2009; *St. George*, 2014]. In most tree ring width studies, tens to hundreds of tree cores are combined into a single chronology, and multiple chronologies may be integrated to reconstruct climate or flow [*Woodhouse et al.*, 2006; *Cook et al.*, 2013]. These population-based approaches amplify the common signal across trees by removing individual-level growth patterns thought to be unrelated to the climatic factors of interest. However, the noise contained in tree rings is not random. By combining cores to create population-level indices, potentially valuable information affecting only some of the individuals is lost [*Ettl and Peterson*, 1995; *Rozas and Olano*, 2013].

The individual tree is the fundamental level at which forests integrate environmental conditions [*Smith*, 2008; *Rozas and Olano*, 2013]. For example, tree sensitivity to growth-limiting climate conditions can increase [*Carrer and Urbinati*, 2004; *Yu et al.*, 2008] or decrease with tree age [*Vieira et al.*, 2008; *Rozas et al.*, 2009] depending on local setting and species-specific physiology [*Rozas and Olano*, 2013]. In dioecious species, male and female trees can differ in water use efficiency [*Leigh and Nicotra*, 2003; *Hultine et al.*, 2013], sensitivity to variation in rainfall [*Rozas et al.*, 2009], and radial growth response to hydroclimatic conditions [*Rood et al.*, 2013]. Biological response is also affected by extrinsic factors creating each tree's

microclimatic, geomorphic, competitive, and resource settings. Tree radial growth can be sensitive to topographic position [*Oberhuber and Kofler*, 2000], elevation [*Zhang and Hebda*, 2004], soil water regime [*Pelfini et al.*, 2006], and soil nutrient content [*Sheppard et al.*, 2001]. One place where resource access varies at small scales is in floodplain forests [*Hughes*, 1997; *Naiman et al.*, 2005].

Rivers and their floodplain environments are some of the most productive, biodiverse, and heterogeneous environments on the landscape [*Ward et al.*, 1999; *Tockner and Stanford*, 2002; *Naiman et al.*, 2005]. Riparian trees form the structural backbone of these forests. In dry regions, floodplain trees rely on groundwater linked to the river through the alluvial water table [*Scott et al.*, 1999; *Amlin and Rood*, 2003]. Dendrochronologic study at the tree-level may reveal factors that promote tree vigor that can be used to inform water and land management.

Populus species are common to rivers throughout the northern hemisphere, and plains cottonwood (*P. deltoides*) is the most common native tree along rivers in the western Great Plains, USA [*Friedman et al.*, 2005b]. Plains cottonwoods establish from overbank flows [*Scott et al.*, 1997; *Amlin and Rood*, 2003; *Cooper et al.*, 2003a], often germinating in very high densities on flood-deposited sediment. Cottonwoods are shade intolerant and grow quickly to outcompete neighbors for sunlight [*Braatne et al.*, 1996]. Cottonwood growth is limited by flow magnitude [*Edmondson et al.*, 2014; *Meko et al.*, 2015; *Schook et al.*, 2016b], and trees can die without river water [*Albertson and Weaver*, 1945; *Scott et al.*, 2000; *Rood et al.*, 2003]. In the western Great Plains, cottonwoods are drought-sensitive species [*Tyree et al.*, 1994] living in a semi-arid landscape, so they rely on streamflow. Water and nutrient access varies greatly across river floodplains. Changes to the river channel have been shown to kill some trees while

having undetectable effects on others [*Scott et al.*, 2000], illustrating that not all trees within floodplain forest are equally susceptible to changing climate and hydrology. As flow regimes and climate rapidly evolve, systematic changes will occur that may be interpreted with focused study of individual cottonwood growth patterns.

In this study, I use dendrochronological techniques to investigate the biological and spatial controls on plains cottonwood tree ring growth along a 25-km reach of the Yellowstone River in the western Great Plains, USA. Specifically, I assess annual ring width correlations to seasonal river flow, precipitation, and climate. The overarching goals of this study were: 1) identify what hydrological and climate variables drive floodplain tree growth patterns, 2) identify potential causes of decreased growth that can lead to tree mortality, and 3) explore strategies for improving hydroclimatic reconstructions that take advantage of tree-scale growth patterns. Several hypotheses were tested, the first four relating to spatial relationships between trees and the water they access.

- *H1* and *H2*: Because river-derived groundwater is expected to be less accessible farther from the river, ring width correlations to river flow should decrease with distance to (*H1*) and elevation above (*H2*) the river.
- *H3* and *H4*: Conversely, tree growth correlations to precipitation should increase with distance to (*H3*) and elevation above (*H4*) the river.

These hypotheses are based on the prediction that cottonwoods will use rain water if river water is less accessible. Biological processes may also affect tree-water relationships:

- *H5*: Older trees should rely more on precipitation relative to flow because they may have more near-surface roots, have less competition for light from neighboring trees, and are generally farther from the channel.
- *H6*: Because light competition is high for young cottonwoods, they devote excess resources to above ground growth in favorable years. In contrast, old trees will have more stable interannual ring widths because they allocate excess resources to maintenance and reproduction. Therefore, young trees will have greater ring width variation between years.
- *H7*: Finally, given that growth patterns differ, strategic combinations of cores can improve flow reconstructions.

4.2 Study Site

4.2.1 Regional setting

The Yellowstone River flows east from the Rocky Mountains and is the largest tributary of the Missouri River. The Yellowstone is 1100 km long and drains the central Rocky Mountains and western Great Plains in Wyoming (48%) and Montana (51%) before joining the Missouri River in North Dakota [*Deacon et al.*, 2015]. The majority of the flow is derived from precipitation at high elevations [*Deacon et al.*, 2015], while the majority of the watershed lies in the relatively low-elevation and semi-arid Great Plains. The lowlands are sagebrush steppe habitat supporting sparsely vegetated landscapes whose main land use is rangeland [*Deacon et al.*, 2015]. In this region, water availability limits plant growth.

4.2.2 Study reach

The study site was located along the Yellowstone River between Glendive and Sidney, Montana (Fig. 4.1). The river has a wandering gravel bed [*Nanson and Croke*, 1992] that includes single and multi-thread sections. This study reach was the most geomorphically active part of the entire Yellowstone River between 1950 and 2001 [*Thatcher and Boyd*, 2006]. The geomorphic processes occurring here are relatively unrestrained by levees and bank stabilization.

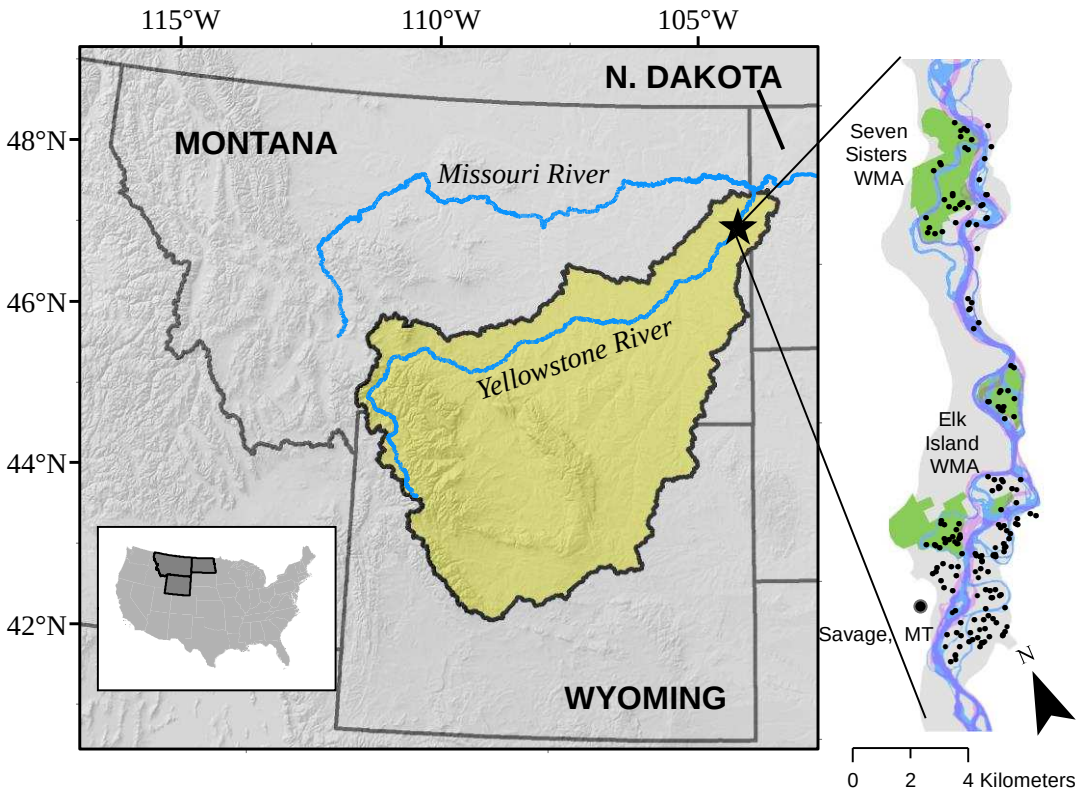

Figure 4.1. The 25-km study reach is located on the Yellowstone River in eastern Montana 70 km above its confluence with the Missouri River. Study trees are black dots, the 1950 and 2001 river channels are blue and purple, the 100-year floodplain is gray, and state Wildlife Management Areas are green.

Temperature and precipitation data were downloaded from PRISM for a point located on the Elk Island Wildlife Management Area in the study reach and south of Sidney, MT at 104.35° W and 47.44° N. The 1911-2010 mean July high temperature was 30.6° C and the mean January low was -16.5°C [*Daly et al.*, 2008]. Mean annual precipitation was 346 mm. The greatest local precipitation occurred in June, which coincides with the season of maximum snowmelt runoff from high elevation snowpack. The study site is 70 km west of the Little Missouri River, where previous research has investigated the connection between cottonwood growth and river flows [*Everitt*, 1968; *Edmondson et al.*, 2014; *Meko et al.*, 2015; *Schook et al.*, 2016b], and 250 km northeast of the Powder River where cottonwood growth has been used to reconstruct river channel migration [*Schook et al*., in review].

The study reach contains the largest floodplain forest on the lower Yellowstone River. Plains cottonwood is the most common tree in the study reach. Russian olive (*Elaeagnus angustifolia*), juniper (*Juniperus virginiana*), peachleaf willow (*Salix amygdaloides*), and green ash (*Fraxinus pennsylvanica*) trees are found among the cottonwoods. Sandbar willow (*Salix exigua*) is a shrub found on young surfaces, but juniper, Russian olive, and ash are most commonly associated with older successional cottonwood forests and former agricultural fields. Cottonwoods were sampled over 28 km^2 of forest in the 25-river km study reach. The largest tracts of contiguous forest were on the Seven Sisters and Elk Island State Wildlife Management Areas and on private ranches. The modern forest is largely contiguous, and within the 100-year floodplain [*Thatcher and Boyd*, 2009], 60% remains forested. I obtained access to 87% of the extant forest, and assume that the sample is representative of the entire floodplain forest throughout the reach.

4.3 Methods

4.3.1 Flow data

I used flow data from USGS streamgage #06329500 near Sidney, MT. The gage is located 15 km downstream from the study reach and had a mean annual flow of 352 m^3/s during the 1911-2015 flow record. The river has a snowmelt-dominated hydrograph, with 76% of peak annual flows in June [*Schook et al.*, 2016b] and 53% of runoff in May, June, and July. River flow and local precipitation have similar seasonal patterns, with the top three months for each being June, July, then May (Fig. 4.2). Temperatures peak later, in July and August, resulting in drying of the floodplain over the growing season.

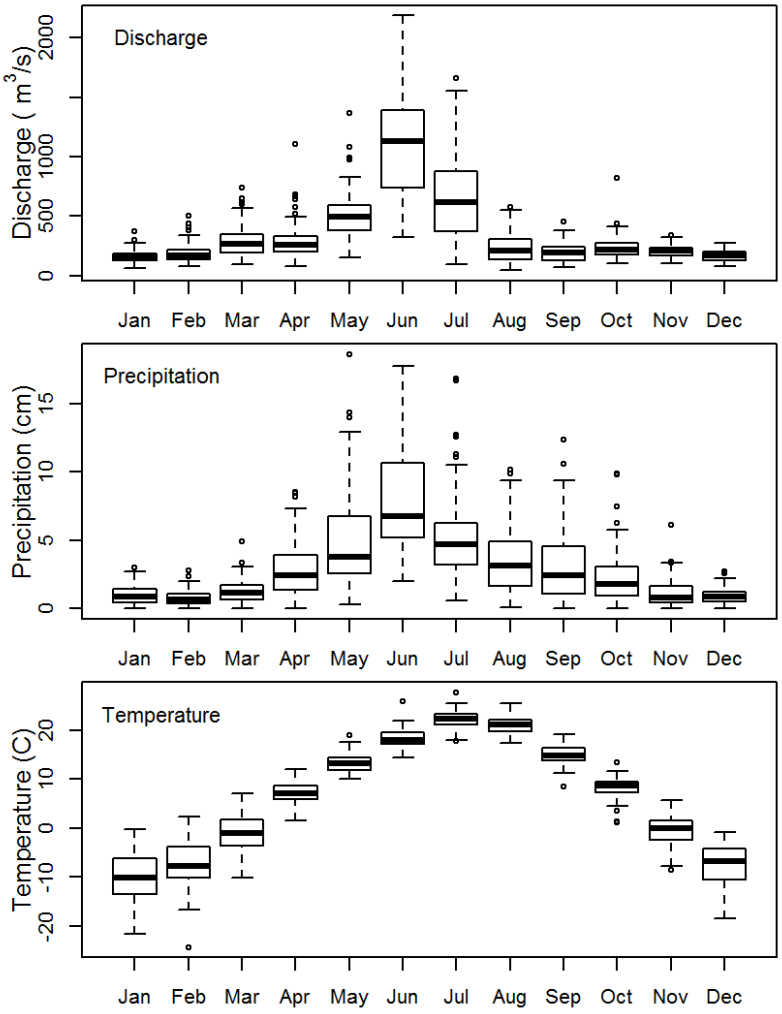

Figure 4.2. 1911-2012 annual patterns of monthly discharge at USGS streamgage #06329500, along with precipitation and temperature data for the study site from PRISM (Daily et al. 2008).

4.3.2 Tree core collection and preparation

Field sampling occurred in 2013 and 2014. 162 of the 178 trees were cored because they were the closest tree on the same geomorphic surface to randomly distributed points. This technique promoted a spatially unbiased sample and included trees of all age classes and growing surfaces. Additional cores were collected from old trees for the primary purpose of lengthening flow reconstructions [*Schook et al.*, 2016b], and the 16 old trees without rot were

included in this analysis to increase sample size. At least two cores were collected at breast height from each tree to facilitate cross-dating and ensure that one was close enough to the center to calculate its age. The sample includes a maximum of two cores per tree (n = 150 trees), and one core was used from the 28 remaining trees for a total of 328 cores. Trees were cored using 4.5-12 mm diameter increment borers that were up to 1 m long. Cores were mounted and sanded to progressively finer grades between 200 and 600 grit. Skeleton plots were used to create a master plot [*Stokes and Smiley*, 1996]. Cores were quality controlled using Cofecha [*Holmes*, 1983; *Grissino-Mayer*, 2001]. I used the R package dplR [*Bunn et al.*, 2016] to detrend tree ring series using cubic smoothing splines [*Cook and Peters*, 1981] with a 50% frequency-response cutoff at 50 years. This procedure removes age-related trends in ring-width [*Fritts*, 1976].

4.3.3 Predictors of tree ring growth patterns

Tree ring width varies between years based on growing conditions. I compared site-averaged ring widths to single- and multi-month values for discharge, precipitation, and temperature (collectively referred to as "Q, P & T") to identify which flow and climate metrics most strongly relate to tree growth. Additionally, I tested four predictor variables that could influence how ring width from individual trees is related to Q, P & T. The predictor variables were both spatial and biological because tree growth integrates the external physical environment and is regulated by internal biological processes. Predictors include 1) tree age, 2) growth rate, 3) elevation above the river, and 4) distance from the river. Age, elevation, and distance are independent variables that were hypothesized to affect tree growth, whereas growth rate could both affect and respond to ring width changes related to Q, P & T. The

predictors were only moderately correlated ($r \leq 0.37$; Table 4.1). I analyzed correlations between annual ring widths and Q, P & T metrics along gradients of each predictor. In this way, I could identify which spatial and biological variables best correspond to cottonwood ring width responses to variable flow and weather conditions. The correlative analyses described do not ascribe causation, but many strongly suggest it.

Table 4.1. Correlations (*r*) among the predictor variables. Distance and elevation are relative to the 2001 location of the Yellowstone River channel.

	Tree Age	Growth rate	Elevation
Growth rate	-0.26	-	-
Elevation	0.37	-0.03	-
Distance to channel	0.15	-0.09	-0.07

Spatial variables were calculated in two ways. For distance to river channel, I used the 1999-2001 air photo channel delineations created in the Yellowstone River Cumulative Effects Assessment study [*U.S. Army Corps of Engineers and Yellowstone River Conservation District Council*, 2015]. Most of the photos were from 2001, so I refer to them with this year. I conducted preliminary analyses using the 1950 and 1976 channel delineations, but these analyses proved redundant and were discontinued. Using ArcGIS, I determined the distance from each tree to the nearest point of any branch of the 2001 river channel. For elevation, geoprocessing tools were used to automatically create valley-spanning cross-sections perpendicular to the valley center and at equal distance spacing [*Jones*, 2006]. Values were derived from a 2.5 m digital elevation model created from a 2007 airborne lidar survey. I generated a raster of floodplain surface elevation above the river by taking land surface

elevation and subtracting elevation of the water surface extended across each valley-spanning cross-section. This method permitted elevation comparisons relative to the river channel for trees throughout the study reach. Uncertainty in elevation data arose because the land surface elevation above the river at each tree varies through time.

Two biological components were included in the predictor variables. First, I determined tree ages by cross-dating tree cores and identifying the pith year. Therefore, all tree ages are for sampling height (1.3 m above ground), not germination point. If pith was not contained in the core, the number of years to pith was calculated by dividing the mean ring width of the last four measured rings by the distance to pith, which was estimated using ring curvature [*Meko et al.*, 2015]. Second, I characterized each tree core's relative growth rate by generating nine Regional Curve Standardization [*Briffa et al.*, 1992] curves in the computer program CRUST [*Melvin and Briffa*, 2014a]. For every core, this method calculated the ring width for each ring compared to the same-aged ring in all other cores. Combining the relative ring widths for a core permitted grouping each core into one of nine equal-sized growth rate classes ranging from 1 (slow) to 9 (fast).

4.3.4 Statistical analysis

Hydroclimatic Metrics and Multiple Linear Regression

I used the best-subsets multiple linear regression technique (BIC selection criterion) to describe tree ring growth as a function of the ten flow (n = 2), precipitation (n = 4), and temperature (n = 4) variables that were the Q, P & T metrics. The metrics were all 1- to 4-month averages of uncorrelated ($r < 0.35$) flow, precipitation, and temperature from the current or prior year. Monthly correlation analyses using seascorr [*Meko et al.*, 2011; *Zang and Biondi*,

2015] identified Mar-Jun (referred to as "spring") to be the most positively correlated period related to ring width, so each of Q, P & T averaged over this period were three of the predictors. July had the highest single-month correlations to tree ring width for both precipitation and temperature, so July precipitation and temperature were two additional predictors. July flow was highly correlated with spring flow, so it was not a predictor. Plains cottonwood tree ring production is essentially complete in July (Friedman et a. 2011), and carbohydrates produced at the end of the summer can be used for root growth and stored for flower and leaf production in the following year [*Loescher et al.*, 1990]. Therefore, I included the previous fall (*p*Aug-*p*Nov, where "*p"* means "previous") averages for each Q, P & T. Although trees are mostly dormant over winter, they may still be affected by climatic conditions. For example, warm winters may cause early initiation of growth, leaving the tree vulnerable to subsequent freezes that could decrease tree ring growth. I therefore included winter (*p*Dec-Feb) precipitation and temperature as two more predictors to evaluate if ring width is affected by dormant-season temperature and local snowpack or soil rewetting. Winter flow was not included because it was moderately correlated to fall and spring flow, ice cover increases measurement error, and mechanistic explanations for ring width variations caused by low-magnitude winter flows were unclear.

Correlation Analysis

I used the R stats package to investigate Pearson correlations (*r*) linking tree ring growth to Q, P & T metrics across gradients of the spatial and biological predictor variables [*Rood et al.*, 2003; *Nakawatase and Peterson*, 2006]. All cores retained in this analysis had ring width measurements for 1960-2012 (53 years, n = 280 cores). This period was a compromise between

retaining a large sample size and including many years in the subsequent analyses. After determining correlation coefficients for each core's ring widths to all Q, P & T metrics, I linearly regressed these *r*-values against each of the predictors (i.e., creating correlations of correlations). In this way, I describe how tree ring width correlated to Q, P & T as a function of spatial and biological traits of each tree. I repeated analyses for three forms of the data: 1) all years, 2) only below average spring flow years (termed "dry" years because spring flow was the strongest cottonwood water source), and 3) all years after removing the effects of age. Using unadjusted probability values, I assigned conservative thresholds of $p < 0.01$ for significance and $p < 0.05$ for marginal significance, in recognition of the possibility of Type 1 errors when observing many *p*-values.

4.3.5 Grouping similar tree cores

In a complementary but opposite approach to the correlation analyses, I grouped cores that had similar correlations to Q, P & T. Grouping cores allowed for 1) interpretation of which predictors most strongly drove different tree ring responses to Q, P & T, 2) one map of similarly responding trees instead of four maps with cores stratified by each predictor, and 3) subsetting cores according to growth responses instead of *a priori* designations, creating groups that could be used in flow reconstructions. I grouped cores using k-means clustering in the R stats package. K-means minimized the within-cluster variance measured by Euclidean distance. I chose four groups *a priori*, a balance between creating enough groups to have small within-group variability while not producing too many groups with small sample sizes and statistical power. For each group I calculated all correlations for flow, precipitation, and temperature

from *p*Aug-Sep using seascorr [*Meko et al.*, 2011] in the treeclim program in R [*Zang and Biondi*, 2015].

I conducted a multivariate analysis of variance (MANOVA) to test for significant differences across groups for each of the predictor variables. Each variable was standardized using a z-scores transformation to facilitate comparisons. MANOVA accounts for the interactions among variables and guards against Type 1 errors introduced by multiple ANOVAs. I conducted post hoc ANOVAs to identify which of the predictors were different, and post hoc pairwise t-tests for each significantly different predictor.

4.3.6 Alternative flow reconstructions

River flow reconstructions are generally created by determining the relationship between annual ring width variations and flow over a period of record overlap, and reconstructions can extend back in time through the length of the tree ring records. To improve flow reconstructions, researchers have retained only cores with ring widths strongly correlated to measured flow [*Woodhouse et al.*, 2011], but stringent selection can produce over-fit models. I explored this issue by first creating a flow reconstruction model using all cores, then comparing it to one created from groups of cores that were selected using a best-subsets regression. Because the four groups were created based on having maximally unique differences for tree ring relationships to Q, P & T, I expected each group to express different signals of hydroclimatic variation. This model selection technique could retain any combination of the four groups, so retention of three or fewer groups was not considered a biased subsetting of the tree cores.

4.4 Results

4.4.1 Tree ring width, flow, and climate

Yellowstone River cottonwood tree ring width was more strongly correlated to flow than to precipitation or temperature. At the population level, more flow and precipitation reliably increased tree ring widths, while warmer temperatures corresponded to decreased ring widths. The most highly correlated single months for each climate variable were for May flow (r = 0.56), Jul precipitation (r = 0.29), and Jul temperature (r = -0.30).

Site-averaged ring widths were 62% more correlated to the ten Q, P & T metrics compared to the average correlation of individual cores (Fig. 4.3). This supported the approach of merging cores into a population index to remove individual variation in order to isolate climate signals. This pattern held during dry years alone, when the site-averaged ring widths were 65% more correlated to Q, P & T metrics compared to the average of individual cores (Fig. 4.3).

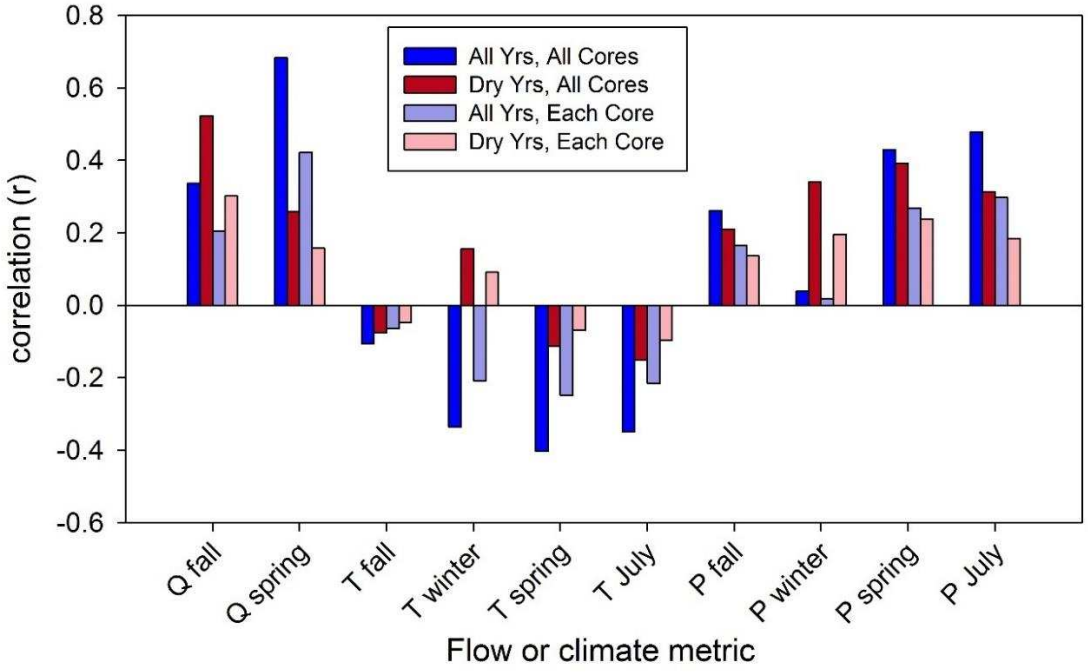

Figure 4.3. Correlations between tree growth and the ten flow (Q), precipitation (P) and temperature (T) metrics. The four analyses are arranged by 1) whether they contain *all* years (1960-2012; blue colors) or only the *driest* half of years (red colors), and 2) whether they were calculated from averaging *all* ring widths in a year and then correlating to Q, P & T metrics (darker colors), or were calculated from *each* core's correlation to Q, P & T metrics and then averaged (lighter colors).

Using all ten Q, P & T metrics as potential predictors of tree ring width, the best model (with unitless standardized coefficients) retained spring (Mar-Jun) flow (1.05), previous fall (*p*Aug-*p*Nov) flow (0.48), spring precipitation (0.41), and July precipitation (0.36) (r = 0.72). All four selected predictors had positive coefficients indicating that more flow and precipitation increased tree ring growth. Even though the predictor pool included twice as many precipitation and temperature variables as flow, flow emerged as the most important Q, P & T metric, reinforcing the importance of river-derived water in riparian forests within dry regions.

4.4.2 Ring width patterns and predictor variables

There were significant ($p < 0.01$) but weak correlations for the ten Q, P & T metrics with tree ring growth along gradients of predictor variables (Fig. 4.4; Table 4.2, which contains all *r*- and *p*-values for correlation analyses). All significant correlations to flow and precipitation were positive (i.e., more water in any season corresponded to wider tree rings), while correlations to temperature were always negative (i.e., warmer temperature at any time corresponded to narrower tree rings because of water stress). The strongest relationships between tree growth patterns and any predictor were that warmer falls and winters (*p*Dec-Feb) reduced ring width the most in older trees ($r = 0.42$; Table 4.2). In contrast to the other seasons, spring temperature was the only Q, P & T metric not significantly correlated to tree ring growth along gradients of any predictor. This suggests that temperature has systematically variable effects on tree growth only when soil moisture and water tables are not high. The most notable difference from analyzing all years (1960-2012) to only dry years was the emergence of spring precipitation relationships along predictor variables (Appendix Fig. 7.12). This result indicated that some trees used precipitation relatively more than others when the water table was deeper. Considering all trees independent of their spatial and biological predictors, spring precipitation is a stronger predictor of tree growth than spring flow in dry years, which contrasts the pattern from all years (2^{nd} and 9^{th} groups in Fig. 4.3). The other noteworthy shift during dry years is the stronger correlation between ring width and previous fall flow compared to current spring flow, which was opposite of the trend when all years were considered.

Table 4.2. Tree ring width relationships to flow (Q), precipitation (P), and temperature (T) metrics along gradients of the predictor variables for all years (A), dry years (B), and all years after removing the effects of age (C). Tree age was never significant in dry years, so partial correlations were not calculated for dry years. "dir." is the direction of the relationship (p = positive, n = negative). "*r*" is the Pearson's R correlation coefficient. Cells are highlighted yellow for marginal significance ($p < 0.05$) and red for significance ($p < 0.01$) for unadjusted *p*-values.

A)

All Years

	Elevation			Distance 2001			Growth rate			Tree Age		
Metric	dir.	*r*	p	dir.	*r*	p	dir.	*r*	p	dir.	*r*	p
Q *p* Aug-*p* Nov	p	0.16	0.01	p	0.00	0.73	p	0.09	0.11	p	0.25	0.00
Q Mar-Jun	n	0.12	0.05	p	0.10	0.08	p	0.16	0.01	n	0.05	0.36
T Mar-Jun	n	0.11	0.07	n	0.09	0.11	p	0.00	0.63	n	0.03	0.53
T *p* Aug-*p* Nov	n	0.10	0.08	n	0.42	0.00	p	0.10	0.09	n	0.31	0.00
T *p* Dec-Feb	n	0.13	0.03	n	0.42	0.00	n	0.00	0.67	n	0.23	0.00
T Jul	n	0.11	0.07	n	0.19	0.00	n	0.00	0.83	n	0.19	0.00
P Mar-Jun	p	0.03	0.58	p	0.15	0.01	p	0.00	0.89	n	0.04	0.41
P *p* Aug-*p* Nov	p	0.11	0.07	p	0.25	0.00	p	0.16	0.01	p	0.30	0.00
P *p* Dec-Feb	p	0.12	0.09	p	0.14	0.02	n	0.07	0.27	p	0.17	0.00
P Jul	n	0.20	0.00	n	0.11	0.07	p	0.11	0.06	n	0.25	0.00

B)

Below average Mar-Jun flow

	Elevation			Distance 2001			Growth rate			Tree Age		
Metric	dir.	*r*	p	dir.	*r*	p	dir.	*r*	p	dir.	*r*	p
Q *p* Aug-*p* Nov	n	0.00	0.68	n	0.10	0.09	p	0.09	0.11	n	0.00	0.64
Q Mar-Jun	n	0.11	0.05	n	0.09	0.14	p	0.15	0.01	n	0.09	0.14
T Mar-Jun	n	0.06	0.27	n	0.09	0.14	p	0.10	0.08	n	0.00	0.69
T *p* Aug-*p* Nov	n	0.12	0.04	n	0.18	0.00	p	0.06	0.31	p	0.06	0.29
T *p* Dec-Feb	n	0.00	0.61	n	0.28	0.00	p	0.10	0.07	n	0.00	0.83
T Jul	p	0.00	0.71	n	0.00	0.85	p	0.00	0.84	p	0.00	0.95
P Mar-Jun	p	0.20	0.00	p	0.26	0.00	n	0.22	0.00	p	0.09	0.14
P *p* Aug-*p* Nov	p	0.00	0.95	n	0.00	0.96	p	0.15	0.01	n	0.05	0.37
P *p* Dec-Feb	n	0.04	0.41	p	0.04	0.41	p	0.00	0.80	p	0.08	0.19
P Jul	p	0.09	0.14	n	0.07	0.21	p	0.00	0.86	p	0.04	0.49

C)

Partial corr. after removing Tree Age

	Elevation			Distance 2001			Growth rate		
Metric	dir.	*r*	p	dir.	*r*	p	dir.	*r*	p
Q *p* Aug-*p* Nov	p	0.08	0.21	n	0.00	0.78	p	0.16	0.01
Q Mar-Jun	n	0.10	0.10	p	0.11	0.06	p	0.14	0.02
T Mar-Jun	n	0.10	0.11	n	0.09	0.13	p	0.00	0.74
T *p* Aug-*p* Nov	p	0.00	0.84	n	0.40	0.00	p	0.00	0.73
T *p* Dec-Feb	n	0.04	0.41	n	0.39	0.00	n	0.09	0.15
T Jul	n	0.03	0.51	n	0.16	0.01	n	0.06	0.28
P Mar-Jun	p	0.05	0.39	p	0.16	0.01	n	0.00	0.94
P *p* Aug-*p* Nov	n	0.00	0.99	p	0.22	0.00	p	0.25	0.00
P *p* Dec-Feb	p	0.03	0.52	p	0.12	0.05	n	0.00	0.74
P Jul	n	0.11	0.06	n	0.07	0.23	p	0.04	0.44

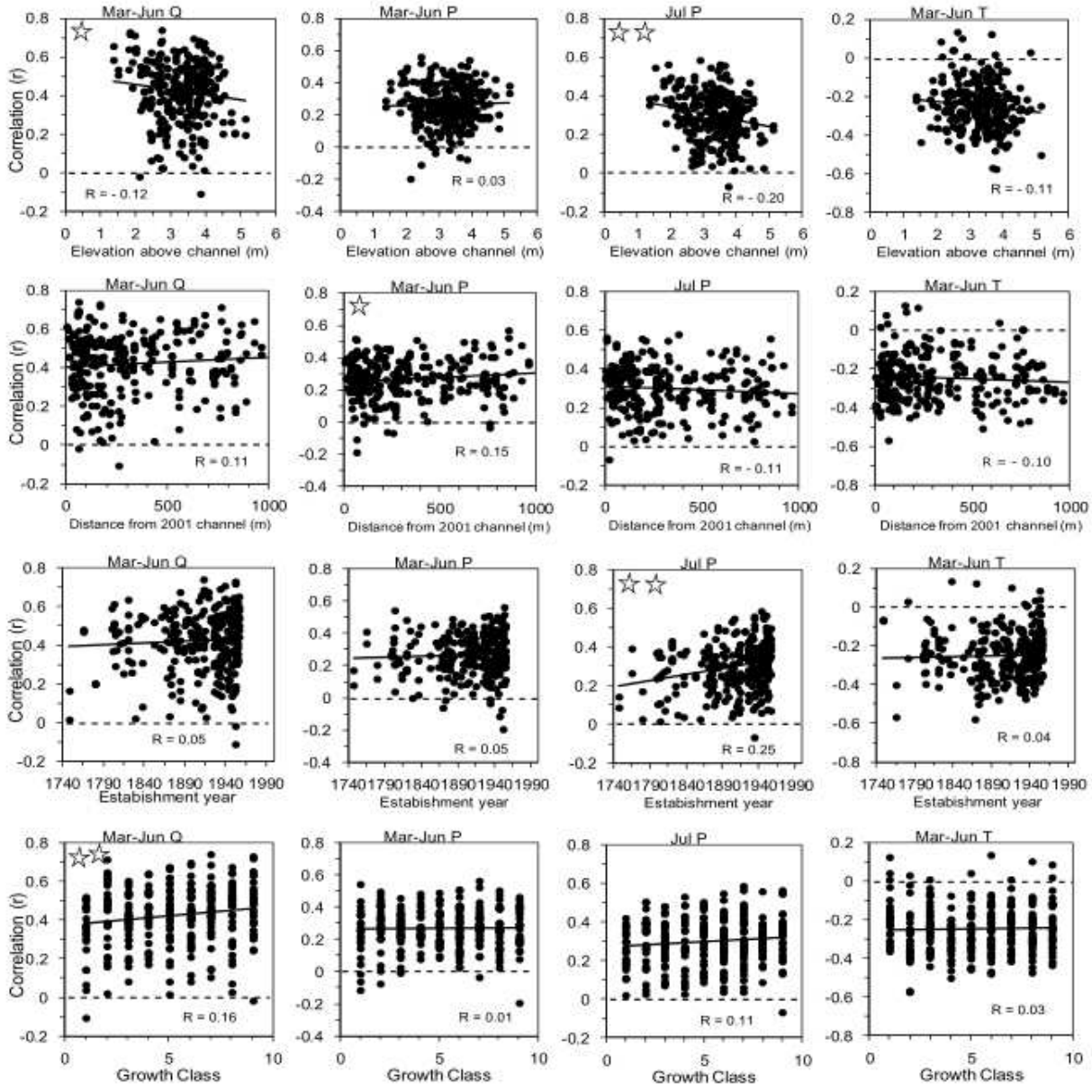

Figure 4.4. Relationships between tree ring width and spring flow, spring precipitation, July precipitation, and spring temperature (columns) for all years, 1960-2012. Rows are predictor variables that could affect correlations to each Q, P & T metric. Dashed line at zero shows no correlation, and solid lines are best-fit lines for the data. One star means $p < 0.05$**,** two stars for $p < 0.01$.

Tree age was the predictor variable most commonly related to tree growth correlations to Q, P & T. Older trees were significantly more negatively related to temperature during all

seasons except during spring (Table 4.2). Older trees were more positively correlated to fall and winter precipitation, but younger trees were more positively correlated to July precipitation. This suggests a longer growing season for the young trees and extended integration of environmental conditions in old trees. In contrast to all years, tree age was not significantly correlated to any predictor when only considering dry years. This unexpected result was found because growth patterns were highly stratified by age class in wet years (Appendix Fig. 7.13).

To isolate the effects of age on tree growth patterns, I separated the 280 tree cores into evenly-sized groups and determined their relationships to *monthly* flow, precipitation, and temperature. Although generally similar, important differences appeared across the four age classes. The most notable difference was that older trees were more strongly correlated to earlier (Mar-Apr) runoff, while younger trees were most strongly correlated to both later (May-Jul) runoff and May and July precipitation (Fig. 4.5). The oldest trees had significantly less autocorrelation than every other age class (ANOVA, $F(3,275) = 7.02$, $p < 0.001$, post hoc t-tests with Bonferroni adjustment $p < 0.05$). Because of the observed strong correlations to tree age and known changes in resource allocation as trees age [*Ryan et al.*, 2004], I also tested first-order partial correlations for the other predictors (growth rate, distance to channel, elevation above channel) after removing the effects of age.

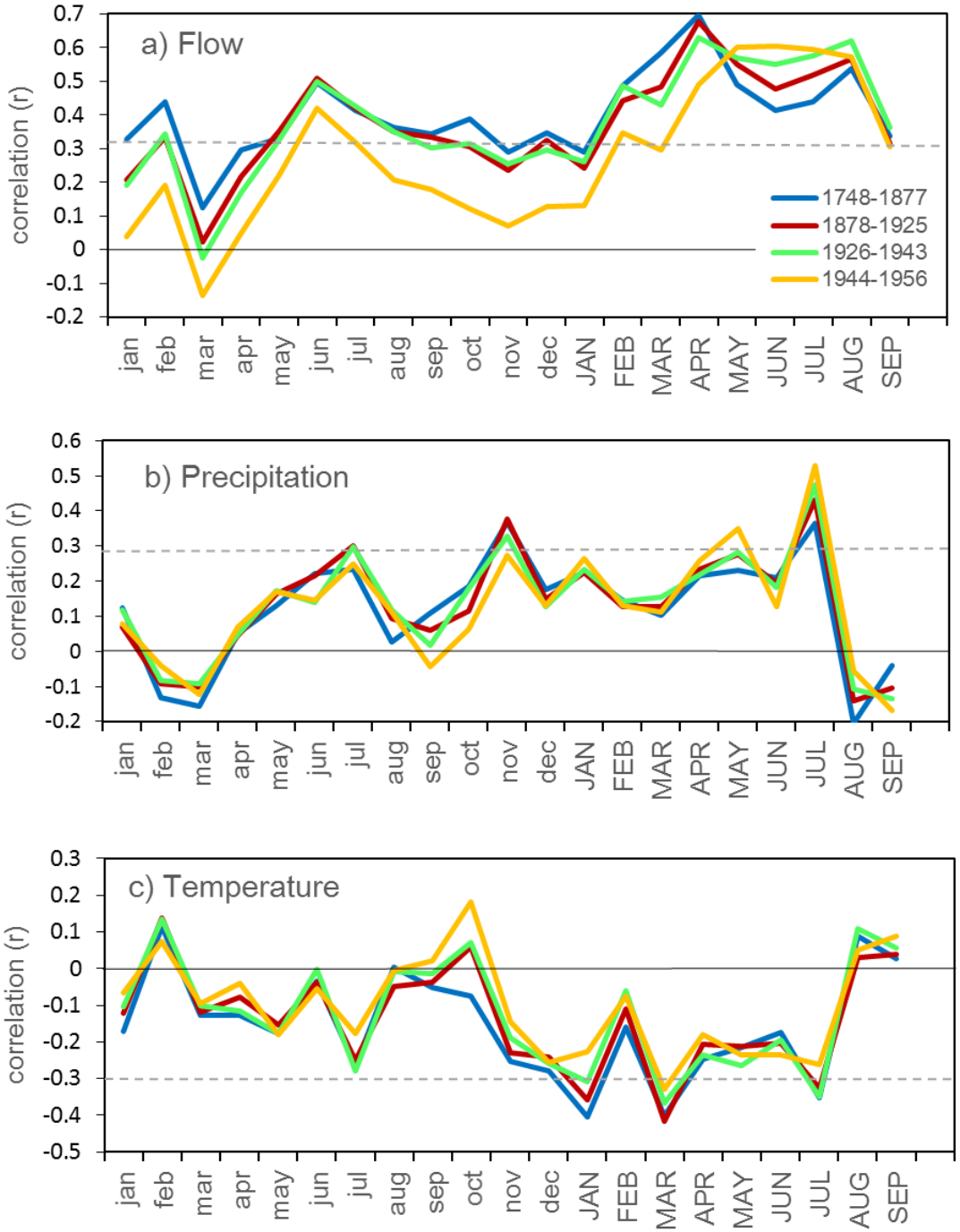

Figure 4.5. 1960-2012 mean correlations between cores within each age class and monthly Q, P and T from the current (capitalized) and previous (lower case) years. Groups are the oldest trees (1748-1877, blue), second oldest (1878-1925, red), second youngest (1926-1943, green), and youngest (1944-1956, yellow). Note that y-axes differ. Horizontal black lines represent $r = 0$ (no correlation). The dashed gray line is the approximate significance level using exact bootstrapping by circulant embedding of tree-ring data, for which monthly correlations higher (Q, P) or lower (T) than the line were significant at $p < 0.05$.

The second biological variable tested was tree growth rate. In all three scenarios (i.e., all years, dry years, and all years after accounting for the effects of age), faster growing trees were at least marginally more positively correlated to spring flow. Similarly, for all three scenarios, faster growing trees were more positively correlated to previous fall precipitation. Additionally, after accounting for tree age, faster growing trees were more correlated to fall flow. These relationships indicate that more water permits faster tree growth. In contrast, in dry years, slower growing trees were more positively correlated to spring precipitation, suggesting that trees that use precipitation instead of flow during the runoff season are less productive.

Distance to the river was one of two spatial variables tested as influencing ring width patterns. Even after accounting for age, trees farther from the channel were more negatively affected by high temperatures in fall, winter, and July (Table 4.2b). Similarly, even after accounting for age, trees farther from the channel were more positively correlated to fall precipitation. This is consistent with the expectation that trees with less groundwater access are more adapted to use precipitation. In all three scenarios, trees farther from the channel were at least marginally more correlated to spring precipitation, highlighting that trees nearer the channel use river water instead of rain during the runoff season. Distance to channel did not significantly affect tree growth patterns in relation to either fall (r = 0.73) or spring flows (r = 0.08).

Tree elevation relative to the river was the second spatial factor tested. Lower trees were marginally more correlated to spring flows in all and dry years, while higher trees were better correlated to spring precipitation in dry years. This pattern was also seen with lateral distance from the channel. In both cases trees with less access to river water were more

strongly supported by precipitation, especially in drier years. Higher trees were unexpectedly more correlated to fall flow, a relationship that disappeared after accounting for tree age. In fact, all Q, P & T relationships to elevation disappeared after accounting for tree age, although it is unclear if elevation or age drove the relationships.

4.4.3 Groups of similar tree cores

The correlation analyses described above directly identified relationships between gradients of predictor variables and tree ring growth patterns. I used a complementary but opposite approach to further investigate growth patterns by clustering cores into four groups that minimized within-group variance to the ten seasonal Q, P & T metrics. This allowed for interpretation of which predictors most strongly separated tree ring responses to Q, P & T, mapping responses to Q, P & T, and data-directed separation of cores for alternative flow reconstructions. Each group contained cores from throughout the study reach, indicating that tree-scale variables dictated growth patterns instead of reach-scale variables (Fig. 4.6). The four groups differed along predictor variables (MANOVA test, Pillai = 0.27, $F(3,324) = 5.25$, $p < 0.001$). Tree age, elevation above water, and distance from the river significantly varied across groups, while growth rate was the same across groups (Fig. 4.7, Table 4.3). Across groups, Group 4 had the most distinct values for predictor variables. This group was comprised of trees older, higher, and farther from the channel. Group 1 cores had opposite characteristics and came from trees that were relatively young, low, and close to the channel. Groups 2 and 3 were not different from each other for any predictor, suggesting that untested variables influenced their differentiation.

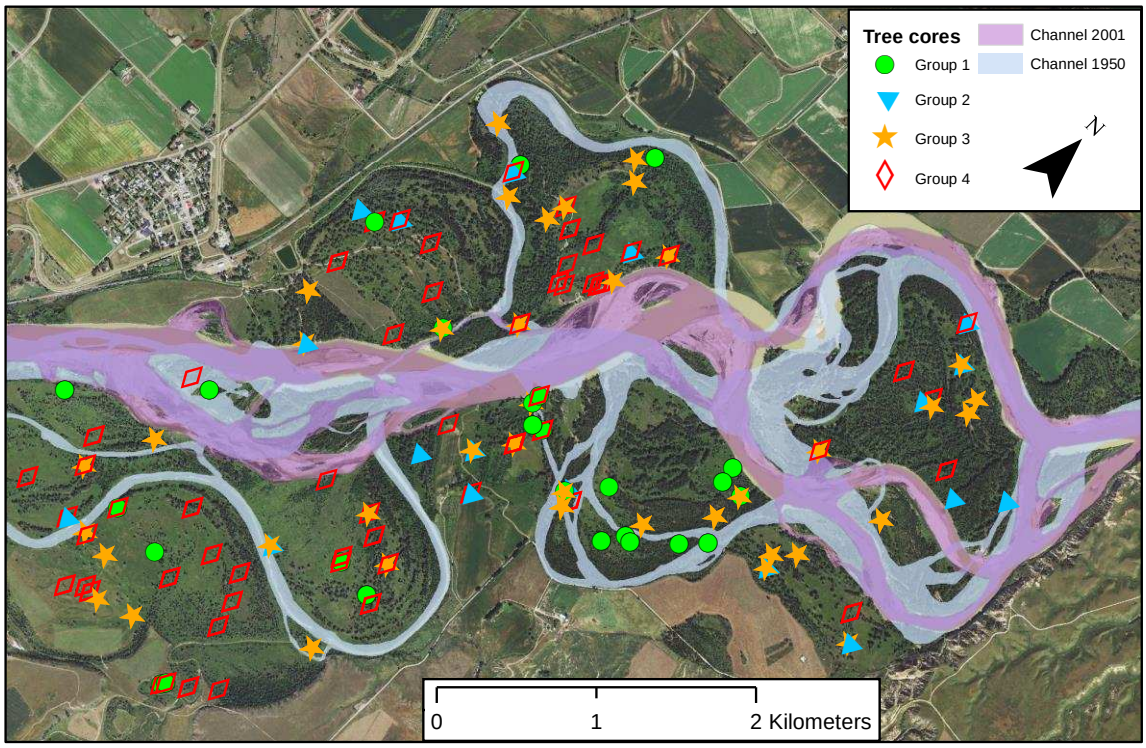

Figure 4.6. Example portion of the study reach showing the locations of the four groups of tree cores, which were determined by the relationships between ring width and flow, temperature, and precipitation. Thirty percent of trees had cores belonging to more than one group, and these were plotted on top of each other. Flow is from left to right.

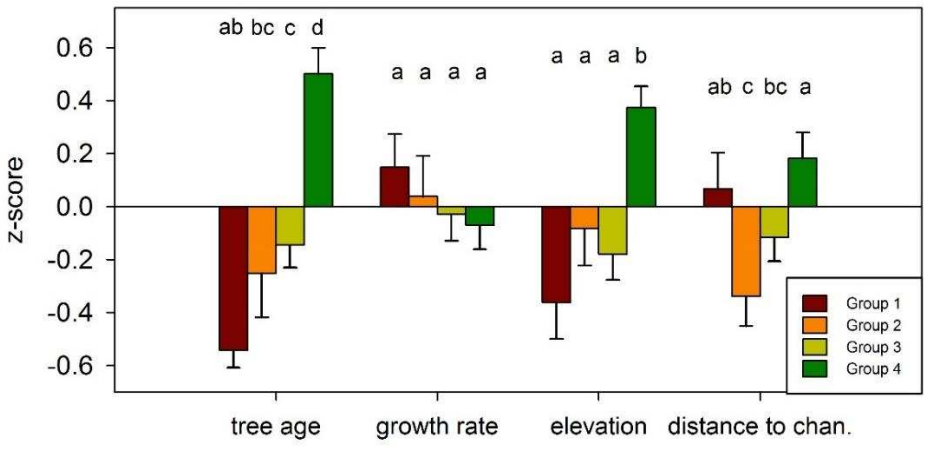

Figure 4.7. Comparisons of predictor variables for the four groups of tree cores. Groups were created by clustering cores that responded similarly to Q, P & T so the relative influence of predictors could be assessed. Variables tested include: 1) tree age (negative values on y-axis = young), 2) growth rate (negative = slow), 3) elevation above river (negative = low), and 4) distances from the 2001 channel (negative = close). Mean and standard error are displayed for the z-scores of standardized groups. The same letter represents a non-significant difference between groups for a given predictor.

Table 4.3. Summary statistics of the predictor variables for each group. Mean and standard deviation are included.

Group	Cores in group (n)	Establishment year	Growth rate (unitless)	Elev. above river (m)	Distance to river (m)
1	64	1940 ± 26	5.4 ± 2.5	3.04 ± 0.76	376 ± 368
2	43	1925 ± 54	5.1 ± 2.5	3.23 ± 0.63	240 ± 248
3	101	1920 ± 42	5.0 ± 2.5	3.17 ± 0.67	315 ± 306
4	120	1888 ± 52	4.9 ± 2.5	3.55 ± 0.61	415 ± 360

I ran monthly correlations to identify inter-group differences in ring width patterns related to Q, P & T metrics. Correlations with flow differed more than with precipitation or temperature among groups (Appendix Fig. 7.15). Group 1 cores had the highest correlations to flow during the May-July runoff season when 53% of annual discharge occurred. Group 1 also had the highest correlation to July precipitation, which was consistent with young tree growth being most correlated with July rain. Group 2 tree core growth was the least correlated to Q, P & T metrics. Group 3 tree cores had low correlation to fall and winter flows, but they had the second highest correlation to spring and summer flows. Group 4 cores were the oldest, highest, and farthest from the river channel. Group 4 had uniquely similar correlations to river flow throughout the year; peak correlation was in April, which preceded high elevation snowmelt runoff (Fig. 4.2) and the peak monthly correlations from all other groups (Appendix Fig. 7.15). Although opposite along predictor variables, Groups 1 and 4 had the strongest negative relationships to summer temperature.

To test if growth patterns were constant around the circumference of a tree, 300 of the 328 cores analyzed were paired with another core that was collected 90-180° away in the same tree (n = 150 trees). If growth patterns were constant throughout a tree, a 100% group match

rate for paired cores would have occurred, whereas uncorrelated and spatially random growth patterns would yield a 25% group match rate. The cores had a 64% match rate, with the highest portion of matched cores coming from Group 4 (77%) and lowest from Group 2 (42%; Table 4.4). For the 36% of cores matched with a core from a different group, the most consistent mismatch was that Group 2 cores were paired with Group 3 cores almost as frequently as with themselves. This was not unexpected given their similar and intermediate values of predictors (Fig. 4.7).

Table 4.4. 300 of the 328 cores were paired with a core collected from a different radius on the same tree. Rows show the group of the first core, and columns the group of its paired core. Values are the proportion of cores from groups listed in rows that were paired by cores from groups listed in columns. The italicized diagonal highlights matched cores.

	Group of paired core				
Group of first core	**1**	**2**	**3**	**4**	**Cores (n)**
1	*0.61*	0.00	0.22	0.17	59
2	0.00	*0.42*	0.37	0.21	38
3	0.14	0.15	*0.62*	0.10	94
4	0.09	0.07	0.08	*0.75*	109

4.4.4 Alternative flow reconstructions

I conducted a sensitivity analysis to investigate how core make-up affects flow reconstruction. For each of the four groups, I developed a simple linear regression model to describe mean annual (*p*Aug-Jul) flow from 1930-2012, which was a longer duration than in correlation analyses where each core included all years. The reconstructed flows differed substantially from each other. The reconstruction from Group 1 cores best matched the measured discharge (r = 0.73). Group 4 was second best (r = 0.67), followed by Group 3 (r =

0.56) and Group 2 (r = 0.25; Appendix Fig. 7.16). The high year-round correlations between Group 4 and flow suggested that these cores would create the most accurate flow reconstructions (Appendix Fig. 7.17). However, Group 1 outperformed Group 4, highlighting the importance of the snowmelt runoff period.

I created two more flow reconstructions from a) a simple linear model developed from all tree cores, and b) a best subsets multiple regression produced using the four groups of cores as potential predictor variables. The best subsets reconstruction (r = 0.76) outperformed the all-core reconstruction (r = 0.68; Fig. 4.8, Fig. 4.9), slightly outperforming the reconstruction of Group 1 alone (r = 0.73). The best subsets model retained Group 1 and Group 2 as predictors. Group 1 had a positive loading (305.9), while Group 2 had a smaller negative loading (-170.4). Thus, Group 2 acted as a suppressor variable and removed some of the ring width variation present in Group 1 that was unrelated to annual flow.

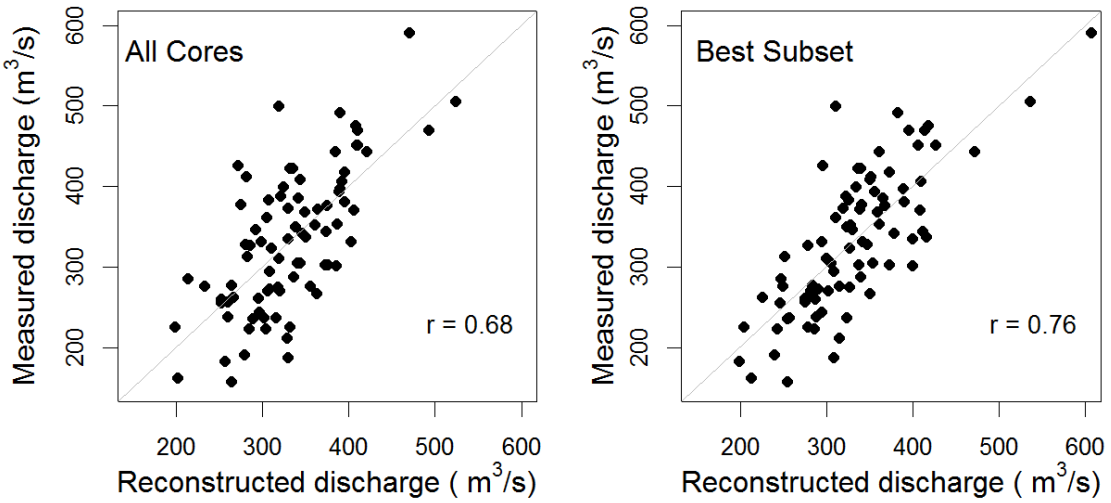

Figure 4.8. Scatterplot showing mean annual discharge for measured vs. reconstructed flows in each year (1930-2012). Panels depict the relationships calculated using all cores (left) or the two groups of cores selected in best subsets regression. Perfect fit indicated by the 1:1 gray line.

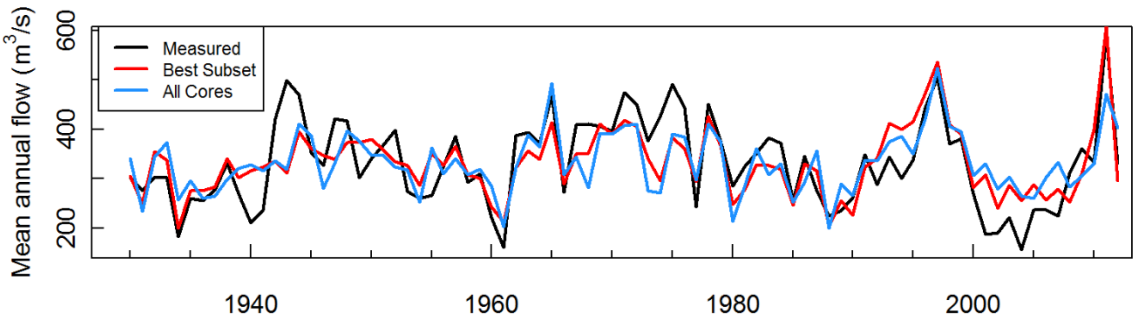

Figure 4.9. Comparison between measured (black) and flow reconstructed from all cores (blue) and the best subset regression (red).

4.4.5 Summary of hypotheses tested

Some of the seven hypotheses that guided this study were supported. Four hypotheses related to trees more proximal to the channel being better correlated to river flow while more distant trees would better correlate to precipitation. The only scenario in which correlations between flow and growth were greater for trees laterally closer to the channel was for spring flow in dry years, so most data did not show closer trees as better correlated to flow (mostly not supporting *H1*). Higher trees were expected to have similar trends as farther trees, but they mostly showed the expected results by being more correlated to spring flows in all years (supporting *H2*). The alternative water source to river-derived groundwater was precipitation, which was more strongly linked to farther trees (supporting *H3*) and higher trees during dry years only (partially supporting *H4*). *H5* stated that older trees would be more correlated to precipitation than younger trees. This relationship was found during winter and spring but it was reversed in July, presumably because younger trees had basal growth later into the summer. *H6* stated that older trees would have more autocorrelation in annual growth because they have greater storage capacity, but the results showed these trees to have the least

autocorrelation. This could have resulted from a decreased prioritization of aboveground growth as trees age, resulting in lower allocation to basal growth during less favorable growing years for older trees. Finally, I used a cluster analysis to subset tree cores, showing that strategic combinations of cores can improve flow reconstructions (supporting *H7*).

4.5 Discussion

4.5.1 Factors affecting tree ring growth

Tree age

A fundamental concept in dendrochronology is that after detrending ring widths, radial growth response to climate is no longer age dependent. However, this study contradicts this concept, as tree age was the predictor variable most consistently affecting the ring width response to Q, P & T. Age-dependent climate responses also occur in *J. thurifera* [*Rozas and Olano*, 2013], *Picea glauca* [*Szeicz and MacDonald*, 1994], and *Larix decidua* [*Carrer and Urbinati*, 2004]. Tree ages in this analysis were confounded with spatial location, as older trees tended to be both higher and farther from the channel (Table 4.1). The importance of age (i.e., establishment year) may be partially due to the fact that it was fixed throughout the study period, unlike spatial relationships that change through natural fluvial processes. Older trees were more positively correlated to precipitation in the winter and spring, but this pattern was reversed in July (partially supporting *H5*). A July reversal is consistent with the hypothesis that young trees put more energy into aboveground growth and continue tree ring growth later into the summer. Young cottonwoods often grow in dense single-aged stands, and their survival depends on outcompeting neighbors for light. Similarly, stronger relationships to the most growth limiting climate variable, June rain, occurred in younger *J. thurifera* [*Rozas et al.*, 2009].

In this species, tree age and sex modulated growth response to climate more than did any environmental variable.

Over their lifetimes, the oldest trees along the Yellowstone River study site had the least autocorrelation in ring width between years (not supporting *H6*). Although contrary to expectations, this finding has an ecologically-plausible explanation. The oldest group of trees had only trees over 135 years old. Most neighboring trees die before reaching this age which makes aboveground competition low, such that adding basal growth serves to maintain functioning connective tissue and outpace rot. With less competition, basal growth would be less prioritized compared to reproduction and maintenance. Because basal growth is marginalized, it is more likely to vary between years, producing the observed lower autocorrelation. In contrast, younger cottonwoods prioritize vertical and basal growth in every year, so greater interannual variation may occur in other processes such as root growth and seed production.

These findings reinforce another fundamental concept in dendrochronology that the common growth patterns of a population correlate more strongly to climate than do the growth patterns of individual trees. This has also been explicitly shown in *Juniperus thurifera* [*Rozas and Olano*, 2013] and *Abies lasiocarpa* [*Ettl and Peterson*, 1995], where researchers identified climate relationships to be highly variable, and even opposite, for some trees compared to that of the population as a whole. In an environment as heterogeneous and dynamic as the Yellowstone River floodplain, I found tree-level growth connections to flow and climate to vary by tree age, growth rate, and distance from and elevation above the river.

Spatial relationships

In all years, even after accounting for age, there were non-significant (p = 0.08 and 0.06) tendencies for trees farther, not closer, from the channel to be better correlated with spring discharge. However, after isolating the driest half of spring flows, this trend was mostly reversed (p = 0.14; partially supporting *H1*). These divergent patterns highlight that proximity to the river affects water acquisition for different trees depending on water availability. During high flow years the trees nearer the channel likely had ample water, so another resource became limiting to tree ring growth. In these same wet years, however, it appears that trees farther from the channel may have a stronger connection to flow because of increased access to groundwater. However, in dry years farther trees appear less connected to river-derived groundwater, and trees closer to the river were more linked to river flow. Correspondingly, trees farther from the channel were always at least marginally more correlated to spring precipitation compared to trees close to the channel (p's < 0.02; supporting *H3*). With less access to river water, precipitation is used more, even though this may be a less preferred strategy in *Populus* [*Snyder and Williams*, 2000]. These spatial relationships that change during wet and dry years impact how reliably dendrochronologists can extract environmental signals through time.

I expected elevation relationships to mirror those for distance to the channel because both represent distance to the river. However, the relationships differed. Lower trees were marginally more correlated to spring flows in all years and dry years (p's = 0.05), a relationship that only slightly weakened after accounting for age (p = 0.10; supporting *H2*). This contrasts the reversal between wet and dry years seen for distance from the channel. This suggests that

lower trees have better access to the alluvial water table compared to high trees that acquire more of their water from rain, a relationship that remained important during wetter years. Compensating for their decreased access to river water, higher trees were more strongly linked to spring precipitation in dry years (partially supporting *H4*). The relationship disappeared when all years were considered, however. This finding supports the idea that river flows are more important than precipitation by suppressing precipitation relationships when river water was abundant.

Additional causes of tree ring variability

The predictor variables tested did not include all factors known to affect tree radial growth. For example, competition has been identified as a strong control on a tree's climatic sensitivity [*Manetti and Cutini*, 2006; *Martín-Benito et al.*, 2007; *Rozas and Olano*, 2013]. I did not measure competition from neighboring trees directly, but there is a well-established seral development of cottonwood floodplain forests, progressing from young dense stands to old sparse stands (i.e., competition decreases through time). One line of evidence that indicated the study trees experience competition is the higher relationship to July precipitation for young trees, which suggested they devote more of their energy derived late in the growing season to above-ground growth.

4.5.2 Emergent trends in dry years

Spatial relationships revealed a divergence in cottonwood water acquisition processes in years of low water availability. Use of both groundwater and rainwater supports findings that *Populus* are facultative phreatophytes [*Rood et al.*, 2011] and that *P. fremontii* with access to groundwater used it more than precipitation even after summer rain [*Snyder and Williams*,

2000]. Spring flow was the Q, P & T metric most correlated to ring width. An extension of this finding is that in dry years faster growing trees were more correlated to spring flow, but slower growing trees were more correlated to spring precipitation. This finding supports the idea that river flow is a preferred water source over precipitation, and better access to groundwater supports higher growth.

Yellowstone River spring runoff will decrease in the future if: a) summer temperature rises and watershed evapotranspiration (ET) increases, b) reservoir storage increases to support growing human populations, or c) irrigated acreage or crop ET increases without increased efficiency in irrigation techniques. The Yellowstone has already experienced marginally significant spring flow declines [*Chase*, 2013; *Schook et al.*, 2016b], and all three mechanisms proposed above are highly plausible. Reductions in early summer flows caused persistent reductions in cottonwood growth in the Green River downstream of Flaming Gorge Dam [*Schook et al.*, 2016a], where recently a fire swept through and killed a large stand of the drought-stressed trees. In addition to fire, greater water stress and increased reliance on summer rain will increase vulnerability to pathogens [*Raffa et al.*, 2008; *van Mantgem et al.*, 2009], further threatening floodplain ecosystems [*Merritt and Cooper*, 2000].

4.5.3 Importance of river water in semi-arid floodplain forests

Both the monthly correlation and the multiple linear regression analyses suggested river flow to be more important to floodplain cottonwood growth compared to local precipitation or temperature. These results are consistent with research documenting tree ring growth in dry regions being moisture-limited [*Fritts*, 1976], and floodplain cottonwoods are phreatophytes that acquire much of their water through the alluvial water table supported by the river [*Butler*

et al., 2007; *Rood et al.*, 2011]. The exercise of clustering tree cores by their common responses to Q, P & T metrics revealed the clearest group separation by flow (Appendix Fig. 7.15). Believably, this indicated that water table access varies to a greater degree across the floodplain compared to precipitation and temperature. The low-volume fall and winter base flows were correlated with ring width for Group 4 trees to a greater degree than expected given that most of these flows occur during tree dormancy when water availability has negligible direct effects. Therefore, dormant season correlations may have been driven by correlations between the previous summer's flow with fall and winter flow.

4.5.4 Within-tree variation

In addition to the biological and spatial factors that vary by tree, I analyzed within-tree growth patterns using the 150 trees that had paired cores. The cluster analysis produced a 64% group match rate for paired cores. The match rate falling between 25% (i.e., randomly matched) and 100% (i.e., perfectly matched) indicated that a) tree ring growth occurred systematically as a function of the interaction between physical and biological processes, and b) one tree can express different growth patterns, so analyzing multiple cores from a tree adds information. In a study of *P. angustifolia* in Alberta, Rood et al. [2013] found no systematic difference in climate relationships according to cardinal direction of the radius cored. However, differing growth patterns could result from asymmetric root and branch distributions, competition, physical or pathogenic wounds, and abiotic factors such as soil water and nutrient availability [*Speer*, 2010]. Of the four tree core groups created in cluster analysis, Group 2 had the lowest match rate and the lowest correlations to Q, P & T. Potential factors leading to Group 2 growth patterns include: a) some trees had growth more influenced by processes

unrelated to weather and flow, b) weather and flow affected tree growth at a scale not captured by the monthly indices, or c) some radii were unresponsive to weather and flow even though other radii within the tree were. Explanation (c) is to be at least partly supported, as Group 2 both had the highest mismatch rate (Table 4.4) and did not strongly distinguish itself from other groups across the predictor variables (Fig. 4.7).

4.5.5 Spatial relationships in dynamic settings

The Yellowstone River in the study reach is a wandering gravel bed river with multiple channels that migrate and avulse within the lifetimes of cottonwood trees. These dynamic fluvial processes complicated identification of a tree's spatial relationship to the river. Elevation is often among the most important spatial drivers of tree growth patterns [*Zhang and Hebda*, 2004; *Nakawatase and Peterson*, 2006; *Peng et al.*, 2008; *Albright and Peterson*, 2013]. However, the elevations in this study were relative to the river surface and varied by less than 4 m. This elevation range is not climatically meaningful, but it is hydrologically relevant considering near-surface floodplain water tables that vary with the river stage [*Rood et al.*, 1995, 2013; *Mahoney and Rood*, 1998]. Relative elevations between the land surface and water change with channel aggradation, erosion, avulsion, downstream translation of bedforms, and when flooding causes floodplain sedimentation [*Pizzuto*, 1994; *Gay et al.*, 1998; *Moody and Meade*, 2008]. Therefore, selecting a static elevation does not fully represent a tree's relationship to the river. Furthermore, tree roots access water, but below-ground root distribution is unknown without mechanical [*Scott et al.*, 1997; *Holloway et al.*, 2016] or hydraulic [*Rood et al.*, 2011] excavation. *Populus* root distribution is a function of soil moisture conditions and water table depth across the continent [*Sprackling and Read*, 1979; *Shafroth et*

al., 2000; *Rood et al.*, 2011]. Therefore, the elevations I identified may poorly represent root distributions and access to groundwater for the sampled trees.

4.5.6 Potential for improved flow reconstructions and study implications

This study supports the tenet that tree ring variability from a population better expresses climate compared to that from individual trees. The simple example presented of creating alternative flow reconstructions from subsetted groups suggests that dendrochronologists can exploit multiple signals within a population. Systematically separating cores and recombining them in a multiple regression framework improved tree ring correspondence to measured flow. The best flow reconstruction model positively loaded Group 1 cores and negatively loaded Group 2 cores, thereby using Group 2 cores to suppress some of the ring width variation in Group 1 that was due to non-flow factors. This strategy of using the growth of some trees to remove some of the undesired signal could have widespread applicability in dendrochronology. This approach could be extended, for example, by explicitly grouping cores by correlations to flow only. Subsetting cores has the potentially undesirable effect of decreasing the length of flow reconstructions, but record shortening may be acceptable depending on goals. Researchers often create flow reconstructions using populations from different locations to create groups of predictors *a priori*. Future flow reconstructions may benefit from exploiting the multiple signals expressed from within a site, thereby allowing the growth patterns themselves to inform groupings to improve reconstructions.

Modern floodplains are shaped by land and water management decisions. Western *Populus* forests require river-derived groundwater for establishment and survival, and

regulated flows reduce tree ring growth [*Schook et al.*, 2016a], cause branch sacrifice (Rood et al 2000), or foreshadow tree death [*Rood et al.*, 1995; *Cooper et al.*, 2003b]. Instead of being a homogenous habitat, floodplain forests are the sum of many individual trees that acquire and process water according to tree-specific characteristics related to proximity from the river and groundwater access [*Singer et al.*, 2014]. When river forms and flows change, some patches of trees may die while others are unaffected [*Scott et al.*, 2000]. Floodplain forests have innate value for the biodiversity and ecosystem processes they support, and this translates to recreational and aesthetic value for people. Given the concurrent dependence on water by people and nature, wise management necessitates science-informed decisions and a watershed perspective.

5. CONCLUSIONS

5.1 Summary

Rivers and floodplains are vital ecosystems in the semi-arid western Great Plains. Because most floodplains in the region have been converted to agriculture, the remaining forest is even more valuable for environmental processes, biota, and people. In this dissertation, I integrated fluvial geomorphology, hydrology, dendrochronology, and ecology to build a multi-disciplinary understanding of how past events have created modern river environments in the Upper Missouri River Basin.

The cottonwood-based flow reconstructions are the first discharge extensions for the Powder and Yellowstone Rivers. Combined with the Little Missouri, all three reconstructed rivers had cottonwood growth that was strongly correlated with log-transformed discharge in the runoff season. The reconstructions explained 57-58% of the variance in historical flows and extended back to 1742, 1729 and 1643 at the Yellowstone, Powder, and Little Missouri Rivers. The Regional Curve Standardization (RCS) detrended chronologies preserved low-frequency variation in the tree ring data and produced reconstructions showing a prolonged wet period from 1870-1980 at all three sites. Reconstructions also revealed droughts and wet periods in the 1800s more extreme than any in the historical record. Declines in cottonwood growth at the Yellowstone and Powder Rivers beginning in the mid-to-late 1900s are partly attributable to water management, which delayed a portion of the runoff until after the early-summer period when most tree ring growth occurs. These flow reconstructions, created from only three cottonwood predictor chronologies, explained at least as much variance as nearby reconstructions for headwater streamgages that incorporated multiple tree ring series, multiple

species, and multiple climate proxies. This study can be used to inform water management and serve as a launching point for future flow reconstructions in the Upper Missouri River Basin and across the Northern Hemisphere, where riparian *Populus* trees are common.

Fluvial geomorphic processes are affected by the layered, complex and delayed responses induced by flows, climate, and land uses. Using historical air photos, repeated cross section surveys and cottonwood age transects, I show that channel migration on the Powder River has decreased, and the recent past (1975-2014) is not representative of fluvial processes over the past two centuries. Even though the Powder River is a snowmelt dominated river where the variability of interannual floods is usually low, the largest floods appear to have produced years-to-decades of channel response. The relatively small peak annual floods from the past three decades contributed to channel migration occurring half as fast in the 39-year channel cross-section period (0.81 m/yr) compared to the 74- and 184-year periods captured by air photos (1.52 m/yr) and cottonwood transects (1.62 m/yr). It is common practice to use annual migration rates to describe geomorphic processes, but scaling measurements need be done with consideration of the temporal scales of data collection and process variability. High flows cause channel migration because they erode and widen the channel, enabling point bar formation. These processes in turn lead to floodplain turnover and habitat creation. Although channel migration occurs at discrete locations in a river channel, the rate at which it occurs results from nested interactions ranging up to watershed-scales, so integrating multiple research approaches builds a stronger understanding of the processes affecting it. Information learned from the Powder River can aid in interpretation of channel migration across geographic and hydroclimatic settings.

I also analyzed tree-scale climate signals in cottonwood tree rings from the Yellowstone River floodplain. The findings support a central concept in dendrochronology, that the average growth of many trees better reflects climate compared to the patterns expressed by individual trees. I found that deviation from the site-level growth patterns was not random, and basic biological and spatial factors affected the relationships between tree rings and flow, precipitation, and temperature. Cottonwood growth was more closely related to river flow than to precipitation or temperature. Proximity to the channel affected the strength of these connections, as did water availability in each year. Trees more proximal to the river were better correlated to flow than more distant trees, and the strongest connections were with the fastest growing trees, further suggesting that river water promotes tree growth. Because river corridors are dynamic environments, a tree's proximity to the river changes through time. These findings suggest that tree ring signals within a tree may evolve with geomorphic changes. Although time-invariance is a common assumption of tree ring-based climate reconstructions, I found older trees to more closely correspond to non-growing season flow and climate, and younger trees better correspond to July rain. This finding would have been problematic if my reconstructions had not been created from multi-aged trees. Separating cores based on common flow and climate responses, then recombining them using a multiple regression framework showed that variable tree ring responses to climate can improve flow reconstructions. Recognition of the factors that affect tree ring growth across trees and years can improve future tree ring collection efforts, interpretation of growth patterns, flow reconstructions, and water management.

5.2 Broader Impacts and Emergent Ideas

In this dissertation, I built on previous research to expand the knowledge and application of cottonwood-based flow reconstructions. Other flow reconstructions have benefited from including multiple species because each can express a different component of the regional hydroclimate. An obstacle of combining floodplain cottonwoods with upland trees is that upland tree rings cannot reflect changes in river flow due to changing runoff processes. Floodplain trees connected to the alluvial water table do reflect changes in runoff, even small ones due to climate or irrigation extraction, such as occurs at the study rivers. Compatibility between floodplain and upland trees would presumably converge prior to the period of manipulated runoff, but calibrating these relationships remains a challenge to overcome.

Cottonwoods grow across a wide variety of rivers in the region, demonstrating that multiple conditions can support their establishment and survival. However, there remains substantial room for exploration of regional cottonwood growth patterns in relation to their local environment. Future research could integrate plains and narrowleaf cottonwoods, as researchers have identified similarities between these and other *Populus* species found within the same region [*Rood et al.*, 2011; *Wilding et al.*, 2014]. Integrating tree core collections across sites will further advance understanding of the factors leading to cottonwood regeneration, growth, and death. Planned cottonwood research in the Wind River Range will complement existing datasets from the Upper Yellowstone, Lower Yellowstone, Powder, Little Missouri, Missouri, Redwater, Upper Green, Lower Green, Yampa, and ephemeral rivers in eastern Colorado [*Friedman and Lee*, 2002; *Merigliano et al.*, 2013; *Edmondson et al.*, 2014; *Meko et al.*, 2015; *Schook et al.*, 2016a, 2016b; *Friedman and Schook*, unpub data]. Increased knowledge of

cottonwood ecology is beneficial to land managers, who recognize floodplain forests as valuable corridors within relatively barren uplands.

The flow regime is the most important aspect of river and floodplain environments, mobilizing sediment, rearranging landforms, creating disturbances, and providing life [*Poff et al.*, 1997; *Wohl et al.*, 2015]. Considering that invasive species are prolific along Western rivers [*Friedman et al.*, 2005b; *Merritt and Poff*, 2010] and at least 90% of total river flow in the USA is strongly affected by channel fragmentation [*Jackson et al.*, 2001], continued research is required to determine how much river alteration is acceptable [*Poff et al.*, 2010]. The Yellowstone, Powder, and Little Missouri Rivers still maintain flow regimes consistent with their historical seasonal variability. I have shown that peak flows in the early summer are the most important for cottonwood growth and channel migration, but it is these peak flows that are often shaved off by flow regulators for later use. Beyond flow regulation, changes to flow are also occurring because of evolving relationships in temperature, precipitation, and runoff processes [*Stewart et al.*, 2005; *Clow*, 2010; *Griffin and Friedman*, in revision]. Moving forward, rivers will continue to express environmental changes, and our enhanced interpretation of these expressions will improve land and water management.

6. REFERENCES

Albertson, F. W., and J. E. Weaver (1945), Injury and death or recovery of trees in prairie climate, Ecol. Monogr., 15(4), 393–433, doi:10.2307/1948428.

Albright, W. L., and D. L. Peterson (2013), Tree growth and climate in the Pacific Northwest, North America: a broad-scale analysis of changing growth environments, J. Biogeogr., 40(11), 2119–2133, doi:10.1111/jbi.12157.

Allen, E. B., T. M. Rittenour, R. J. DeRose, M. F. Bekker, R. Kjelgren, and B. M. Buckley (2013), A tree-ring-based reconstruction of Logan River streamflow, northern Utah, Water Resour. Res., 8579-8588, doi:10.1002/2013WR014273.

Amlin, N. M., and S. B. Rood (2003), Drought stress and recovery of riparian cottonwoods due to water table alteration along Willow Creek, Alberta, Trees, 17(4), 351–358, doi:10.1007/s00468-003-0245-3.

Andersen, D. C., D. J. Cooper, and K. Northcott (2007), Dams, floodplain land use, and riparian forest conservation in the semiarid Upper Colorado River Basin, USA, Environ. Manage., 40(3), 453–475, doi:10.1007/s00267-006-0294-7.

Auble, G. T., and M. L. Scott (1998), Fluvial disturbance patches and cottonwood recruitment along the upper Missouri River, Montana, Wetlands, 18(4), 546–556, doi:10.1007/BF03161671.

Ault, T. R., J. E. Cole, J. T. Overpeck, G. T. Pederson, S. St. George, B. Otto-Bliesner, C. A. Woodhouse, and C. Deser (2013), The continuum of hydroclimate variability in western North America during the last millennium, J. Clim., 26(16), 5863–5878, doi:10.1175/JCLI-D-11-00732.1.

Ault, T. R., J. E. Cole, J. T. Overpeck, G. T. Pederson, and D. M. Meko (2014), Assessing the risk of persistent drought using climate model simulations and paleoclimate data, J. Clim., 27(20), 7529–7549, doi:10.1175/JCLI-D-12-00282.1.

Barlow, M., S. Nigam, and E. H. Berbery (2001), ENSO, pacific decadal variability, and U.S. summertime precipitation, drought, and stream flow, J. Clim., 14(9), 2105–2128, doi:10.1175/1520-0442(2001)014<2105:EPDVAU>2.0.CO;2.

Belmecheri, S., F. Babst, E. R. Wahl, D. W. Stahle, and V. Trouet (2016), Multi-century evaluation of Sierra Nevada snowpack, Nat. Clim. Change, 6, 2–3, doi:10.1038/nclimate2809.

Benito, G. et al. (2004), Use of systematic, palaeoflood and historical data for the improvement of flood risk estimation. Review of scientific methods, Nat. Hazards, 31(3), 623–643, doi:10.1023/B:NHAZ.0000024895.48463.eb.

Benjankar, R., M. Burke, E. Yager, D. Tonina, G. Egger, S. B. Rood, and N. Merz (2014), Development of a spatially-distributed hydroecological model to simulate cottonwood seedling recruitment along rivers, J. Environ. Manage., 145, 277–288, doi:10.1016/j.jenvman.2014.06.027.

Birken, A. S., and D. J. Cooper (2006), Processes of Tamarix invasion and floodplain development along the lower Green River, Utah, Ecol. Appl., 16(3), 1103–1120.

Black, B. A., J. J. Colbert, and N. Pederson (2008), Relationships between radial growth rates and lifespan within North American tree species, Ecoscience, 15(3), 349–357, doi:10.2980/15-3-3149.

Bradley, R. S., and P. D. Jonest (1993), "Little Ice Age" summer temperature variations: their nature and relevance to recent global warming trends, The Holocene, 3(4), 367–376, doi:10.1177/095968369300300409.

Brandt, S. A. (2000), Classification of geomorphological effects downstream of dams, CATENA, 40(4), 375–401, doi:10.1016/S0341-8162(00)00093-X.

Brienen, R. J. W., E. Gloor, and P. A. Zuidema (2012), Detecting evidence for CO2 fertilization from tree ring studies: The potential role of sampling biases, Glob. Biogeochem. Cycles, 26(1), GB1025, doi:10.1029/2011GB004143.

Briffa, K. R., and T. M. Melvin (2011), A closer look at regional curve standardization of tree-ring records: justification of the need, a warning of some pitfalls, and suggested improvements in its application, in Dendroclimatology, edited by M. K. Hughes, T. W. Swetnam, and H. F. Diaz, pp. 113–145, Springer Netherlands.

Briffa, K. R., P. D. Jones, T. S. Bartholin, D. Eckstein, F. H. Schweingruber, W. Karlén, P. Zetterberg, and M. Eronen (1992), Fennoscandian summers from AD 500: temperature changes on short and long timescales, Clim. Dyn., 7(3), 111–119, doi:10.1007/BF00211153.

Briffa, K. R., T. M. Melvin, T. J. Osborn, R. M. Hantemirov, A. V. Kirdyanov, V. S. Mazepa, S. G. Shiyatov, and J. Esper (2013), Reassessing the evidence for tree-growth and inferred temperature change during the Common Era in Yamalia, northwest Siberia, Quat. Sci. Rev., 72, 83–107, doi:10.1016/j.quascirev.2013.04.008.

Brown, D. P., and A. C. Comrie (2004), A winter precipitation "dipole" in the western United States associated with multidecadal ENSO variability, Geophys. Res. Lett., 31(9), L09203, doi:10.1029/2003GL018726.

Bunde, A., U. Büntgen, J. Ludescher, J. Luterbacher, and H. von Storch (2013), Is there memory in precipitation?, Nat. Clim. Change, 3(3), 174–175, doi:10.1038/nclimate1830.

Bunn, A. et al. (2016), dplR: Dendrochronology Program Library in R, v 1.6.4, http://cran.r-project.org/web/packages/dplR/index.html.

Büntgen, U., D. Frank, R. Wilson, M. Carrer, C. Urbinati, and J. Esper (2008), Testing for tree-ring divergence in the European Alps, Glob. Change Biol., 14(10), 2443–2453, doi:10.1111/j.1365-2486.2008.01640.x.

Butler, J. J., G. J. Kluitenberg, D. O. Whittemore, S. P. Loheide, W. Jin, M. A. Billinger, and X. Zhan (2007), A field investigation of phreatophyte-induced fluctuations in the water table, Water Resour. Res., 43(2), W02404, doi:10.1029/2005WR004627.

Cadol, D., S. L. Rathburn, and D. J. Cooper (2011), Aerial photographic analysis of channel narrowing and vegetation expansion in Canyon De Chelly National Monument, Arizona, USA, 1935–2004, River Res. Appl., 27(7), 841–856, doi:10.1002/rra.1399.

Carrer, M., and C. Urbinati (2004), Age-dependent tree-ring growth responses to climate in *Larix decidua* and *Pinus cembra*, Ecology, 85(3), 730–740, doi:10.1890/02-0478.

Ceulemans, R., and J. G. Isebrands (1996), Carbon acquisition and allocation, in Biology of *Populus* and its implications for management and conservation., pp. 355–400, NRC Research Press, Ottawa.

Chase, K. J. (2013), Streamflow statistics for unregulated and regulated conditions for selected locations on the Yellowstone, Tongue, and Powder Rivers, Montana, 1928-2002, Scientific Investigations Report, U.S. Geological Survey 2013-5173.

Chase, K. J. (2014), Streamflow statistics for unregulated and regulated conditions for selected locations on the upper Yellowstone and Bighorn Rivers, Montana and Wyoming, 1928-2002, Scientific Investigations Report, U.S. Geological Survey 2014-5115.

Cleaveland, M. K. (2000), A 963-year reconstruction of summer (JJA) streamflow in the White River, Arkansas, USA, from tree-rings, The Holocene, 10(1), 33–41, doi:http://dx.doi.org/10.1191/095968300666157027.

Clow, D. W. (2010), Changes in the timing of snowmelt and streamflow in Colorado: a response to recent warming, J. Clim., 23(9), 2293–2306, doi:10.1175/2009JCLI2951.1.

Coble, A. P., and T. E. Kolb (2012), Riparian tree growth response to drought and altered streamflow along the Dolores River, Colorado, West. J. Appl. For., 27(4), 205–211, doi:10.5849/wjaf.12-001.

Cook, E. R., and L. A. Kairiukstis (2013), Methods of dendrochronology: Applications in the environmental sciences, Springer Science & Business Media.

Cook, E. R., and K. Peters (1981), The smoothing spline: a new approach to standardizing forest interior tree-ring width series for dendroclimatic studies., Tree Ring Bull 41, 45-53.

Cook, E. R., C. A. Woodhouse, Eakin, C. Mark, D. M. Meko, and Stahle, David W. (2004), Long-term aridity changes in the western United States, Science, 306, 1015–1018, doi:10.1126/science.1102586.

Cook, E. R., et al. (2008), North American summer PDSI reconstructions, version 2a. IGBP PAGES/World Data Center for Paleoclimatology Data Contribution Series # 2008-046, NOAA/NGDC Paleoclimatology Program, Boulder, CO.

Cook, E. R., J. G. Palmer, M. Ahmed, C. A. Woodhouse, P. Fenwick, M. U. Zafar, M. Wahab, and N. Khan (2013), Five centuries of Upper Indus River flow from tree rings, J. Hydrol., 486, 365–375, doi:10.1016/j.jhydrol.2013.02.004.

Cooper, D. J., and D. C. Andersen (2012), Novel plant communities limit the effects of a managed flood to restore riparian forests along a large regulated river, River Res. Appl., 28(2), 204–215, doi:10.1002/rra.1452.

Cooper, D. J., D. C. Andersen, and R. A. Chimner (2003a), Multiple pathways for woody plant establishment on floodplains at local to regional scales, J. Ecol., 91(2), 182–196.

Cooper, D. J., D. R. D'Amico, and M. L. Scott (2003b), Physiological and morphological response patterns of *Populus deltoides* to alluvial groundwater pumping, Environ. Manage., 31(2), 215–226, doi:10.1007/s00267-002-2808-2.

Costa, M. H., A. Botta, and J. A. Cardille (2003), Effects of large-scale changes in land cover on the discharge of the Tocantins River, Southeastern Amazonia, J. Hydrol., 283(1–4), 206–217, doi:10.1016/S0022-1694(03)00267-1.

Daly, C., M. Halbleib, J. I. Smith, W. P. Gibson, M. K. Doggett, G. H. Taylor, J. Curtis, and P. P. Pasteris (2008), Physiographically sensitive mapping of climatological temperature and precipitation across the conterminous United States, Int. J. Climatol., 28(15), 2031–2064, doi:10.1002/joc.1688.

D'Arrigo, R., R. Wilson, and G. Jacoby (2006), On the long-term context for late twentieth century warming, J. Geophys. Res. Atmospheres, 111(D3), D03103, doi:10.1029/2005JD006352.

D'Arrigo, R., R. Wilson, B. Liepert, and P. Cherubini (2008), On the "divergence problem" in northern forests: a review of the tree-ring evidence and possible causes, Glob. Planet. Change, 60(3–4), 289–305, doi:10.1016/j.gloplacha.2007.03.004.

Deacon, J. R., C. J. Lee, P. L. Toccalino, M. P. Warren, N. T. Baker, C. G. Crawford, R. G. Gilliom, and M. D. Woodside (2015), Tracking water-quality of the Nation's rivers and streams, USGS Fact Sheet 149-97.

Dean, D. J., M. L. Scott, P. B. Shafroth, and J. C. Schmidt (2011), Stratigraphic, sedimentologic, and dendrogeomorphic analyses of rapid floodplain formation along the Rio Grande in Big Bend National Park, Texas, Geol. Soc. Am. Bull., 123(9–10), 1908–1925, doi:10.1130/B30379.1.

Dettinger, M. D., D. R. Cayan, H. F. Diaz, and D. M. Meko (1998), North-south precipitation patterns in western North America on interannual-to-decadal timescales, J. Clim., 11(12), 3095–3111.

Dickmann, D. I., Z. Liu, P. V. Nguyen, and K. S. Pregitzer (1992), Photosynthesis, water relations, and growth of two hybrid *Populus* genotypes during a severe drought, Can. J. For. Res., 22(8), 1094–1106, doi:10.1139/x92-145.

Dixon, M. D., W. C. Johnson, M. L. Scott, D. E. Bowen, and L. A. Rabbe (2012), Dynamics of plains cottonwood (*Populus deltoides*) forests and historical landscape change along unchannelized segments of the Missouri River, USA, Environ. Manage., 49(5), 990–1008, doi:10.1007/s00267-012-9842-5.

Dufour, S., M. Rinaldi, H. Piégay, and A. Michalon (2015), How do river dynamics and human influences affect the landscape pattern of fluvial corridors? Lessons from the Magra River, Central–Northern Italy, Landsc. Urban Plan., 134, 107–118, doi:10.1016/j.landurbplan.2014.10.007.

Edmondson, J., J. Friedman, D. Meko, R. Touchan, J. Scott, and A. Edmondson (2014), Dendroclimatic potential of plains cottonwood (*Populus deltoides* Subsp. *monilifera*) from the northern Great Plains, USA, Tree-Ring Res., 70(1), 21–30, doi:10.3959/1536-1098-70.1.21.

Enfield, D. B., A. M. Mestas-Nuñez, and P. J. Trimble (2001), The Atlantic Multidecadal Oscillation and its relation to rainfall and river flows in the continental U.S., Geophys. Res. Lett., 28(10), 2077–2080, doi:10.1029/2000GL012745.

Erskine, W., C. McFadden, and P. Bishop (1992), Alluvial cutoffs as indicators of former channel conditions, Earth Surf. Process. Landf., 17(1), 23–37, doi:10.1002/esp.3290170103.

Erskine, W., A. Keene, R. Bush, M. Cheetham, and A. Chalmers (2012), Influence of riparian vegetation on channel widening and subsequent contraction on a sand-bed stream since European settlement: Widden Brook, Australia, Geomorphology, 147–148, 102–114, doi:10.1016/j.geomorph.2011.07.030.

Ettl, G. J., and D. L. Peterson (1995), Extreme climate and variation in tree growth: individualistic response in subalpine fir (*Abies lasiocarpa*), Glob. Change Biol., 1(3), 231–241, doi:10.1111/j.1365-2486.1995.tb00024.x.

Everitt, B. L. (1968), Use of the cottonwood in an investigation of the recent history of a flood plain, Am. J. Sci., 266(6), 417–439, doi:10.2475/ajs.266.6.417.

Favaro, E. A., and S. F. Lamoureux (2015), Downstream patterns of suspended sediment transport in a High Arctic river influenced by permafrost disturbance and recent climate change, Geomorphology, 246, 359–369, doi:10.1016/j.geomorph.2015.06.038.

Fenn, E. A. (2014), Encounters at the heart of the world : a history of the Mandan people, First Edition., Hill and Wang, New York City.

Fonstad, M. A., J. T. Dietrich, B. C. Courville, J. L. Jensen, and P. E. Carbonneau (2013), Topographic structure from motion: a new development in photogrammetric measurement, Earth Surf. Process. Landf., 38(4), 421–430, doi:10.1002/esp.3366.

Franke, J., D. Frank, C. C. Raible, J. Esper, and S. Brönnimann (2013), Spectral biases in tree-ring climate proxies, Nat. Clim. Change, 3(4), 360–364, doi:10.1038/nclimate1816.

Fremier, A. K., E. H. Girvetz, S. E. Greco, and E. W. Larsen (2014), Quantifying process-based mitigation strategies in historical context: separating multiple cumulative effects on river meander migration, PLoS ONE, 9(6), doi:10.1371/journal.pone.0099736.

Friedman, J. M., and V. J. Lee (2002), Extreme floods, channel change, and riparian forests along ephemeral streams, Ecol. Monogr., 72(3), 409–425.

Friedman, J. M., W. R. Osterkamp, M. L. Scott, and G. T. Auble (1998), Downstream effects of dams on channel geometry and bottomland vegetation: Regional patterns in the Great Plains, Wetlands, 18(4), 619–633.

Friedman, J. M., K. R. Vincent, and P. B. Shafroth (2005a), Dating floodplain sediments using tree-ring response to burial, Earth Surf. Process. Landf., 30(9), 1077–1091, doi:10.1002/esp.1263.

Friedman, J. M., G. T. Auble, P. B. Shafroth, M. L. Scott, M. F. Merigliano, M. D. Freehling, and E. R. Griffin (2005b), Dominance of non-native riparian trees in western USA, Biol. Invasions, 7(4), 747–751, doi:http://dx.doi.org/10.1007/s10530-004-5849-z.

Friedman, J. M., J. E. Roelle, and B. S. Cade (2011), Genetic and environmental influences on leaf phenology and cold hardiness of native and introduced riparian trees, Int. J. Biometeorol., 55(6), 775–87, doi:http://dx.doi.org.ezproxy2.library.colostate.edu:2048/10.1007/s00484-011-0494-6.

Fritts, H. C. (1976), Tree rings and climate, Academic Press, New York.

Gay, G. R., H. H. Gay, W. H. Gay, H. A. Martinson, R. H. Meade, and J. A. Moody (1998), Evolution of cutoffs across meander necks in Powder River, Montana, USA, Earth Surf. Process. Landf., 23(7), 651–662, doi:10.1002/(SICI)1096-9837(199807)23:7<651::AID-ESP891>3.0.CO;2-V.

Gottesfeld, A. S., and L. M. J. Gottesfeld (1990), Floodplain dynamics of a wandering river, dendrochronology of the Morice River, British Columbia, Canada, Geomorphology, 3(2), 159–179.

Graumlich, L. J., M. F. J. Pisaric, L. A. Waggoner, J. S. Littell, and J. C. King (2003), Upper Yellowstone River flow and teleconnections with Pacific basin climate variability during the past three centuries, Clim. Change, 59(1), 245–262.

Gray, S. T., and G. J. McCabe (2010), A combined water balance and tree ring approach to understanding the potential hydrologic effects of climate change in the central Rocky Mountain region, Water Resour. Res., 46(5), W05513, doi:10.1029/2008WR007650.

Grissino-Mayer, H. D. (2001), Evaluating crossdating accuracy: A manual and tutorial for the computer program COFECHA, Tree-Ring Res., 57(2), 205–221.

Grover, N. C. (1925), Contributions to the hydrology of the United States, 1923-1924, Water Supply Paper 520, USGS, Washington, D.C.

Güneralp, İ., J. D. Abad, G. Zolezzi, and J. Hooke (2012), Advances and challenges in meandering channels research, Geomorphology, 163–164, 1–9, doi:10.1016/j.geomorph.2012.04.011.

Hickin, E. J., and G. C. Nanson (1975), The character of channel migration on the Beatton River, northeast British Columbia, Canada, Geol. Soc. Am. Bull., 86(4), 487–494.

HKM Engineering Inc. (2003), Lake DeSmet level II master plan and reservoir rehabilitation plan, Final Report, Sheridan, WY.

Hobo, N., B. Makaske, J. Wallinga, and H. Middelkoop (2014), Reconstruction of eroded and deposited sediment volumes of the embanked River Waal, the Netherlands, for the period AD 1631-present, Earth Surf. Process. Landf., 39(10), 1301–1318, doi:10.1002/esp.3525.

Holloway, J. V., M. C. Rillig, and A. M. Gurnell (2016), Underground riparian wood: Buried stem and coarse root structures of black poplar (*Populus nigra* L), Geomorphology, doi:10.1016/j.geomorph.2016.08.002.

Holmes, R. L. (1983), Computer-assisted quality control in tree-ring dating and measurement, Tree-Ring Bull., 43, 69–78.

Hooke, J. (1980), Magnitude and distribution of rates of river bank erosion, Earth Surf. Process. Landf., 5(2), 143–157, doi:10.1002/esp.3760050205.

Hooke, J. M. (2007), Spatial variability, mechanisms and propagation of change in an active meandering river, Geomorphology, 84(3–4), 277–296, doi:10.1016/j.geomorph.2006.06.005.

Hudson, P. F., and R. H. Kesel (2000), Channel migration and meander-bend curvature in the lower Mississippi River prior to major human modification, Geology, 28(6), 531–534, doi:10.1130/0091-7613(2000)28<531:CMAMCI>2.0.CO;2.

Hughes, F. M. R. (1997), Floodplain biogeomorphology, Prog. Phys. Geogr., 21(4), 501–529, doi:10.1177/030913339702100402.

Hughes, M. L., P. F. McDowell, and W. A. Marcus (2006), Accuracy assessment of georectified aerial photographs: Implications for measuring lateral channel movement in a GIS, Geomorphology, 74(1–4), 1–16, doi:10.1016/j.geomorph.2005.07.001.

Hultine, K. R., K. G. Burtch, and J. R. Ehleringer (2013), Gender specific patterns of carbon uptake and water use in a dominant riparian tree species exposed to a warming climate, Glob. Change Biol., 19, 3390–3405, doi: 10.1111/gcb.12230.

Hurrell, J. W. (1996), Influence of variations in extratropical wintertime teleconnections on northern hemisphere temperature, Geophys. Res. Lett., 23(6), 665–668, doi:10.1029/96GL00459.

Jackson, R. B., S. R. Carpenter, C. N. Dahm, D. M. McKnight, R. J. Naiman, S. L. Postel, and S. W. Running (2001), Water in a Changing World, Ecol. Appl., 11(4), 1027–1045, doi:10.2307/3061010.

Johnson, W. C. (1994), Woodland expansions in the Platte River, Nebraska: Patterns and causes, Ecol. Monogr., 64(1), 45–84, doi:10.2307/2937055.

Johnson, W. C., M. D. Dixon, M. L. Scott, L. Rabbe, G. Larsen, M. Volke, and B. Werner (2012), Forty years of vegetation change on the Missouri River floodplain, BioScience, 62(2), 123–135, doi:10.1525/bio.2012.62.2.6.

Jones, J. L. (2006), Side channel mapping and fish habitat suitability analysis using lidar topography and orthophotography, Photogramm. Eng. Remote Sens., 72(11), 1202.

Jones, P. D. et al. (2009), High-resolution palaeoclimatology of the last millennium: a review of current status and future prospects, The Holocene, 19(1), 3–49, doi:http://dx.doi.org.ezproxy2.library.colostate.edu:2048/10.1177/0959683608098952.

Knighton, D. (1998), Fluvial Forms and Processes: A New Perspective, Routledge, pp. 404.

Konrad, C. P. (2012), Reoccupation of floodplains by rivers and its relation to the age structure of floodplain vegetation, J. Geophys. Res. Biogeosciences, 117(G4), G00N13, doi:10.1029/2011JG001906.

Lauer, J. W. (2012), Channel planform statistics toolbox, v 2.0, National Center for Earth-surface Dynamics.

Lawler, D. M. (1993), The measurement of river bank erosion and lateral channel change: A review, Earth Surf. Process. Landf., 18(9), 777–821, doi:10.1002/esp.3290180905.

Leigh, A., and A. B. Nicotra (2003), Sexual dimorphism in reproductive allocation and water use efficiency in *Maireana pyramidata* (Chenopodiaceae), a dioecious, semi-arid shrub, Aust. J. Bot., 51(5), 509, doi:10.1071/BT03043.

Loescher, W. H., T. McCamant, and J. D. Keller (1990), Carbohydrate reserves, translocation, and storage in woody plant roots, HortScience, 25(3), 274–281.

Mahoney, J. M., and S. B. Rood (1998), Streamflow requirements for cottonwood seedling recruitment—An integrative model, Wetlands, 18(4), 634–645, doi:10.1007/BF03161678.

Malevich, S. B., C. A. Woodhouse, and D. M. Meko (2013), Tree-ring reconstructed hydroclimate of the Upper Klamath basin, J. Hydrol., 495, 13–22, doi:10.1016/j.jhydrol.2013.04.048.

Manetti, M. C., and A. Cutini (2006), Tree-ring growth of silver fir (*Abies alba* Mill.) in two stands under different silvicultural systems in central Italy, Dendrochronologia, 23(3), 145–150, doi:10.1016/j.dendro.2005.11.002.

van Mantgem, P. J., N.L. Stephenson, J.C. Byrne, L.D. Daniels, J.F. Franklin, P.Z. Fule, M.E. Harmon, A.J. Larson, J.M. Smith, A.H. Taylor, T.T. Veblen (2009), Widespread increase of tree mortality rates in the western United States, Science, 323(5913), 521–524, doi:10.1126/science.1165000.

Marchetto, A. (2015), rkt: Mann-Kendall Test, Seasonal and Regional Kendall Tests. R package version 1.4.

Markonis, Y., and D. Koutsoyiannis (2016), Scale-dependence of persistence in precipitation records, Nat. Clim. Change, 6, 399–401, doi:10.1038/nclimate2894.

Martín-Benito, D., P. Cherubini, M. del Río, and I. Cañellas (2007), Growth response to climate and drought in *Pinus nigra* Arn. trees of different crown classes, Trees, 22(3), 363–373, doi:10.1007/s00468-007-0191-6.

Martinson, H. A., and R. H. Meade (1983), Channel changes of Powder River, 1938-1978, Powder River County, Montana, U.S. Geological Survey Hydrologic Investigations Atlas.

McCabe, G. J., M. A. Palecki, and J. L. Betancourt (2004), Pacific and Atlantic Ocean influences on multidecadal drought frequency in the United States, Proc. Natl. Acad. Sci. U. S. A., 101(12), 4136–4141, doi:10.1073/pnas.0306738101.

Meade, R. H., and J. A. Moody (2013), Erosional and depositional changes wrought by the flood of May 1978 in the channels of Powder River, southeastern Montana, Scientific Investigations Report, USGS Numbered Series, U.S. Geological Survey, Reston, VA.

Meade, R. H., J. A. Moody, and H. A. Martinson (2013), Inundated areas and channel changes wrought by the flood of May 1978 in Powder River between Moorhead and Broadus, southeastern Montana, Scientific Investigations Report, U.S. Geological Survey 2013-5035.

Meko, D. M., R. Touchan, and K. J. Anchukaitis (2011), Seascorr: A MATLAB program for identifying the seasonal climate signal in an annual tree-ring time series, Comput. Geosci., 37(9), 1234–1241, doi:10.1016/j.cageo.2011.01.013.

Meko, D. M., C. A. Woodhouse, and K. Morino (2012), Dendrochronology and links to streamflow, J. Hydrol., 412–413, 200–209, doi:10.1016/j.jhydrol.2010.11.041.

Meko, D. M., J. M. Friedman, R. Touchan, J. R. Edmondson, E. R. Griffin, and J. A. Scott (2015), Alternative standardization approaches to improving streamflow reconstructions with ring-width indices of riparian trees, The Holocene, 25(7), 1093–1101, doi:10.1177/0959683615580181.

Melvin, T. M., and K. R. Briffa (2014a), CRUST: Software for the implementation of Regional Chronology Standardisation: Part 1. Signal-Free RCS, Dendrochronologia, 32(1), 7–20, doi:10.1016/j.dendro.2013.06.002.

Melvin, T. M., and K. R. Briffa (2014b), CRUST: Software for the implementation of Regional Chronology Standardisation: Part 2. Further RCS options and recommendations, Dendrochronologia, 32(4), 343–356, doi:10.1016/j.dendro.2014.07.008.

Merigliano, M. F., J. M. Friedman, and M. L. Scott (2013), 12.10 Tree-ring records of variation in flow and channel geometry, in Treatise on Geomorphology, edited by J. F. Shroder, pp. 145–164, Academic Press, San Diego.

Merritt, D. M., and D. J. Cooper (2000), Riparian vegetation and channel change in response to river regulation: a comparative study of regulated and unregulated streams in the Green River Basin, USA, Regul. Rivers Res. Manag., 16(6), 543–564, doi:10.1002/1099-1646(200011/12)16:6<543::AID-RRR590>3.0.CO;2-N.

Merritt, D. M., and N. L. R. Poff (2010), Shifting dominance of riparian *Populus* and *Tamarix* along gradients of flow alteration in western North American rivers, Ecol. Appl., 20(1), 135–152, doi:10.1890/08-2251.1.

Milan, D. J., G. L. Heritage, and D. Hetherington (2007), Application of a 3D laser scanner in the assessment of erosion and deposition volumes and channel change in a proglacial river, Earth Surf. Process. Landf., 32(11), 1657–1674, doi:10.1002/esp.1592.

Miller, J. R., and J. M. Friedman (2009), Influence of flow variability on floodplain formation and destruction, Little Missouri River, North Dakota, Geol. Soc. Am. Bull., 121(5–6), 752–759, doi:10.1130/B26355.1.

Miřijovský, J., M. Š. Michalková, O. Petyniak, Z. Máčka, and M. Trizna (2015), Spatiotemporal evolution of a unique preserved meandering system in Central Europe — The Morava River near Litovel, CATENA, 127, 300–311, doi:10.1016/j.catena.2014.12.006.

Moody, J. A., and R. H. Meade (1990), Channel changes at cross sections of the Powder River between Moorhead and Broadus, Montana, 1975-88, Open-File Report, USGS Numbered Series, U.S. Geological Survey 2002-4219.

Moody, J. A., and R. H. Meade (2008), Terrace aggradation during the 1978 flood on Powder River, Montana, USA, Geomorphology, 99(1–4), 387–403, doi:10.1016/j.geomorph.2007.12.002.

Moody, J. A., and R. H. Meade (2014), Ontogeny of point bars on a river in a cold semi-arid climate, Geol. Soc. Am. Bull., 126(9–10), 1301–1316, doi:10.1130/B30992.1.

Moody, J. A., J. E. Pizzuto, and R. H. Meade (1999), Ontogeny of a flood plain, Geol. Soc. Am. Bull., 111(2), 291–303, doi:10.1130/0016-7606(1999)111<0291:OOAFP>2.3.CO;2.

Moody, J. A., R. H. Meade, and H. A. Martinson (2002), Erosion and deposition of sediment at channel cross sections on Powder River between Moorhead and Broadus, Montana, 1980-98, Water-Resources Investigations Report, USGS Numbered Series 2002-4219.

Nadler, C. T., and S. A. Schumm (1981), Metamorphosis of South Platte and Arkansas Rivers, Eastern Colorado, Phys. Geog., 2(2), 95-115.

Naiman, R. J., H. Décamps, and M. E. McClain (2005), Riparia: Ecology, Conservation, and Management of Streamside Communities, Elsevier Academic Press, London.

Nakamura, F. and S. Kikuchi (1996), Some methodological developments in the analysis of sediment transport processes using age distribution of floodplain deposits, Geomorphology, 16(2), 139-145, doi:10.1016/0169-555X(95)00139-V.

Nakawatase, J. M., and D. L. Peterson (2006), Spatial variability in forest growth – climate relationships in the Olympic Mountains, Washington, Can. J. For. Res., 36(1), 77–91, doi:10.1139/x05-224.

Nanson, G. C., and J. C. Croke (1992), A genetic classification of floodplains, Geomorphology, 4(6), 459-486, doi:10.1016/0169-555X(92)90039-Q.

Nanson, G., and E. Hickin (1983), Channel migration and incision on the Beatton River, J. Hydraul. Eng., 109(3), 327–337, doi:10.1061/(ASCE)0733-9429(1983)109:3(327).

Nanson, G. C. (1986), Episodes of vertical accretion and catastrophic stripping: A model of disequilibrium flood-plain development, Geol. Soc. Am. Bull., 97(12), 1467–1475, doi:10.1130/0016-7606(1986)97<1467:EOVAAC>2.0.CO;2.

Nicault, A., E. Boucher, C. Bégin, J. Guiot, J. Marion, L. Perreault, R. Roy, M. M. Savard, and Y. Bégin (2014), Hydrological reconstruction from tree-ring multi-proxies over the last two centuries at the Caniapiscau Reservoir, northern Québec, Canada, J. Hydrol., 513, 435–445, doi:10.1016/j.jhydrol.2014.03.054.

Nilsson, C., C. A. Reidy, M. Dynesius, and C. Revenga (2005), Fragmentation and flow regulation of the world's large river systems, Science, 308(5720), 405–408, doi:10.1126/science.1107887.

Oberhuber, W., and W. Kofler (2000), Topographic influences on radial growth of Scots pine (*Pinus sylvestris* L.) at small spatial scales, Plant Ecol., 146(2), 229–238, doi:10.1023/A:1009827628125.

O'Connor, J. E., M. A. Jones, and T. L. Haluska (2003), Flood plain and channel dynamics of the Quinault and Queets Rivers, Washington, USA, Geomorphology, 51(1), 31–59.

Osterkamp, W. R., and E. R. Hedman (1982), Perennial-streamflow characteristics related to channel geometry and sediment in Missouri River basin, Professional Paper, USGS Numbered Series 1242.

Palmer, M. A., C. A. R. Liermann, C. Nilsson, M. Flörke, J. Alcamo, P. S. Lake, and N. Bond (2008), Climate change and the world's river basins: Anticipating management options, Front. Ecol. Environ., 6(2), 81–89.

Patten, D. T. (1998), Riparian ecosystems of semi-arid North America: Diversity and human impacts, Wetlands, 18(4), 498–512.

Pederson, G. T., S. T. Gray, T. Ault, W. Marsh, D. B. Fagre, A. G. Bunn, C. A. Woodhouse, and L. J. Graumlich (2010), Climatic controls on the snowmelt hydrology of the northern Rocky Mountains, J. Clim., 24(6), 1666–1687, doi:10.1175/2010JCLI3729.1.

Pederson, G. T., S. T. Gray, C. A. Woodhouse, J. L. Betancourt, D. B. Fagre, J. S. Littell, E. Watson, B. H. Luckman, and L. J. Graumlich (2011), The unusual nature of recent snowpack declines in the North American cordillera, Science, 333(6040), 332–335, doi:10.1126/science.1201570.

Pederson, G. T., J. L. Betancourt, and G. J. McCabe (2013), Regional patterns and proximal causes of the recent snowpack decline in the Rocky Mountains, U.S., Geophys. Res. Lett., 40(9), 1811–1816, doi:10.1002/grl.50424.

Pederson, G. T. et al. (2016), Multi-century perspectives on current and future streamflow in the Missouri River Basin, Poster, Ameridendro Conference, Mendoza, Argentina.

Pelfini, M., G. Leonelli, and M. Santilli (2006), Climatic and Environmental Influences on Mountain Pine (*Pinus montana* Miller) Growth in the Central Italian Alps, Arct. Antarct. Alp. Res., 38(4), 614–623.

Peng, J., X. Gou, F. Chen, J. Li, P. Liu, and Y. Zhang (2008), Altitudinal variability of climate–tree growth relationships along a consistent slope of Anyemaqen Mountains, northeastern Tibetan Plateau, Dendrochronologia, 26(2), 87–96, doi:10.1016/j.dendro.2007.10.003.

Perry, L. G., P. B. Shafroth, D. M. Blumenthal, J. A. Morgan, and D. R. LeCain (2013), Elevated CO_2 does not offset greater water stress predicted under climate change for native and exotic riparian plants, New Phytol., 197(2), 532–543, doi:10.1111/nph.12030.

Pizzuto, J. E. (1994), Channel adjustments to changing discharges, Powder River, Montana, Geol. Soc. Am. Bull., 106(11), 1494–1501, doi:10.1130/0016-7606(1994)106<1494:CATCDP>2.3.CO;2.

Poff, N. L., J. D. Allan, M. B. Bain, J. R. Karr, K. L. Prestegaard, B. D. Richter, R. E. Sparks, and J. C. Stromberg (1997), The natural flow regime, BioScience, 47(11), 769–784, doi:10.2307/1313099.

Poff, N. L. et al. (2010), The ecological limits of hydrologic alteration (ELOHA): a new framework for developing regional environmental flow standards, Freshw. Biol., 55(1), 147–170, doi:10.1111/j.1365-2427.2009.02204.x.

Powder River County Examiner (1923), Wide open range on Powder River, 12th October.

Radoane, M., C. Nechita, F. Chiriloaei, N. Radoane, I. Popa, C. Roibu, and D. Robu (2015), Late Holocene fluvial activity and correlations with dendrochronology of subfossil trunks: Case studies of northeastern Romania, Geomorphology, 239, 142–159, doi:10.1016/j.geomorph.2015.02.036.

Raffa, K. F., B. H. Aukema, B. J. Bentz, A. L. Carroll, J. A. Hicke, M. G. Turner, and W. H. Romme (2008), Cross-scale drivers of natural disturbances prone to anthropogenic amplification: The dynamics of bark beetle eruptions, BioScience, 58(6), 501–517, doi:10.1641/B580607.

Rannie, W. F. (1999), A survey of hydroclimate, flooding, and runoff in the Red River basin prior to 1870, Geological Survey of Canada, Open File 3705.

Reily, P., and W. Johnson (1982), The effects of altered hydrologic regime on tree growth along the Missouri River in North Dakota, Can. J. Bot.-Rev. Can. Bot., 60(11), 2410–2423.

Richter, B. D., R. Mathews, D. L. Harrison, and R. Wigington (2003), Ecologically sustainable water management: Managing river flows for ecological integrity, Ecol. Appl., 13(1), 206–224.

Rood, S. B., and S. Heinze-Milne (1989), Abrupt downstream forest decline following river damming in southern Alberta, Can. J. Bot., 67(6), 1744–1749, doi:10.1139/b89-221.

Rood, S. B., J. M. Mahoney, D. E. Reid, and L. Zilm (1995), Instream flows and the decline of riparian cottonwoods along the St. Mary River, Alberta, Can. J. Bot., 73(8), 1250–1260.

Rood, S. B., J. H. Braatne, and F. M. R. Hughes (2003), Ecophysiology of riparian cottonwoods: stream flow dependency, water relations and restoration, Tree Physiol., 23(16), 1113–1124, doi:10.1093/treephys/23.16.1113.

Rood, S. B., G. M. Samuelson, J. K. Weber, and K. A. Wywrot (2005), Twentieth-century decline in streamflows from the hydrographic apex of North America, J. Hydrol., 306(1), 215–233.

Rood, S. B., L. A. Goater, J. M. Mahoney, C. M. Pearce, and D. G. Smith (2007), Floods, fire, and ice: disturbance ecology of riparian cottonwoods, Can. J. Bot., 85(11), 1019–1032, doi:10.1139/B07-073.

Rood, S. B., S. G. Bigelow, and A. A. Hall (2011), Root architecture of riparian trees: river cut-banks provide natural hydraulic excavation, revealing that cottonwoods are facultative phreatophytes, Trees, 25(5), 907–917, doi:10.1007/s00468-011-0565-7.

Rood, S. B., D. J. Ball, K. M. Gill, S. Kaluthota, M. G. Letts, and D. W. Pearce (2013), Hydrologic linkages between a climate oscillation, river flows, growth, and wood Δ 13 C of male and female cottonwood trees: Hydrological linkages for riparian cottonwoods, Plant Cell Environ., 36(5), 984–993, doi:10.1111/pce.12031.

Rose, J. R., and D. J. Cooper (2016), The influence of floods and herbivory on cottonwood establishment and growth in Yellowstone National Park: Yellowstone cottonwood establishment, Ecohydrology, doi:10.1002/eco.1768.

Rozas, V., and J. M. Olano (2013), Environmental heterogeneity and neighbourhood interference modulate the individual response of *Juniperus thurifera* tree-ring growth to climate, Dendrochronologia, 31(2), 105–113, doi:10.1016/j.dendro.2012.09.001.

Rozas, V., L. DeSoto, and J. M. Olano (2009), Sex-specific, age-dependent sensitivity of tree-ring growth to climate in the dioecious tree *Juniperus thurifera*, New Phytol., 182(3), 687–697, doi:10.1111/j.1469-8137.2009.02770.x.

Ryan, M. G., D. Binkley, J. H. Fownes, C. P. Giardina, and R. S. Senock (2004), An experimental test of the causes of forest growth decline with stand age, Ecol. Monogr., 74(3), 393–414, doi:10.1890/03-4037.

Salas, J. D., Z. Tarawneh, and F. Biondi (2015), A hydrological record extension model for reconstructing streamflows from tree-ring chronologies, Hydrol. Process., 29(4), 544–556, doi:10.1002/hyp.10160.

Schook, D. M., E. A. Carlson, J. S. Sholtes, and D. J. Cooper (2016a), Effects of moderate and extreme flow regulation on *Populus* growth along the Green and Yampa Rivers, Colorado and Utah, River Res. Appl., 32, 1698–1708, doi:10.1002/rra.3020.

Schook, D. M., J. M. Friedman, and S. L. Rathburn (2016b), Flow reconstructions in the Upper Missouri River Basin using riparian tree rings, Water Resour. Res., 52, 8159-8173, doi:10.1002/2016WR018845.

Schook, D. M., S. L. Rathburn, J. M. Friedman, and J. M. Wolf (in review), Declining channel migration rates on a free-flowing meandering river, Geomorphology.

Schumm, S. A. (1973), Geomorphic thresholds and complex response of drainage systems, Fluv. Geomorphol., 6, 69–85.

Schumm, S. A., and R. W. Lichty (1963), Channel widening and flood-plain construction along Cimarron River in southwestern Kansas, Professional Paper, USGS Numbered Series 352-D.

Scott, M. L., J. M. Friedman, and G. T. Auble (1996), Fluvial process and the establishment of bottomland trees, Geomorphology, 14(4), 327–339, doi:10.1016/0169-555X(95)00046-8.

Scott, M. L., G. T. Auble, and J. M. Friedman (1997), Flood dependency of cottonwood establishment along the Missouri River, Montana, USA, Ecol. Appl., 7(2), 677–690, doi:10.1890/1051-0761(1997)007[0677:FDOCEA]2.0.CO;2.

Scott, M. L., P. B. Shafroth, and G. T. Auble (1999), Responses of riparian cottonwoods to alluvial water table declines, Environ. Manage., 23(3), 347–358, doi:10.1007/s002679900191.

Scott, M. L., G. C. Lines, and G. T. Auble (2000), Channel incision and patterns of cottonwood stress and mortality along the Mojave River, California, J. Arid Environ., 44(4), 399–414, doi:10.1006/jare.1999.0614.

Shafroth, P. B., J. C. Stromberg, and D. T. Patten (2000), Woody riparian vegetation response to different alluvial water table regimes, West. North Am. Nat., 60(1), 66–76.

Shafroth, P. B., J. C. Stromberg, and D. T. Patten (2002), Riparian vegetation response to altered disturbance and stress regimes, Ecol. Appl., 12(1), 107–123, doi:10.1890/1051-0761(2002)012[0107:RVRTAD]2.0.CO;2.

Sheppard, P. A., P. Cassals, and E. Gutiérrez (2001), Relationships between ring-width variation and soil nutrient availability at the tree scale, Tree-Ring Res, 51(1), 105-113.

Shindell, D. T., G. A. Schmidt, R. L. Miller, and M. E. Mann (2003), Volcanic and solar forcing of climate change during the preindustrial era, J. Clim., 16(24), 4094–4107, doi:10.1175/1520-0442(2003)016<4094:VASFOC>2.0.CO;2.

Sieg, C. H., D. Meko, A. D. DeGaetano, and W. Ni (1996), Dendroclimatic potential in the northern Great Plains, *in* Tree Rings, Environment and Humanityedited by J. S. Dean, D. M. Meko, and T. W. Swetnam, pp. 295–302 Proceedings of the International Conference, Tucson, Arizona, 17–21 May 1994, Tucson, Radiocarbon.

Sigafoos, R. S. (1964), Botanical evidence of floods and flood-plain deposition, Geological Survey Professional Paper 485-A, USGS, Washington, D.C.

Singer, M. B., C. I. Sargeant, H. Piégay, J. Riquier, R. J. S. Wilson, and C. M. Evans (2014), Floodplain ecohydrology: Climatic, anthropogenic, and local physical controls on partitioning of water sources to riparian trees, Water Resour. Res., 50(5), 4490–4513, doi:10.1002/2014WR015581.

Slack, J. R., and J. M. Landwehr (1992), Hydro-climatic data network (HCDN); a U.S. Geological Survey streamflow data set for the United States for the study of climate variations, 1874-1988, Open-File Report 92-129, USGS.

Smith, K. T. (2008), An organismal view of dendrochronology, Dendrochronologia, 26(3), 185–193, doi:10.1016/j.dendro.2008.06.002.

Snyder, K. A., and D. G. Williams (2000), Water sources used by riparian trees varies among stream types on the San Pedro River, Arizona, Agric. For. Meteorol., 105(1–3), 227–240, doi:10.1016/S0168-1923(00)00193-3.

Speer, J. H. (2010), Fundamentals of Tree-Ring Research, The University of Arizona Press, Tuscon, AZ.

Sprackling, J. A., and R. E. Read (1979), Tree root systems in eastern Nebraska, Neb. Conserv. Bull. Linc. NE, 37, 73pp.

St. George, S. (2014), An overview of tree-ring width records across the Northern Hemisphere, Quat. Sci. Rev., 95, 132–150, doi:10.1016/j.quascirev.2014.04.029.

Stahle, D. W., E. R. Cook, M. K. Cleaveland, M. D. Therrell, D. M. Meko, H. D. Grissino-Mayer, E. Watson, and B. H. Luckman (2000), Tree-ring data document 16th century megadrought over North America, Eos Trans. Am. Geophys. Union, 81(12), 121–125, doi:10.1029/00EO00076.

St. Jacques, J.-M., D. J. Sauchyn, and Y. Zhao (2010), Northern Rocky Mountain streamflow records: Global warming trends, human impacts or natural variability?, Geophys. Res. Lett., 37(6), L06407, doi:10.1029/2009GL042045.

Stella, J. C., M. K. Hayden, J. J. Battles, H. Piégay, S. Dufour, and A. K. Fremier (2011), The role of abandoned channels as refugia for sustaining pioneer riparian forest ecosystems, Ecosystems, 14(5), 776–790, doi:10.1007/s10021-011-9446-6.

Stettler, R. F., and N. R. C. Canada (1996), Biology of *Populus* and its implications for management and conservation, NRC Research Press.

Stewart, I., D. Cayan, and M. Dettinger (2005), Changes toward earlier streamflow timing across western North America, J. Clim., 18(8), 1136–1155, doi:10.1175/JCLI3321.1.

Stockton, C. W., and D. M. Meko (1983), Drought recurrence in the Great Plains as reconstructed from long-term tree-ring records, J. Clim. Appl. Meteorol., 22(1), 17–29, doi:10.1175/1520-0450(1983)022<0017:DRITGP>2.0.CO;2.

Stokes, M. A., and T. L. Smiley (1996), An introduction to tree-ring dating, University of Arizona Press.

Szeicz, J. M., and G. M. MacDonald (1994), Age-dependent tree-ring growth responses of subarctic white spruce to climate, Can. J. For. Res., 24(1), 120–132, doi:10.1139/x94-017.

Thatcher, T., and K. Boyd (2006), Geomorphic parameters and GIS development, Yellowstone River, Report. Bozeman, MT.

Thatcher, T., and K. Boyd (2009), Yellowstone River channel migration zone mapping, Report. Bozeman, MT.

Therrell, M. D., and M. J. Trotter (2011), Waniyetu Wówapi: Native American records of weather and climate, Bull. Am. Meteorol. Soc., 92(5), 583–592, doi:10.1175/2011BAMS3146.1.

Tockner, K., and J. A. Stanford (2002), Riverine flood plains: Present state and future trends, Environ. Conserv., 29(3), 308–330.

Tyree, M. T., K. J. Kolb, S. B. Rood, and S. Patiño (1994), Vulnerability to drought-induced cavitation of riparian cottonwoods in Alberta: a possible factor in the decline of the ecosystem? Tree Phys., 14(5), 455-466, doi:10.1093/treephys/14.5.455.

U.S. Army Corps of Engineers (2013), Hydrologic Statistics, Technical Report, U.S. Army Corps of Engineers, Omaha, NE.

U.S. Army Corps of Engineers, and Yellowstone River Conservation District Council (2015), Yellowstone River Cumulative Effects Analysis, U.S. Army Corps of Engineers, Omaha, NE.

U.S. Bureau of Rec. (2005), A study to determine the historic and present-level streamflow depletions in the Missouri River Basin for the period 1929 to 2002, USBR, Billings, MT.

U.S. Bureau of Rec. (2013), Missouri River Basin depletions database, USBR, Billings, MT.

Vanstone, J. R. (2012), Investigation and reconstructions of the hydroclimatic variability of the Souris River Basin, Thesis, University of Regina.

Vieira, J., F. Campelo, and C. Nabais (2008), Age-dependent responses of tree-ring growth and intra-annual density fluctuations of *Pinus pinaster* to Mediterranean climate, Trees, 23(2), 257–265, doi:10.1007/s00468-008-0273-0.

Ward, J. V., K. Tockner, and F. Schiemer (1999), Biodiversity of floodplain river ecosystems: Ecotones and connectivity, Regul. Rivers Res. Manag., 15(1), 125–139.

Watson, T. A., F. A. Barnett, S. T. Gray, and G. A. Tootle (2009), Reconstructed streamflows for the headwaters of the Wind River, Wyoming, United States, J. Am. Water Resour. Assoc., 45(1), 224–236.

Wigley, T. M. L., K. R. Briffa, and P. D. Jones (1984), On the average value of correlated time series, with applications in dendroclimatology and hydrometeorology, J. Clim. Appl. Meteorol., 23(2), 201–213, doi:10.1175/1520-0450(1984)023<0201:OTAVOC>2.0.CO;2.

Wilcox, A. C., and P. B. Shafroth (2013), Coupled hydrogeomorphic and woody-seedling responses to controlled flood releases in a dryland river, Water Resour. Res., 49(5), 2843–2860, doi:10.1002/wrcr.20256.

Wilding, T. K., J. S. Sanderson, D. M. Merritt, S. B. Rood, and N. L. Poff (2014), Riparian responses to reduced flood flows: Comparing and contrasting narrowleaf and broadleaf cottonwoods, Hydrol. Sci. J., 1–13, doi:10.1080/02626667.2014.880786.

Winters, D. S. et al. (2004), Aquatic, riparian and wetland ecosystem assessment for the Bighorn National Forest., USDA Forest Service, Rocky Mountain Region, Denver, CO.

Wise, E. K. (2010a), Spatiotemporal variability of the precipitation dipole transition zone in the western United States, Geophys. Res. Lett., 37(7), L07706, doi:10.1029/2009GL042193.

Wise, E. K. (2010b), Tree ring record of streamflow and drought in the upper Snake River, Water Resour. Res., 46(11), W11529, doi:10.1029/2010WR009282.

Wohl, E. (2013), Floodplains and wood, Earth-Sci. Rev., 123, 194-212, doi:10.1016/j.earscirev.2013.04.009.

Wohl, E., B. P. Bledsoe, R. B. Jacobson, N. L. Poff, S. L. Rathburn, D. M. Walters, and A. C. Wilcox (2015), The natural sediment regime in rivers: Broadening the foundation for ecosystem management, BioScience, doi:10.1093/biosci/biv002.

Wolman, M. G., and R. Gerson (1978), Relative scales of time and effectiveness of climate in watershed geomorphology, Earth Surf. Process., 3(2), 189–208, doi:10.1002/esp.3290030207.

Woodhouse, C. A., S. T. Gray, and D. M. Meko (2006), Updated streamflow reconstructions for the Upper Colorado River Basin, Water Resour. Res., 42(5), doi:10.1029/2005WR004455.

Woodhouse, C. A., G. T. Pederson, and S. T. Gray (2011), An 1800-yr record of decadal-scale hydroclimatic variability in the upper Arkansas River basin from bristlecone pine, Quat. Res., 75(3), 483–490, doi:10.1016/j.yqres.2010.12.007.

Woodhouse, C. A., D. M. Meko, D. Griffin, and C. L. Castro (2013), Tree rings and multiseason drought variability in the lower Rio Grande Basin, USA, Water Resour. Res., 49(2), 844–850, doi:10.1002/wrcr.20098.

Xu, D., Y. Bai, J. Ma, and Y. Tan (2011), Numerical investigation of long-term planform dynamics and stability of river meandering on fluvial floodplains, Geomorphology, 132(3-4), 195-207, doi:10.1016/j.geomorph.2011.05.009.

Yu, G., Y. Liu, X. Wang, and K. Ma (2008), Age-dependent tree-ring growth responses to climate in Qilian juniper (*Sabina przewalskii* Kom.), Trees, 22(2), 197–204, doi:10.1007/s00468-007-0170-y.

Zang, C., and F. Biondi (2015), treeclim: an R package for the numerical calibration of proxy-climate relationships, Ecography, 38(4), 431-436, doi:10.1111/ecog.01335.

Zhang, Q.-B., and R. J. Hebda (2004), Variation in radial growth patterns of *Pseudotsuga menziesii* on the central coast of British Columbia, Canada, Can. J. For. Res., 34(9), 1946–1954, doi:10.1139/x04-078.

7. APPENDICES

7.1 Appendix 1: Chapter 2 Supplementary Material

7.1.1 Introduction

The Supplementary material that follows elaborates on methods and results that were related to, but not necessary for, the presentation of the findings in Chapter 2. I conducted many background analyses before deciding to present the material as occurs in the manuscript. All information included in this appendix supports, adds context to, or elaborates on the primary findings of Chapter 2.

7.1.2 Regional Curve Standardization and tree core detrending

I performed signal-free detrending using CRUST software to create tree ring indices for each site [*Melvin and Briffa*, 2014a, 2014b]. In choosing the number of growth curves to use, I attempted to find the best solution among the competing goals of reducing sample bias, maintaining high sample sizes per curve, and preserving low-frequency trends. Using higher numbers of growth curves reduced sample size per curve and the magnitude of the low-frequency trends. I chose to use two growth curves, which is consistent with previous work [*Briffa et al.*, 2013]. This divided each site's cores into fast and slow growing subsets (Fig. 7.1). Each tree core was detrended from whichever growth curve it more closely resembled. Ring width indices were generated from the ratio of measured to expected ring width in each year. Using more growth curves reduced but did not reverse or eliminate any of the low-frequency patterns reported (Fig. 7.2).

7.1.3 Flow reconstruction models

Flow reconstructions were created from multiple linear regression models using only three cottonwood chronologies as predictor datasets. Many upland chronologies are available from the region on the International Tree Ring Data Bank (http://www.ncdc.noaa.gov/data-access/paleoclimatology-data/datasets/tree-ring), but I chose to isolate riparian cottonwoods as the sole predictors to identify their ability to model discharge. I used the entire period of record (1931-2010) to create the models, instead of subsetting the data into calibration and validation periods. This validation exercise is commonly performed to support the methods used. I expect this would have produced similar results with my data, but I deemed it more important to create the models using longer datasets (i.e., 80 years instead of 40 years) to incorporate greater environmental and temporal variability.

The final flow reconstructions are for four months of log-transformed discharge in the early summer (March-June at Yellowstone and Powder, April-July at Little Missouri). However, I created models for other types of discharge as well, including annual. These models explained less variance and were not retained. Table 7.1 reports 12 of the models created in all-subsets regressions.

7.1.4 Correlations between environmental drivers and tree ring width

I used the MATLAB program seascorr [*Meko et al.*, 2011] to correlate the cottonwood chronologies at each site to three possible environmental variables driving growth: river discharge, local precipitation, and local temperature. Environmental data were divided into monthly means (discharge, temperature) or totals (precipitation). Then all years during the period of discharge record were separated into monthly values, which were correlated to the

tree ring index during that year. Months were regressed against ring width index individually or as a group of 4, 8, or 12 consecutive months. In general, river discharge was the best predictor, and I only present figures displaying when discharge was the primary variable (Figs. S3, S4).

The first column and row of Figures S3 and S4 reveals that winter discharge was poorly correlated to ring width across sites. Spring discharge shows the strongest correlation, and the previous fall's discharge is positively correlated at the Yellowstone and Little Missouri. After accounting for discharge, the partial correlations between precipitation and ring width were nominal at the Yellowstone, small at the Powder and larger at the Little Missouri. Although this pattern suggests that local precipitation was more important at the Little Missouri, this interpretation is conflated by the high correlation between discharge and precipitation at the small lowland Little Missouri watershed, while the variables are less related at the Yellowstone. Further analysis is in the primary text. Analyses not shown confirmed discharge to be a better predictor than precipitation.

Temperature was negatively related to cottonwood ring width across sites (Table 2.2; Fig. 7.4). Winter and spring temperatures were the most negatively related to ring width. Higher winter and spring temperature may cause snow to melt and runoff in the dormant season before trees are able to access the water.

7.1.5 Temperature and precipitation trends

Watershed-averaged temperature and precipitation PRISM data [*Daly et al.*, 2008] were downloaded from WestMap (Figs. S5, S6; http://www.cefa.dri.edu/Westmap). WestMap watersheds did not directly line up with the contributing area above each streamgage, but the overlap was reasonable. The Yellowstone data are a weighted average based on area of the

Upper Yellowstone, Powder, Bighorn, and Lower Yellowstone hydrologic units. The Powder data are from the Powder hydrologic unit. The Little Missouri data are from the Lake Sakakawea hydrologic unit.

7.1.6 Flow regulation statistics

The Yellowstone and Powder Rivers lack mainstem dams, but other factors such as irrigation, reservoir operations, and municipal water development in the watersheds alter flow magnitude and timing. The Yellowstone River Conservation District Council and U.S. Army Corps of Engineers partnered to conduct a cumulative effects study to assess the differences in flows between regulated and unregulated conditions at several locations across the basin. The USGS partnered with these organizations to calculate streamflow statistics for rivers in the Yellowstone River Basin (Table 7.2) [*Chase*, 2013, 2014]. The U.S. Bureau of Reclamation estimated extractions based on climate records, irrigation methods and area, and municipal and industrial uses for each year 1929-2002 for the Missouri River Basin [*U.S. Bureau of Rec.*, 2005]. They later extended this record to 2007 [*U.S. Bureau of Rec.*, 2013]. USBR identified ten categories as contributing to total depletions (e.g., irrigation, conveyance losses, non-beneficial consumptive use, return flow redistribution), but they focused on irrigation because it was the primary water depletion. To determine irrigation effects across the basin, crop irrigation requirement, diversion requirement, and a return flow component of the irrigation were computed at each of 118 points in the Missouri River Basin, including the Yellowstone River at Sidney, MT and the Powder River near Locate, MT. USBR calculated daily flows for both unregulated and regulated conditions for 1929-2002. “Regulation” describes flows under the hypothetical situation assuming that all depletions existing in 2002 or 2007 were present

through the entire period, while unregulated statistics characterize flows if none of the depletions occurred. Values for regulated flows were generated using the historically measured weather conditions but imposing the number of irrigated acres present in 2002 or 2007 across the study period. Historical data on the actual annual depletions do not exist. To estimate historical extractions, USBR calculated monthly diversion, return flow, depletion data, and each year's irrigated area, monthly weather, and other depletion statistics. To generate statistics characterizing unregulated flows, USBR added the calculated historical depletions to measured flows.

7.1.7 Autocorrelation

I found different degrees of autocorrelation in annual flows and annual ring width across sites. Flow autocorrelations can result from 1) autocorrelation in weather between years, 2) slow flow paths that take more than one year to route water through a watershed, or 3) artificial storage such as that which occurs in reservoirs. Trees survive multiple years, and stored carbohydrates affect subsequent years' productivity. Cottonwood tree rings at all three rivers had positive autocorrelation in ring width between years. Autocorrelation differed by river, however, with the Yellowstone, Powder, and Little Missouri tree rings having significant positive autocorrelations for lags of 7, 3, and 1 years. Tree ring autocorrelations were greater than those for the reconstructed discharge at all sites over the periods of flow record. Although the Little Missouri had slightly more 1935-2014 mean annual discharge than the Powder River (15.1 vs. 12.5 m^3/s), it had less May-July growing season discharge (23.2 vs. 27.0 m^3/s). Annual runoff patterns were more erratic at the Little Missouri, illustrated by the standard deviation of mean monthly flows being much greater than at the Powder (20.0 vs. 8.9 m^3/s). The flow

regime at the Little Missouri may have caused lower autocorrelations in both discharge and cottonwood ring width. Additionally, much of the Little Missouri runoff occurs in March during cottonwood dormancy, providing further explanation for the lower correlations between river flow and ring growth at the Little Missouri.

I created Yellowstone, Powder, and Little Missouri tree ring chronologies using prewhitening to remove autocorrelation from the tree ring chronologies, but flow reconstructions did not change substantially so I used the standard chronologies instead. For example, I performed model selection for Yellowstone River flows using prewhitened Yellowstone, Powder, and Little Missouri chronologies at t, t-1 and t-2 as nine possible predictors. The lagged predictors were introduced to enable persistence to enter the model after it was removed during prewhitening. This model selected the Yellowstone cores at t, t-1 and t-2 and the Powder cores at t and t-1, which was very similar to selecting the autocorrelated Yellowstone and Powder chronologies retained in the original model.

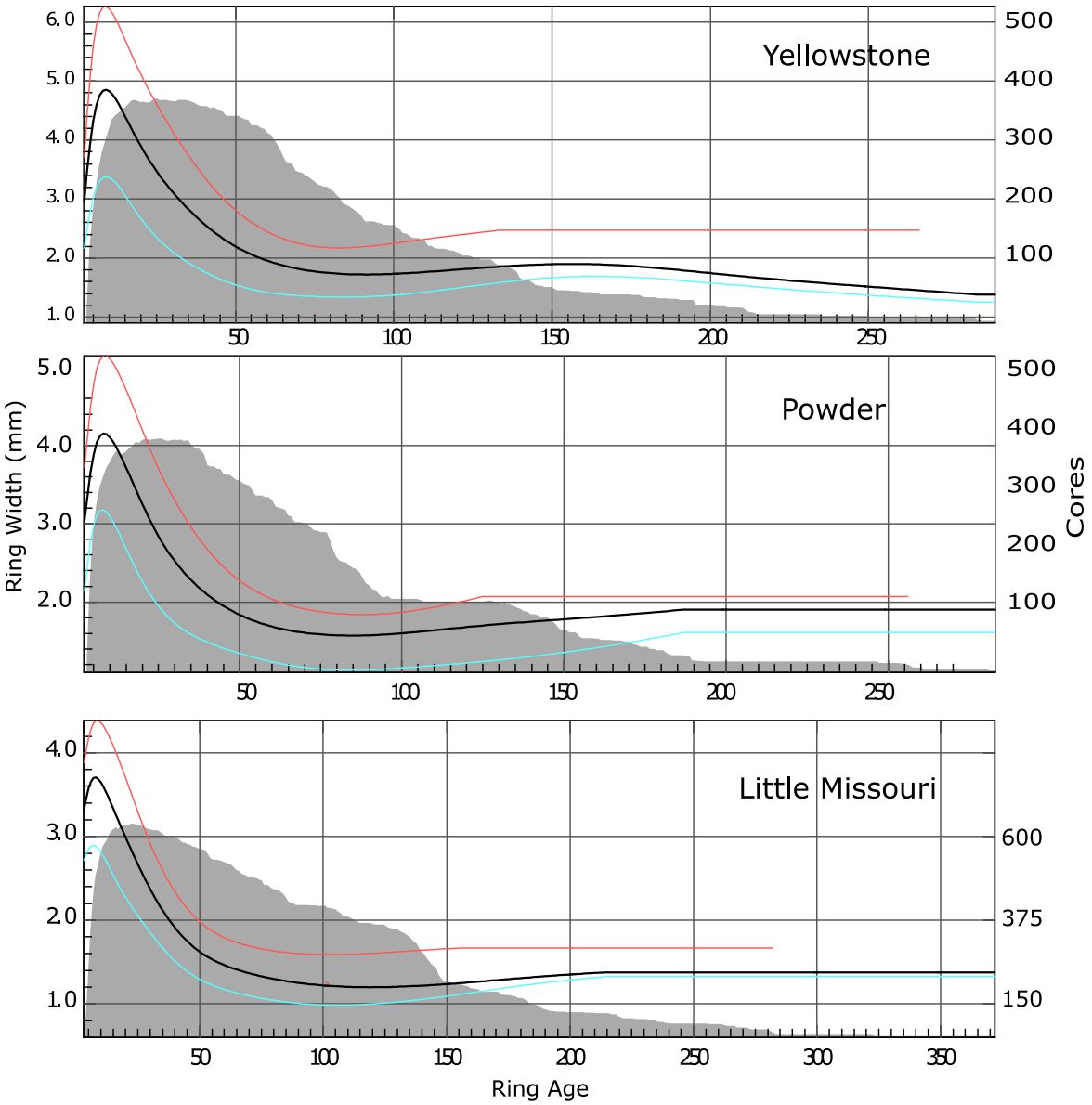

Figure 7.1. The growth curves used in the RCS reconstructions from each site. Cores were separated into fast- (red) and slow-growing (blue) groups and separate growth curves were used to detrend each. Black lines are mean growth curve from all cores from each site.

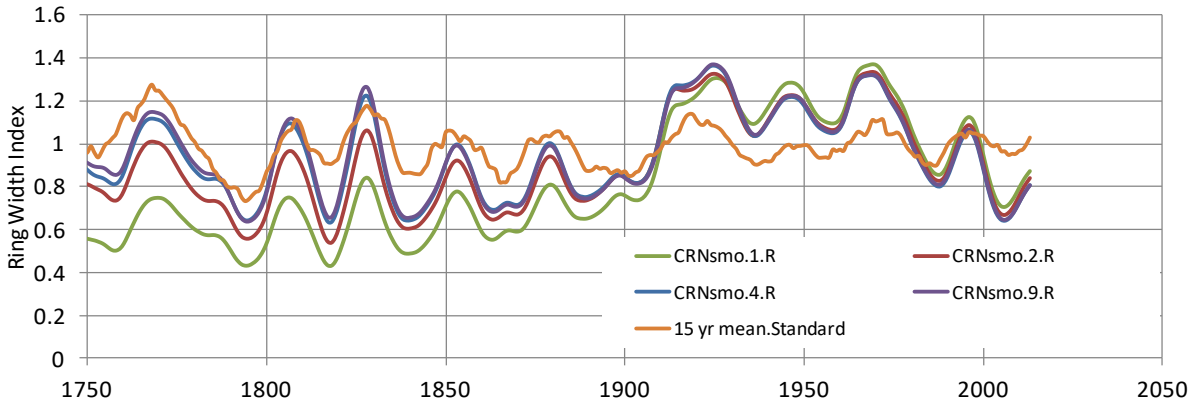

Figure 7.2. Comparison of Yellowstone cottonwood chronologies generated using different detrending methods. Displayed are signal-free chronologies created using 1, 2, 4, and 9 RCS curves, as well as a 15-year moving average (orange) of ring width indices created using a more traditional detrending approach (each core detrended using a 50% frequency response cutoff at 67% of the measured series length). The traditional chronology retained no low-frequency (century-scale) variation and had mean values oscillating around and index of 1. More RCS curves yielded less low frequency change, but even nine curves showed a low-frequency increase through 1980.

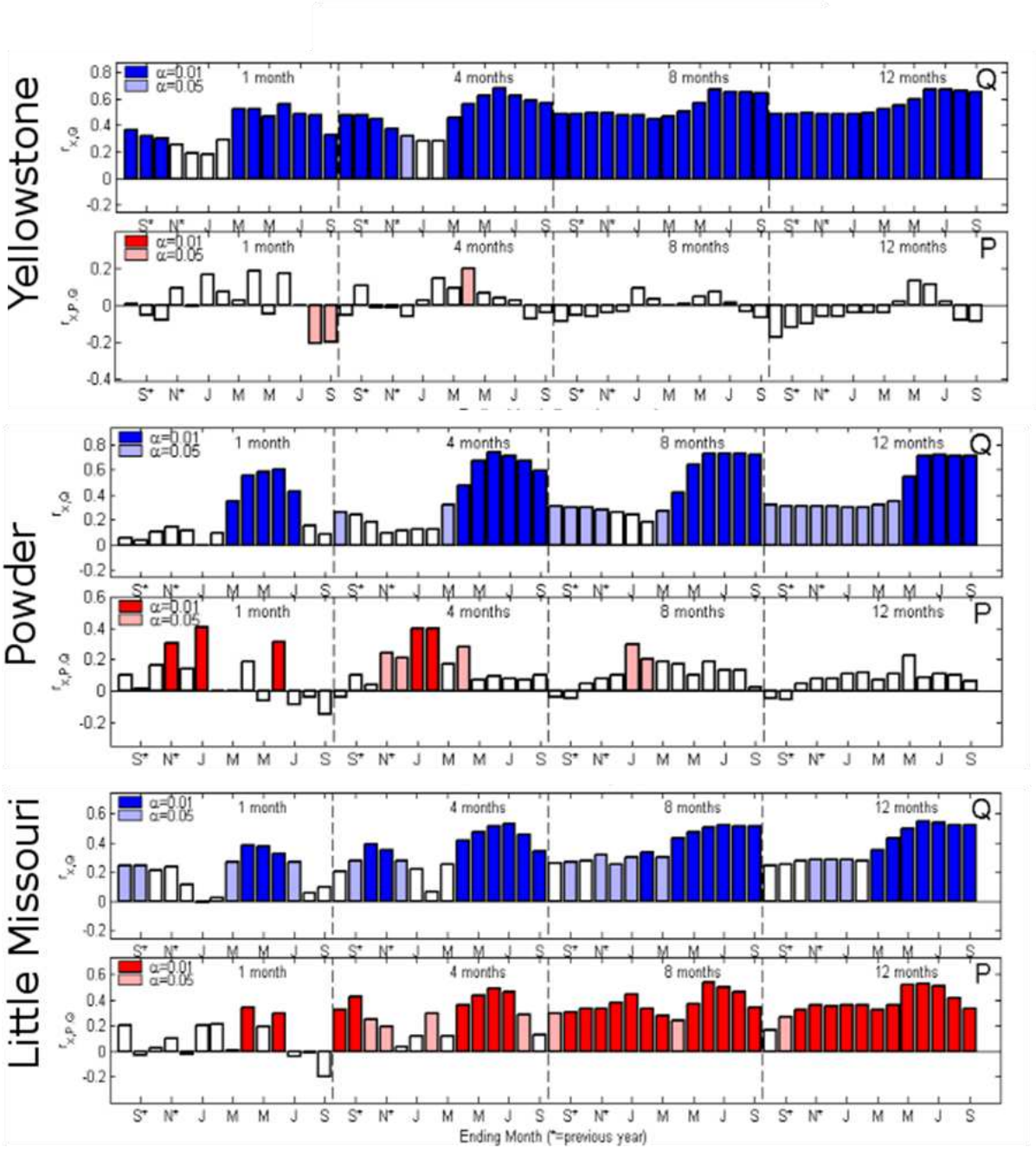

Figure 7.3. Seascorr results showing correlations and partial correlation values (*r*) for the relationship between environmental drivers and cottonwood tree ring width indices (RWI). Top rows (blue) for each site show the correlations between mean monthly discharge and RWI, and bottom rows (red) show the partial correlations between local precipitation and RWI after accounting for discharge. Columns display number of months over which values are calculated, and bars display values for the last month of the given period.

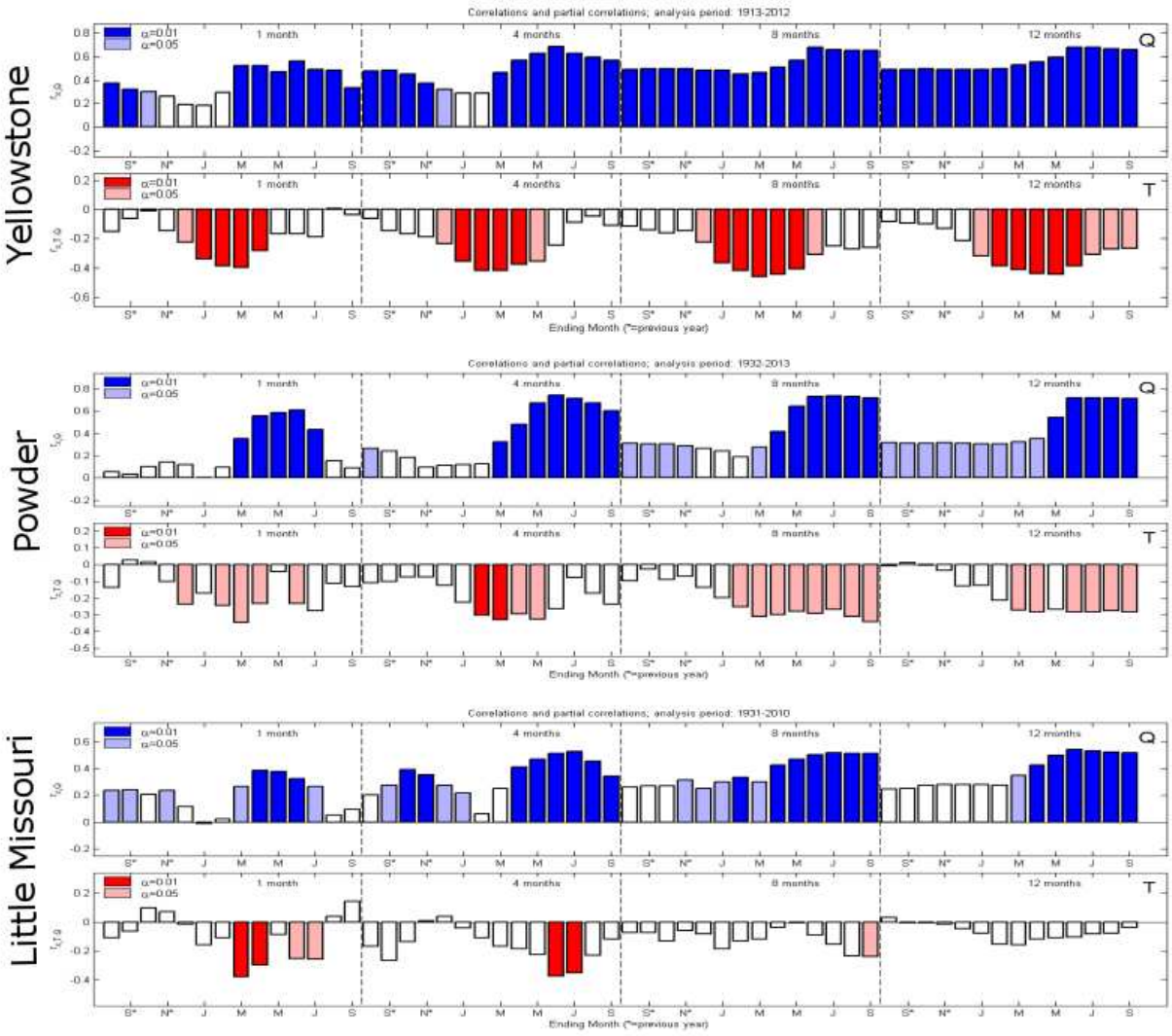

Figure 7.4. Seascorr results showing correlations and partial correlation values (*r*) for the relationship between environmental drivers and cottonwood tree ring width indices (RWI). Top rows (blue) for each site show the correlations between mean monthly discharge and RWI, and bottom rows (red) show the partial correlations between local temperature and RWI after accounting for discharge. Columns display number of months over which values are calculated, and bars display values for the last month of the given period.

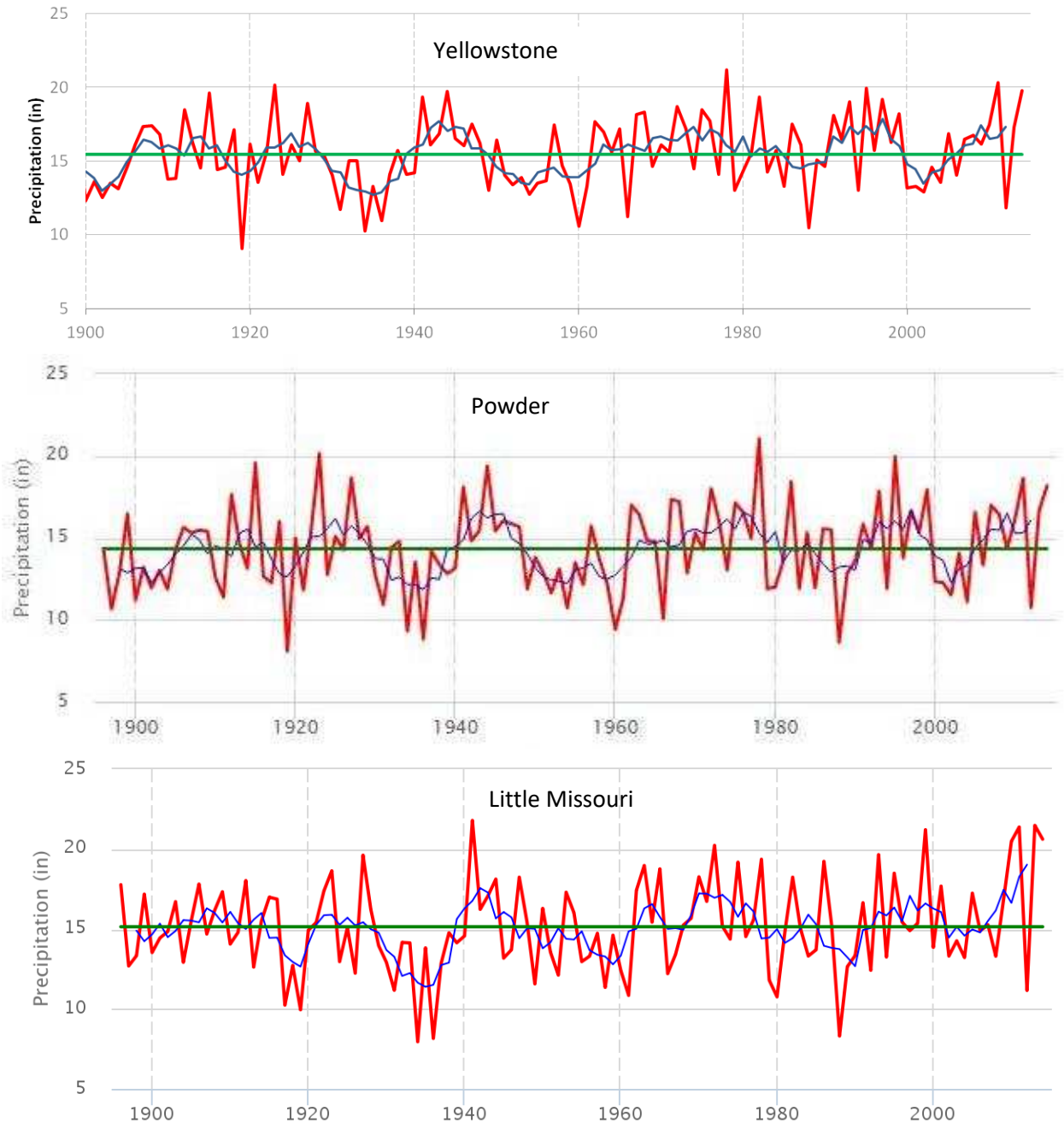

Figure 7.5. Water year precipitation for the Yellowstone, Powder, and Little Missouri watersheds. Red line is annual values, blue line is 5-year running mean, and green line is the average for the entire 1896-2014 period. Note that units are inches.

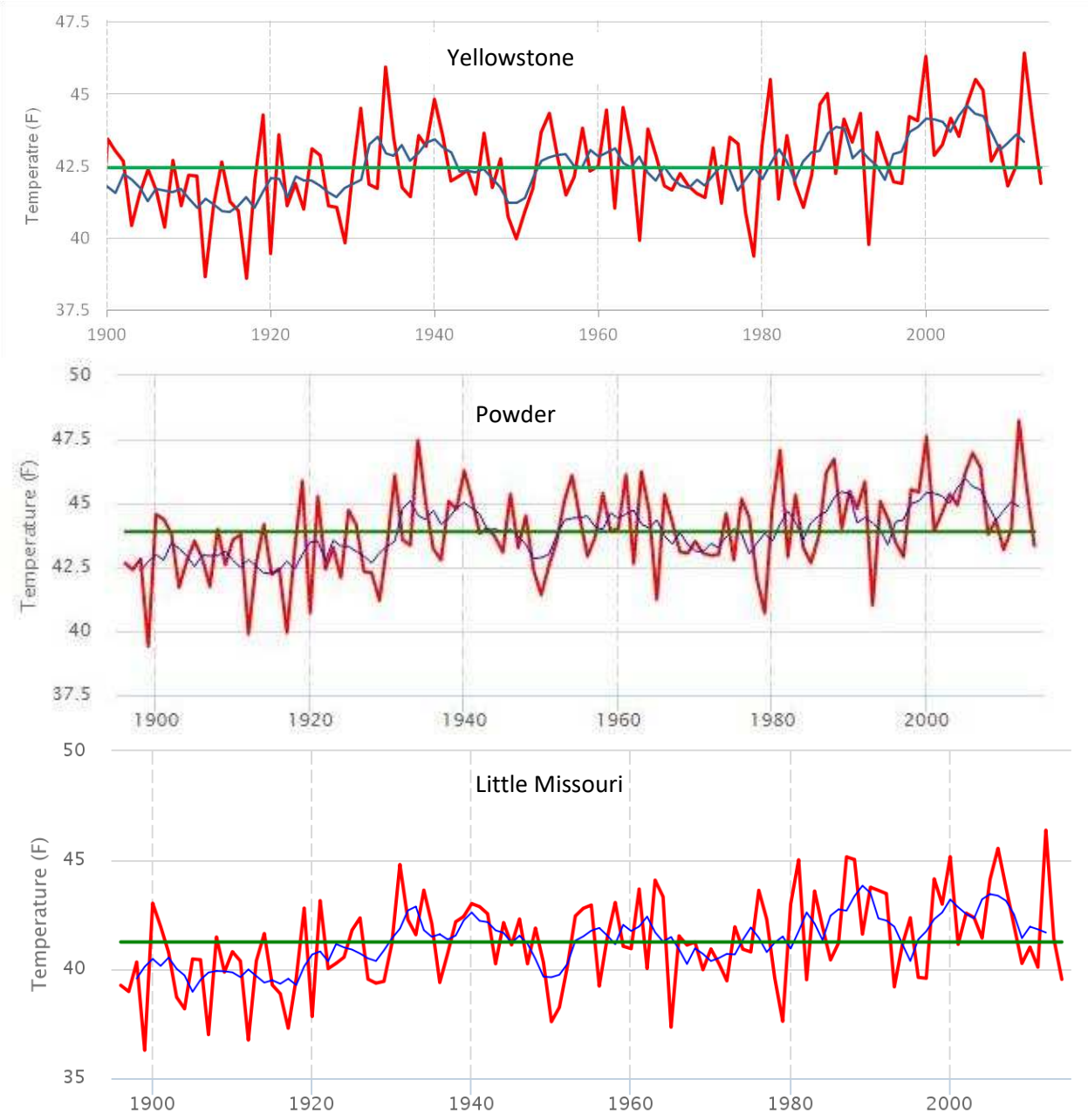

Figure 7.6. Water year mean temperature for the Yellowstone, Powder, and Little Missouri watersheds. Red line is annual values, blue line is 5-year running mean, and green line is the average for the entire 1896-2014 period. Note that units are Fahrenheit.

Site	Reconstructed Flow	Model
Yellowstone	12-mo	45.69 + 170.84*YL + 110.71*PW
	log(12-mo)	2.128 + 0.213*YL + 0.156*PW
	4-mo	12.17 + 291.38*YL + 200.04*PW
	log(4-mo)	**2.266 + 0.2285*YL + 0.1871*PW**
Powder	12-mo	-2.86 + 15.68*PW
	log(12-mo)	0.43965 + 0.627*PW
	4-mo	-13.789 + 39.204*PW
	log(4-mo)	**0.5539 + 0.788*PW**
Little Missouri	12-mo	-15.041 + 10.57*PW + 9.90*LM + 9.13*YL
	log(12-mo)	-0.0188 + 0.5156*PW + 0.5725*LM
	4-mo	-41.56 + 43.56*PW + 25.08*LM
	log(4-mo)	**-0.1675 + 0.675*LM + 0.758*PW**

Table 7.1. The best models for each of the flow conditions and sites. Models are for four different types of flow. The log 4-month flow (bold) was selected as the final model for each site. Predictors are in a unitless tree ring index, and the response flow is in m^3/s. YL = Yellowstone, PW = Powder, and LM = Little Missouri.

	Lower Yellowstone			Powder		
	Unregulated	**Actual**	**% Change**	**Unregulated**	**Actual**	**% Change**
Jan	131	160	0.22	3.3	4.0	0.22
Feb	173	196	0.14	11.3	12.3	0.09
Mar	289	304	0.05	34.0	35.0	0.03
Apr	317	273	-0.14	21.8	21.1	-0.03
May	784	495	-0.37	50.7	32.7	-0.36
Jun	1362	1020	-0.25	62.3	45.8	-0.27
Jul	929	603	-0.35	36.5	16.2	-0.56
Aug	426	222	-0.48	18.4	6.1	-0.67
Sep	265	195	-0.27	9.6	4.8	-0.50
Oct	199	229	0.15	5.3	7.1	0.35
Nov	165	210	0.27	4.5	6.2	0.39
Dec	132	167	0.27	3.1	4.2	0.35
Annual	430	339	-0.21	21.6	16.3	-0.25

Table 7.2. Seasonal flows (m^3/s) for the Yellowstone River near Sidney, MT and the Powder River near Locate, MT. The Locate gage is downstream from the reconstructed Powder River gage at Moorhead and has a similar annual hydrograph. Mean annual flow at Moorhead was 78% of that at Locate. Modified from Chase [2013].

7.2 Appendix 2: Chapter 3 Supplementary Material

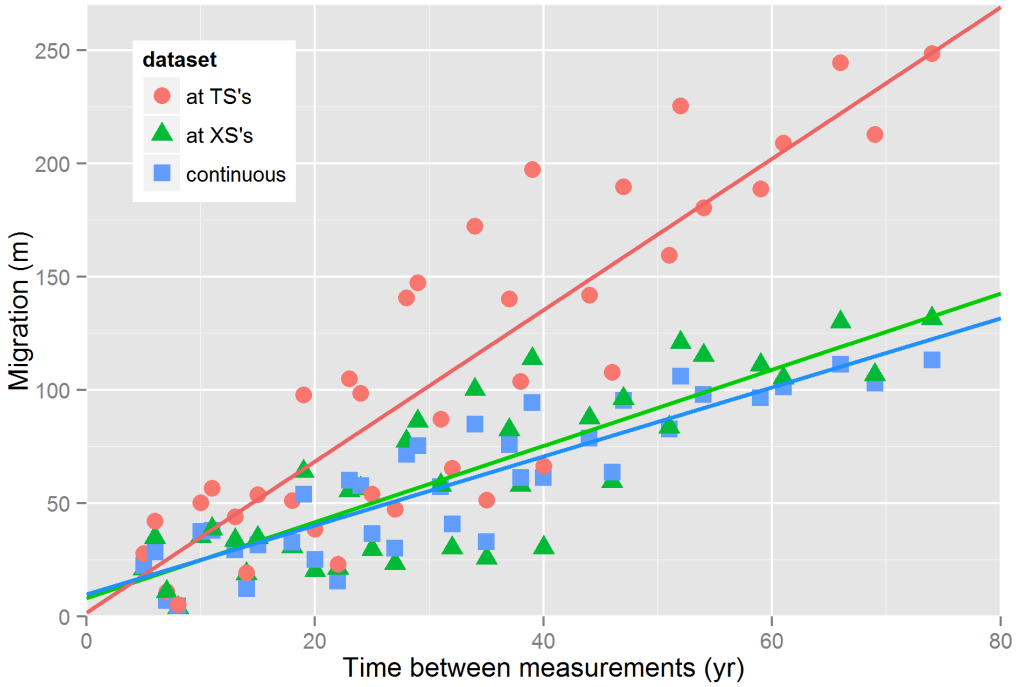

Figure 7.7. Air photo-derived channel migration distance as a function of the number of years between measurements. These are separated by locations in the floodplain and slopes were used to standardize the XS and TS data to the entire reach. AP's at TS locations (red circles) are averages for the 13 TS's, photos at XS locations (green triangles) are averages for the 20 XS's, and continuous air photos (blue squares) are integrated over the entire reach and are considered to be a complete and reference dataset.

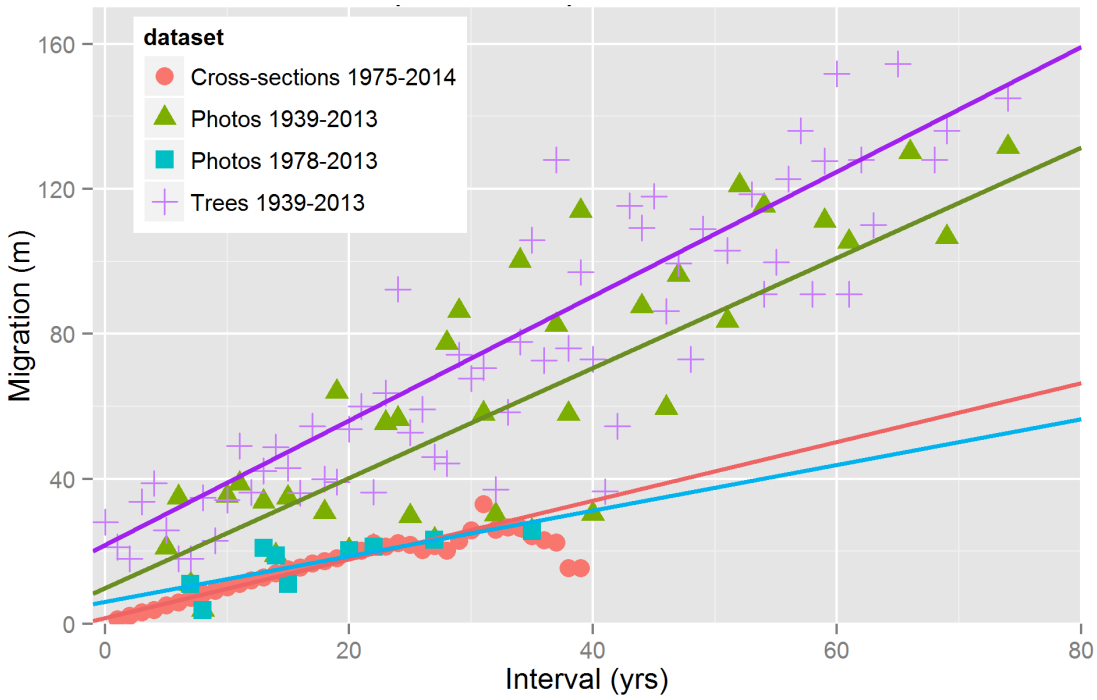

Figure 7.8. Channel migration pattern for air photos (triangles) and the trees (crosses) subsetted to the concurrent period (top lines), and cross-sections (circles) and air photos (squares) subsetted to the concurrent period (bottom lines). Faster migration rates occurred in the longer period compared to the recent cross-section era.

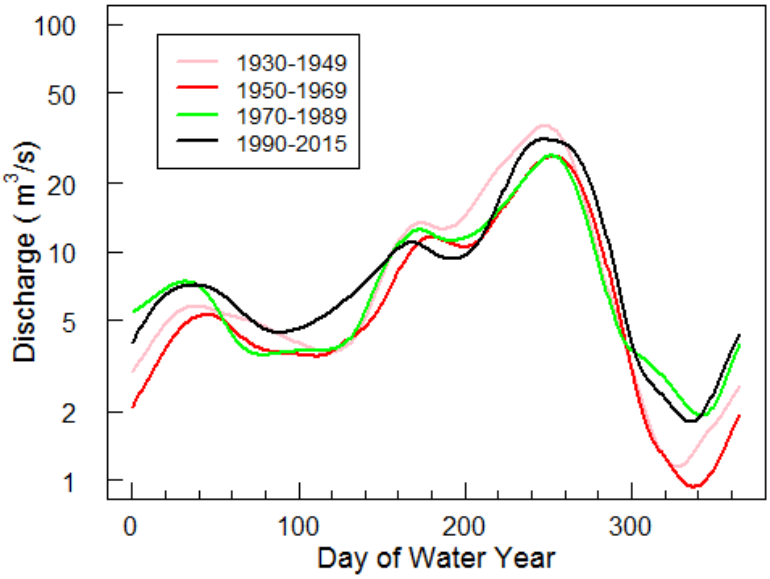

Figure 7.9. Median hydrographs over 20-year increments of Powder River flows smoothed with a smoothing spline. Through time, there has been a slight tendency toward higher base-flows. Note the logged y-axis. However, this view of the flow regime makes changes look small.

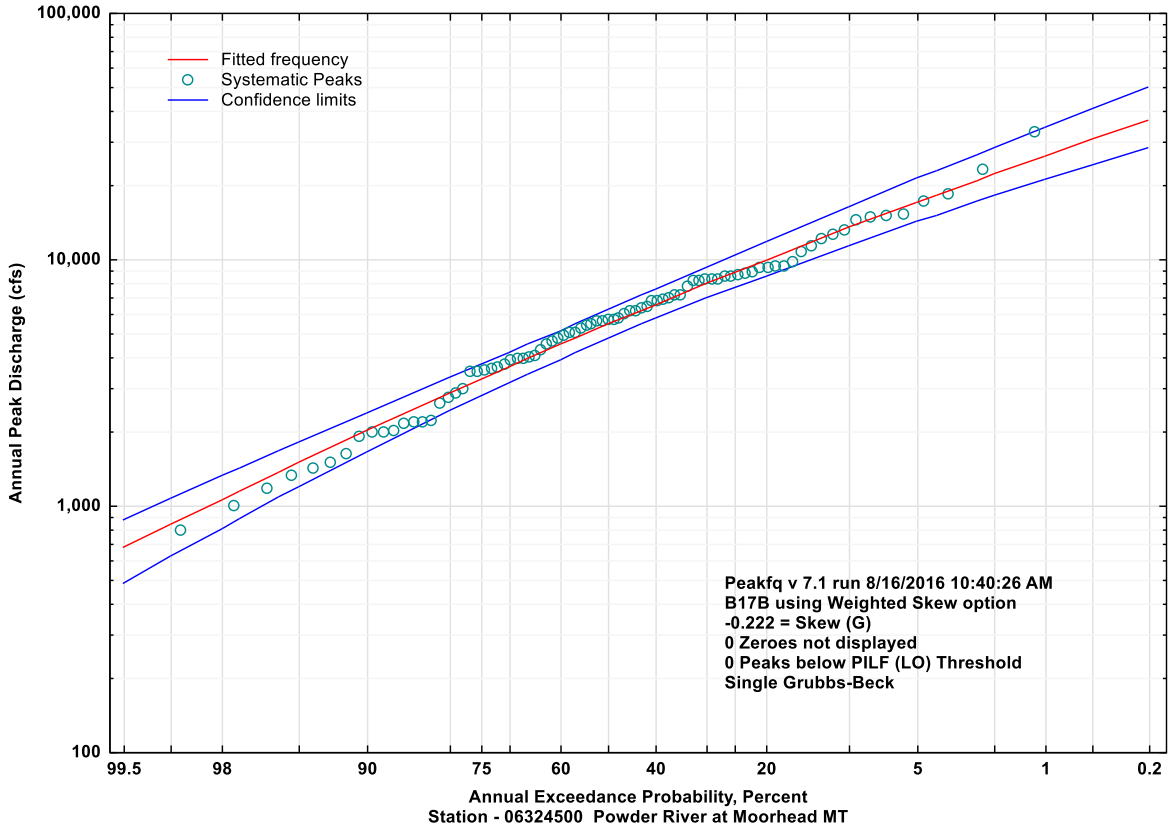

Figure 7.10. Flood frequency curve of peak annual floods for the Powder River, 1930-2014. Note that the 1923 flood was 100,000 cfs, so it would fall well outside of the 95% confidence interval created from 1930-2014 data.

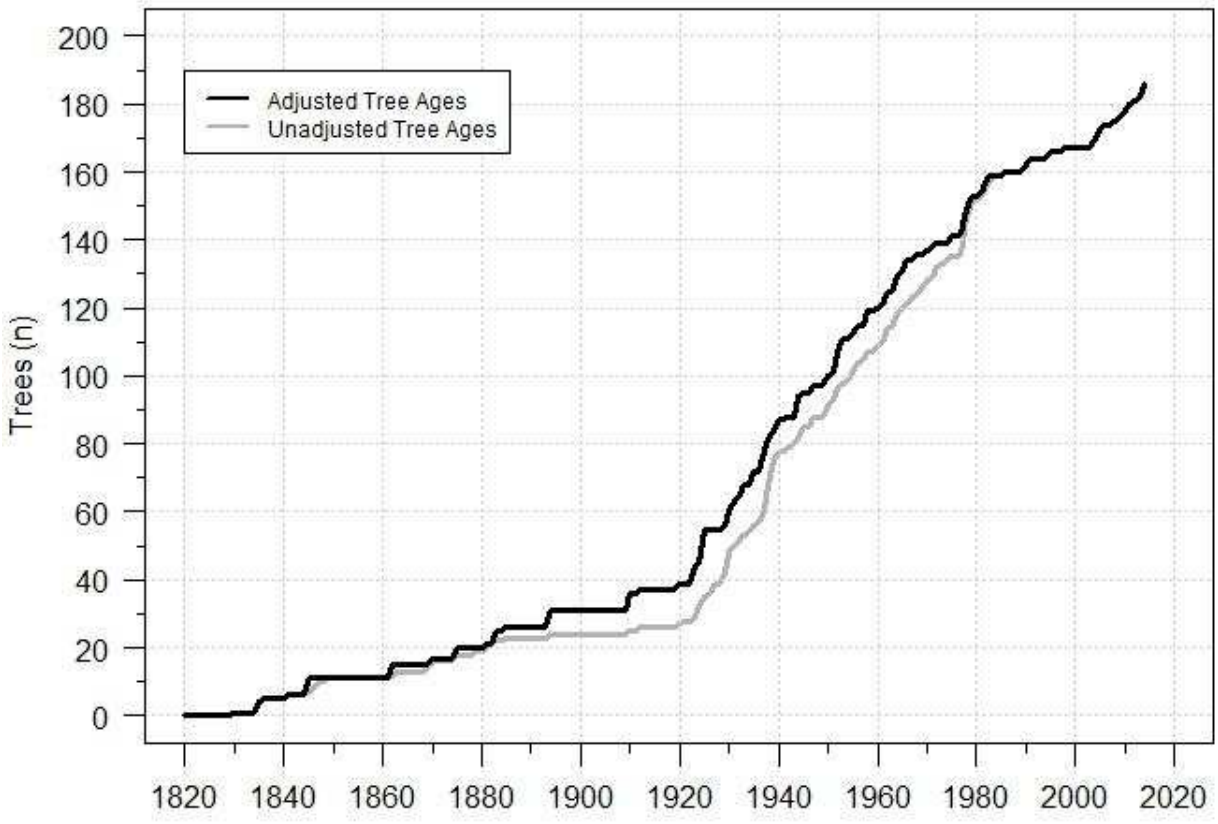

Figure 7.11. Cumulative number of sampled trees dating back in time (x-axis). Lines show the unadjusted tree ages (gray line) and ages adjusted so that tree age could not decrease as distance from channel increased (black line).

Table 7.3. The Powder River cross-sections analyzed [*Moody and Meade*, 1990].

.

Cross-section name	First Survey	Last Survey	Maximum interval (yr)	Years surveyed (n)
PR116	1975	2014	39	20
PR120	1975	2014	39	27
PR122A	1979	2014	35	29
PR125	1975	2014	39	28
PR130	1975	2014	39	27
PR136	1975	2014	39	23
PR141A	1979	2014	35	29
PR147	1975	2013	38	21
PR151	1975	2014	39	24
PR156A	1978	2014	36	24
PR163	1977	2014	37	28
PR166.6	1979	1998	19	5
PR167	1977	2014	37	22
PR168.5	1979	1998	19	5
PR169.2	1979	1998	19	5
PR175	1977	1998	21	20
PR180	1977	2014	37	25
PR183	1977	2014	37	21
PR191	1977	2014	37	21
PR194	1977	2014	37	21

Table 7.4. Air photo metadata.

Year	Dates flown	Source	Resolution	Delineators
1939	27-May-38 – 28-Jun-39	US Forest Service	1:20,000	Martinson and Meade (1983)
1944	28-Jul – 10-Aug	Aero Service, Western Geophysical Company of America	1:40,000	Martinson and Meade (1983)
1954	27-Aug – 26-Sep	USDA-ASCS[1]	1:20,000	Martinson and Meade (1983)
1967	21-Jun – 15-Aug	USDA-ASCS	1:20,000	Martinson and Meade (1983)
1973	4-Jul – 5-Jul	Intrasearch, Inc.	1:24,000	Martinson and Meade (1983)
1978	26-Jul	USDA-ASCS	1:40,000	Both (Schook et al. used for analysis)
1991	2-Jul – 30-Aug	USGS National Aerial Photography Program (NAPP)	1:40,000	Schook et al.
1998	8-Jul-96 – 12-Jul-98	7.5' USGS topographic quadrangles (DOQ) (NAPP derived)	1:40,000	Schook et al.
2005	8-Jul – 5-Aug	National Agriculture Imagery Program (NAIP)	1 m	Schook et al.
2013	21-Jul – 22-Jul	National Agriculture Imagery Program (NAIP)	1 m	Schook et al.

[1] US Department of Agriculture – Agricultural Stabilization and Conservation Service, Aerial Photography Field Office

Table 7.5. Differences in channel boundary locations between air photos for locations that were assumed to have not moved during the entire period. This imprecision estimates were used to correct the air photo migration rates (Table 3.1).

Location[1]	1939-1944	1944-1954	1954-1967	1967-1973	1973-1978b[2]	1978a-1978b[2]	1978b-1991[2]	1991-1998	1998-2005	2005-2013
PR119	2.9	3.7	6.1	1.1	3.3	5	NA[3]	NA[3]	NA[3]	1.2
PR122.3	7.8	10.6	6	2.3	1.2	2.4	2.7	NA[3]	NA[3]	0.3
PR133	29	29.6	15.1	5.2	1.1	0.8	0.5	4.6	6.5	5.2
PR151.2	3.3	19	15.3	4.2	0.6	3.2	2.5	3.5	0.2	3.9
PR165	20.6	14.4	12.5	15.4	3.7	7.4	7.9	0	5.4	5.2
PR172	19.6	20.1	19.5	4.8	9.1	4.6	4.3	3	1.6	2
PR183	16.1	8.1	20.5	3	1	2	15.2	4.6	4.9	4.3
Interval (yr)	5	10	13	6	5	0	13	7	7	8
Mean(m)	14.2	15.1	13.6	5.1	2.9	3.6	5.5	3.1	3.7	3.2
Median (m)	16.1	14.4	15.1	4.2	1.2	3.2	3.5	3.5	4.9	3.9
Standard dev. (m)	9.8	8.7	5.8	4.7	3.0	2.2	5.4	1.9	2.7	2.0
Imprecision (m/yr)	**3.22**	**1.44**	**1.16**	**0.7**	**0.24**	**NA**	**0.27**	**0.5**	**0.7**	**0.49**

[1] Locations are river kilometers as in Moody and Meade [1990]

[2] 1978a is the Martinson and Meade (1983) channel delineation, and 1978b is my re-delineation for the same year.

[3] 1991 and 1998 air photos did not cover the upstream anchor points. However, at PR119 the 1978-2005 difference was 2.5 m, and at PR122.3 the difference was 0.9 m. Both of these longer intervals fall within the range of the values from other years and suggest that the imprecision adjustment would not have altered substantially if they were included.

Table 7.6. Channel migration distance and rate as a function of the interval between measurements. The inferred annual migration rate tends to underestimate the 1.34 m/yr annual migration rate calculated from surveys in consecutive years.

Interval (yr)	Number of comparisons	Mean mig. distance (m)	Median mig. distance (m)	Mean mig. rate (m/yr)	Underestimate of 1-year mig. rate (%)
1	337	1.34	0.30	1.34	0
2	330	2.30	0.63	1.15	14
3	292	3.23	1.03	1.08	19
4	273	3.89	1.35	0.97	28
5	272	5.18	2.25	1.04	22
6	253	6.01	2.95	1.00	25
7	253	7.22	4.35	1.03	23
8	230	8.30	5.90	1.04	22
9	221	9.08	7.05	1.01	25
10	208	10.08	7.45	1.01	25
11	197	11.10	8.80	1.01	25
12	191	12.01	9.75	1.00	25
13	182	12.81	10.65	0.99	26
14	162	13.97	11.25	1.00	25
15	148	15.14	12.55	1.01	25
16	146	15.56	12.80	0.97	28
17	132	16.73	13.85	0.98	27
18	127	17.36	14.20	0.96	28
19	114	18.05	15.08	0.95	29
20	98	19.74	15.35	0.99	26
21	84	20.28	15.63	0.97	28
22	72	22.35	17.35	1.02	24
23	63	21.35	15.05	0.93	31
24	54	22.36	15.28	0.93	31
25	47	21.74	14.60	0.87	35
26	45	20.44	15.15	0.79	41
27	42	21.46	15.58	0.79	41
28	34	20.17	15.18	0.72	46
29	31	23.01	19.35	0.79	41
30	27	25.80	19.65	0.86	36
31	16	32.99	24.40	1.06	21
32	29	26.02	20.25	0.81	40
33	22	26.68	21.60	0.81	40
34	33	26.48	21.10	0.78	42
35	27	24.24	20.25	0.69	49
36	19	23.04	18.40	0.64	52
37	16	22.41	17.15	0.61	54
38	5	15.41	17.95	0.41	69
39	5	15.45	17.10	0.40	70

Table 7.7. Annual migration distance calculated from cottonwood TSs. Because trees age to discrete years, the age distribution suggests erratic migration rates. However, the data are more interpretable and realistic when smoothed (Fig. 3.5).

Year	Migration (m)	Year	Migration (m)	Year	Migration (m)	Year	Migration (m)
1830	18.18	1877	0.00	1924	2.27	1971	1.40
1831	0.00	1878	0.00	1925	22.73	1972	1.40
1832	0.00	1879	0.00	1926	0.00	1973	0.00
1833	0.00	1880	0.00	1927	0.00	1974	0.00
1834	0.00	1881	3.64	1928	0.00	1975	2.80
1835	54.55	1882	0.00	1929	2.02	1976	0.00
1836	9.09	1883	12.12	1930	8.08	1977	1.40
1837	0.00	1884	0.00	1931	6.06	1978	9.79
1838	0.00	1885	3.03	1932	4.04	1979	5.59
1839	0.00	1886	0.00	1933	6.06	1980	0.00
1840	0.00	1887	0.00	1934	0.00	1981	1.40
1841	6.06	1888	0.00	1935	8.08	1982	5.59
1842	0.00	1889	0.00	1936	0.00	1983	1.40
1843	0.00	1890	0.00	1937	12.12	1984	0.00
1844	0.00	1891	0.00	1938	6.06	1985	0.00
1845	30.30	1892	0.00	1939	5.45	1986	1.40
1846	0.00	1893	0.00	1940	5.45	1987	0.00
1847	0.00	1894	12.99	1941	0.00	1988	0.00
1848	0.00	1895	0.00	1942	1.82	1989	0.00
1849	0.00	1896	0.00	1943	0.00	1990	2.80
1850	0.00	1897	0.00	1944	10.91	1991	2.80
1851	0.00	1898	0.00	1945	1.65	1992	0.00
1852	0.00	1899	0.00	1946	0.00	1993	0.00
1853	0.00	1900	0.00	1947	3.31	1994	0.00
1854	0.00	1901	0.00	1948	0.00	1995	2.80
1855	0.00	1902	0.00	1949	0.00	1996	0.00
1856	0.00	1903	0.00	1950	4.55	1997	0.00
1857	0.00	1904	0.00	1951	1.52	1998	1.40
1858	0.00	1905	0.00	1952	9.09	1999	0.00
1859	0.00	1906	0.00	1953	6.06	2000	0.00
1860	0.00	1907	0.00	1954	0.00	2001	0.00
1861	0.00	1908	0.00	1955	1.52	2002	0.00
1862	18.18	1909	0.00	1956	4.55	2003	0.00
1863	0.00	1910	11.36	1957	0.00	2004	4.20
1864	0.00	1911	0.00	1958	6.06	2005	2.80
1865	0.00	1912	2.27	1959	0.00	2006	2.80
1866	0.00	1913	0.00	1960	1.52	2007	0.00
1867	0.00	1914	0.00	1961	1.52	2008	1.40
1868	0.00	1915	0.00	1962	6.06	2009	1.40
1869	0.00	1916	0.00	1963	0.00	2010	2.80
1870	9.09	1917	0.00	1964	5.59	2011	2.80
1871	0.00	1918	0.00	1965	2.80	2012	1.40
1872	0.00	1919	0.00	1966	4.20	2013	1.40
1873	0.00	1920	4.55	1967	0.00	2014	5.59
1874	0.00	1921	0.00	1968	2.80		
1875	13.64	1922	0.00	1969	0.00		
1876	0.00	1923	11.36	1970	1.40		

Table 7.8. Channel characteristics through the study reach (PR130 to PR194) as determined from air photos.

Year	Channel length (km)	Width (m)	Slope (%)	Sinuosity
1939	57.3	111	0.117	1.55
1944	59.2	111	0.113	1.60
1954	61.1	76	0.110	1.65
1967	62.2	117	0.108	1.68
1973	67.6	77	0.099	1.82
1978a[1]	66.6	94	0.101	1.80
1978b[1]	66.6	98	0.100	1.80
1991	70.7	60	0.095	1.91
1998	71.9	64	0.093	1.94
2005	73.6	54	0.091	1.99
2013	74.5	52	0.090	2.01

[1] 1978a is the original delineation by Martinson and Meade [1983], and 1978b is my re-delineation that supports the continuity of delineations through time.

7.3 Appendix 3: Chapter 4 Supplementary Material

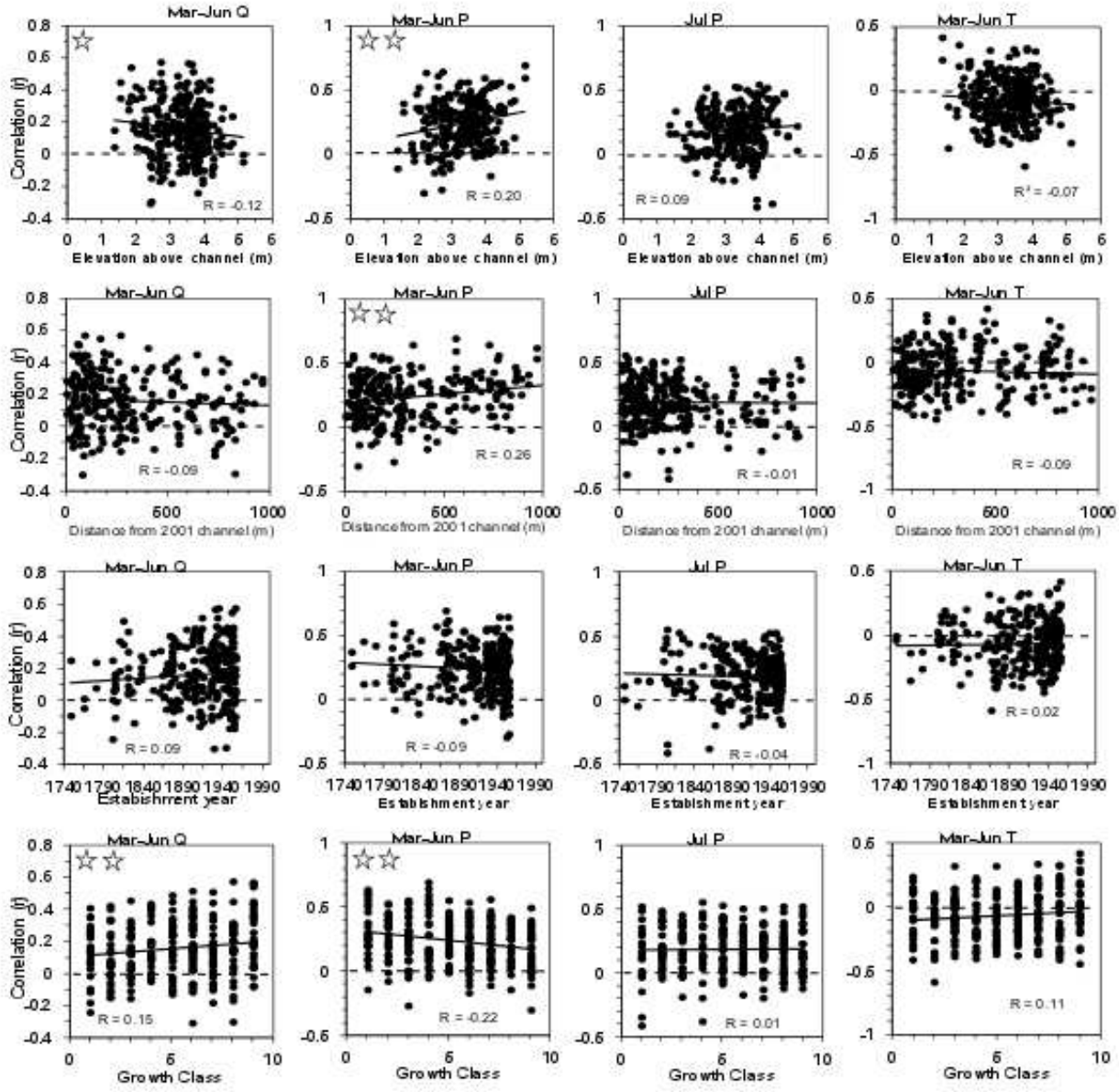

Figure 7.12. Relationships between tree ring width and spring flow, spring, precipitation, July precipitation, and spring temperature (columns) for the *driest half* of years. Rows are predictor variables that could affect correlations to each Q, P & T metric. Dashed line at zero is no correlation, and solid lines are best-fit lines for the data. One star means $p < 0.05$, two stars for $p < 0.01$.

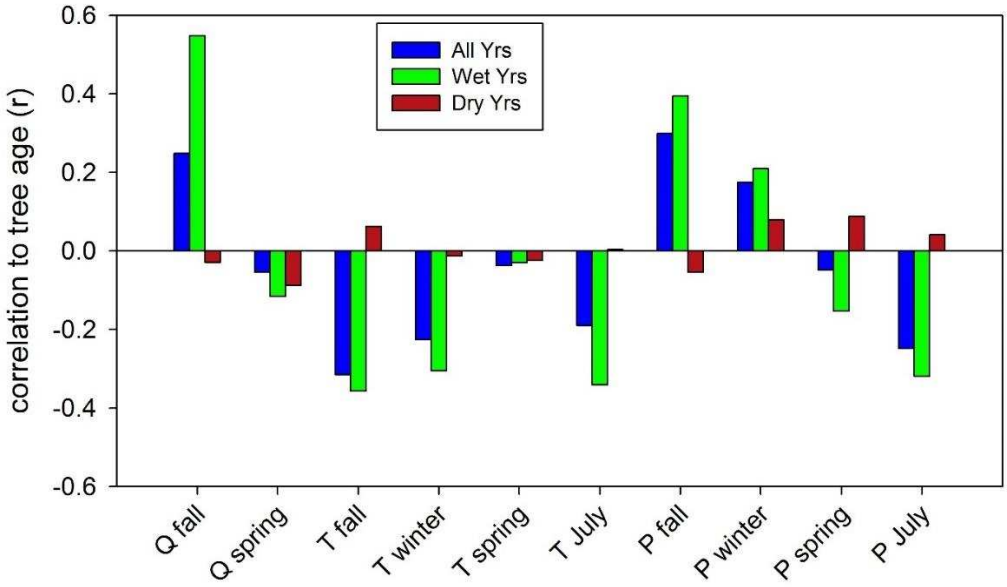

Figure 7.13. Correlations between tree age and ring width correlations to flow (Q), precipitation (P) and temperature (T) metrics (i.e., how strongly does tree age predict tree-ring relationships to seasonal Q, P & T?). The three groups are all years (blue) wet years (green), or dry years (red). Positive correlations mean older trees were more positively correlated to the given metric. The greater sample size in "all years" stabilized the variation, which usually resulted in all years having stronger correlations than would result from averaging the wet and dry years.

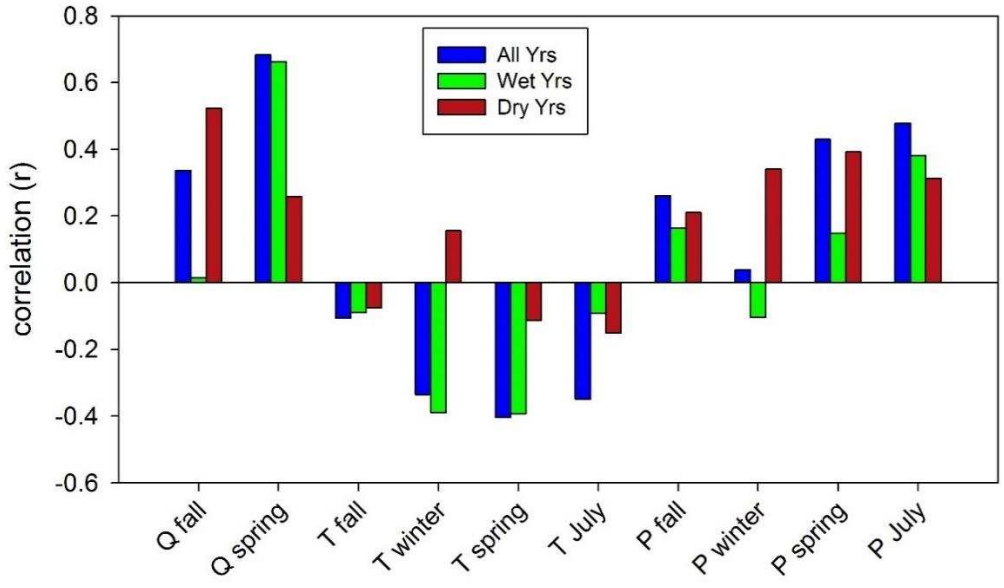

Figure 7.14. Correlations between tree cores and the ten flow (Q), precipitation (P) and temperature (T) metrics. The three groups are all years (blue) wet years (green), or dry years (red). Values were calculated from averaging all ring widths in a year and then correlating to Q, P & T metrics; the greater sample size in "all years" stabilized the variation, which usually resulted in all years having stronger correlations than would result from averaging the wet and dry years.

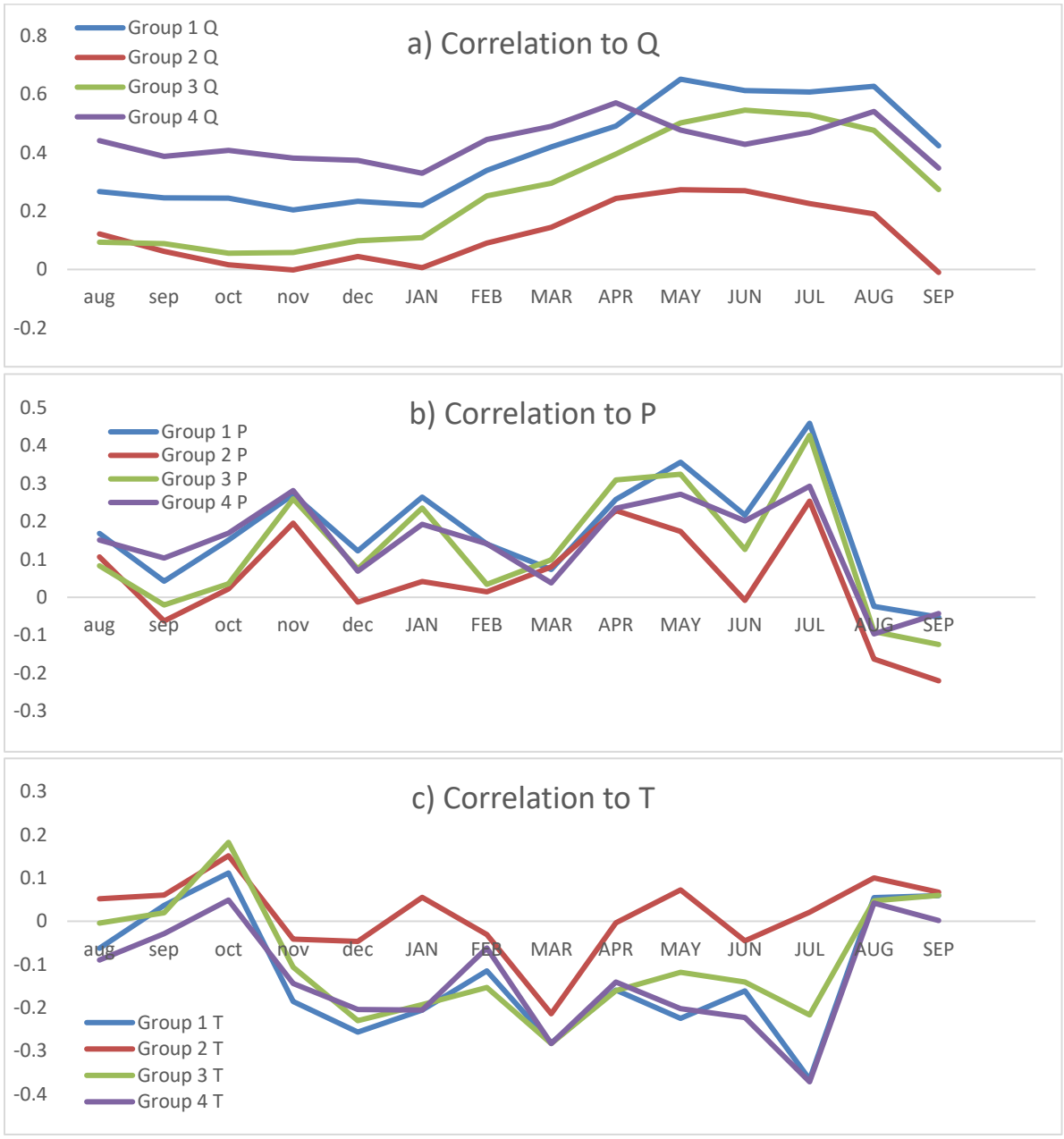

Figure 7.15. Mean 1930-2012 correlations for cores within each group produced in cluster analysis and monthly flow (a), precipitation (b) and temperature (c).

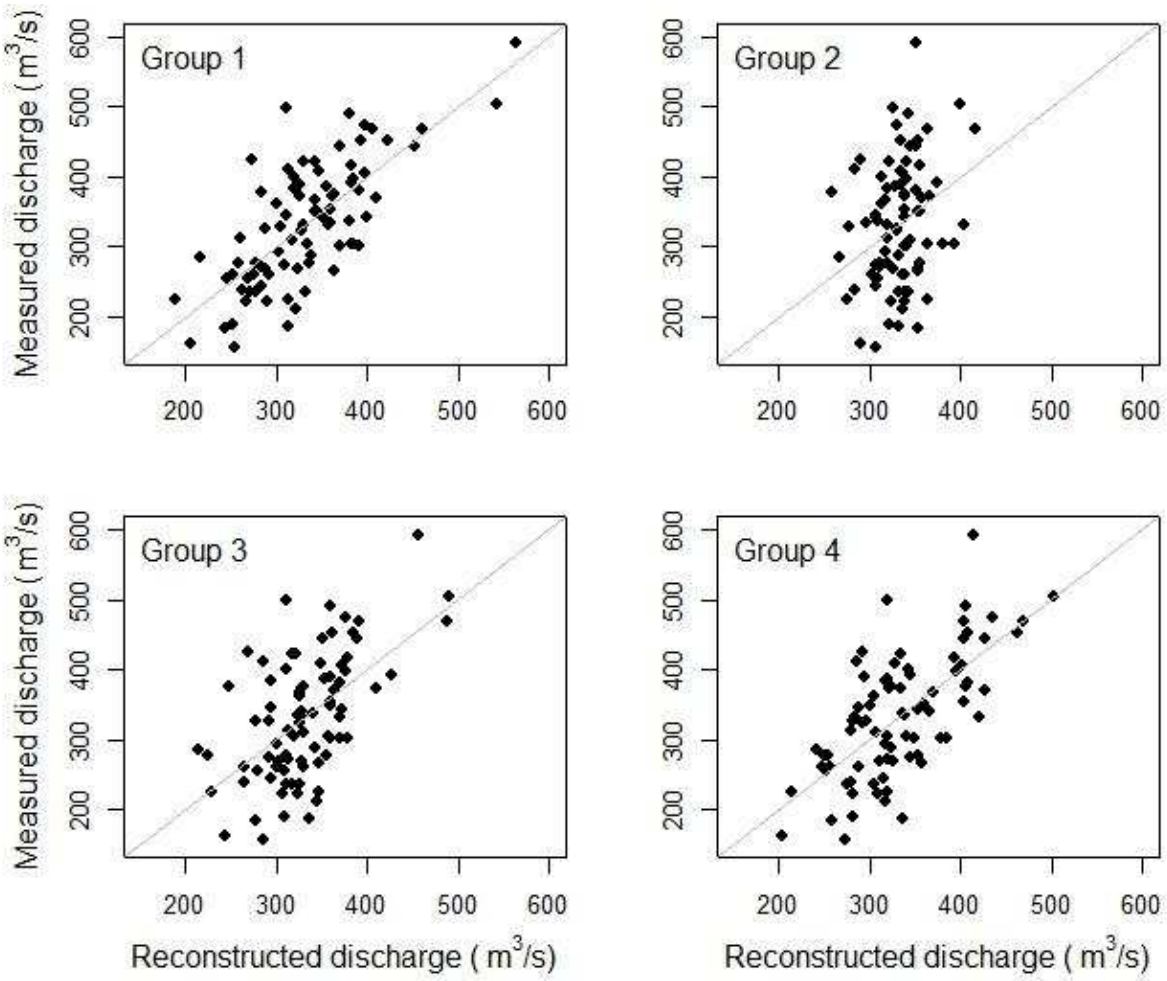

Figure 7.16. Scatterplot showing mean annual discharge for measured vs. reconstructed flows in each year (1930-2012). Panels depict the relationships calculated using cores from each of the four groups. Perfect reconstructions represented by the 1:1 gray line. Correlation coefficients (*r*) for groups 1-4 are 0.73, 0.25, 0.56, and 0.67.

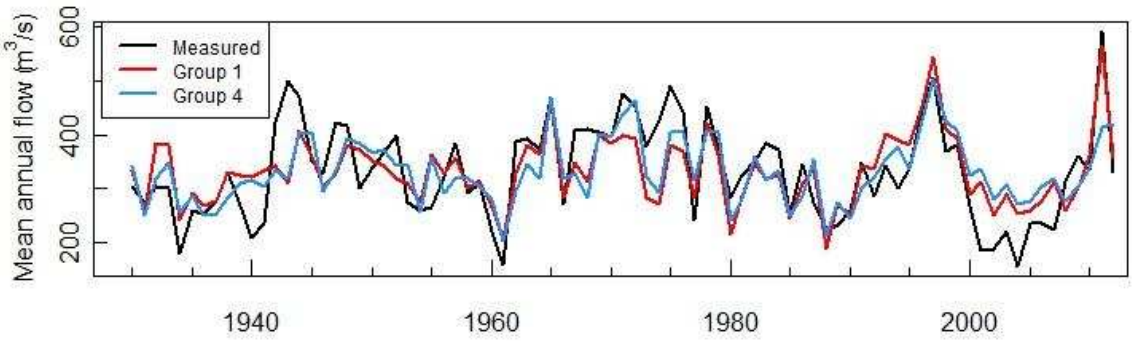

Figure 7.17. Comparison between measured (black) and flow reconstructed from the best two groups of tree cores, Group 1 (red) and Group 4 (blue).

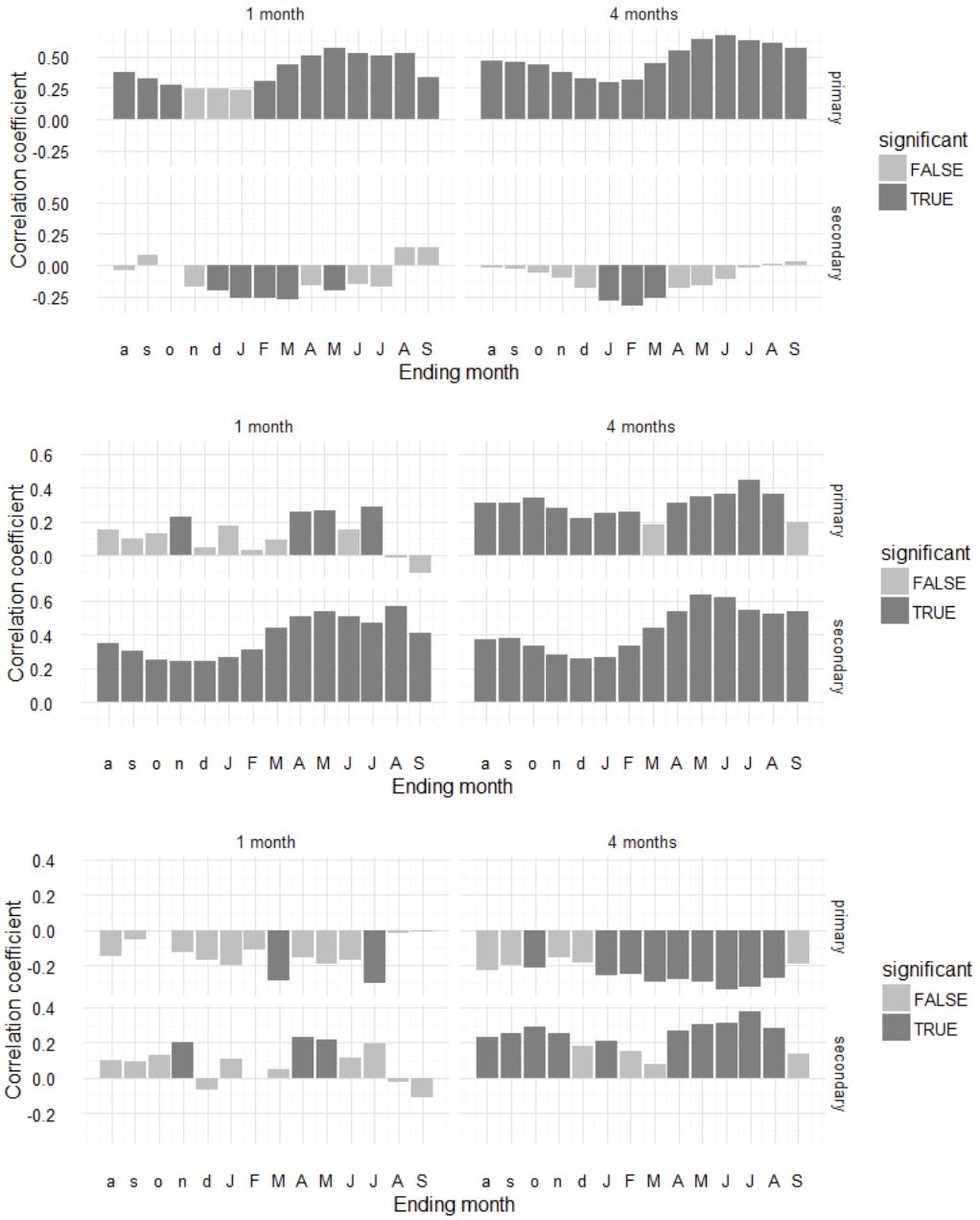

Figure 7.18. All of the cores from the Yellowstone River study site. Primary variables are Q (top panel), P (middle), and T (bottom); secondary variables are T, Q, and P, respectively.

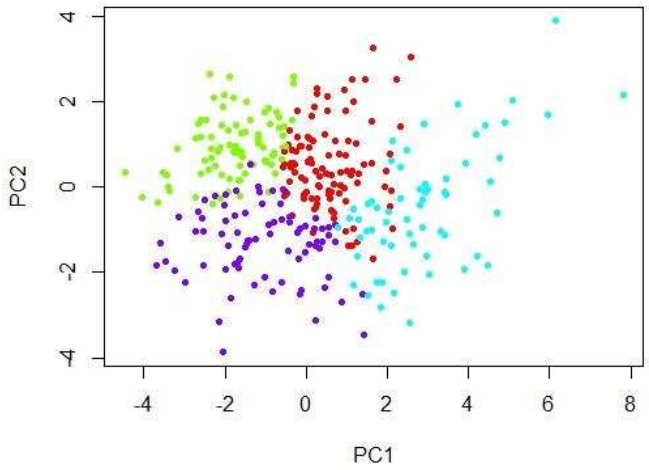

Figure 7.19. The four clusters creating Groups 1-4 of tree cores whose ring widths responded similarly to the ten flow, precipitation, and temperature metrics. Cores are plotted on their first two principal components (PC's). PC's 1 and 2 explained 55.6% of the variance.

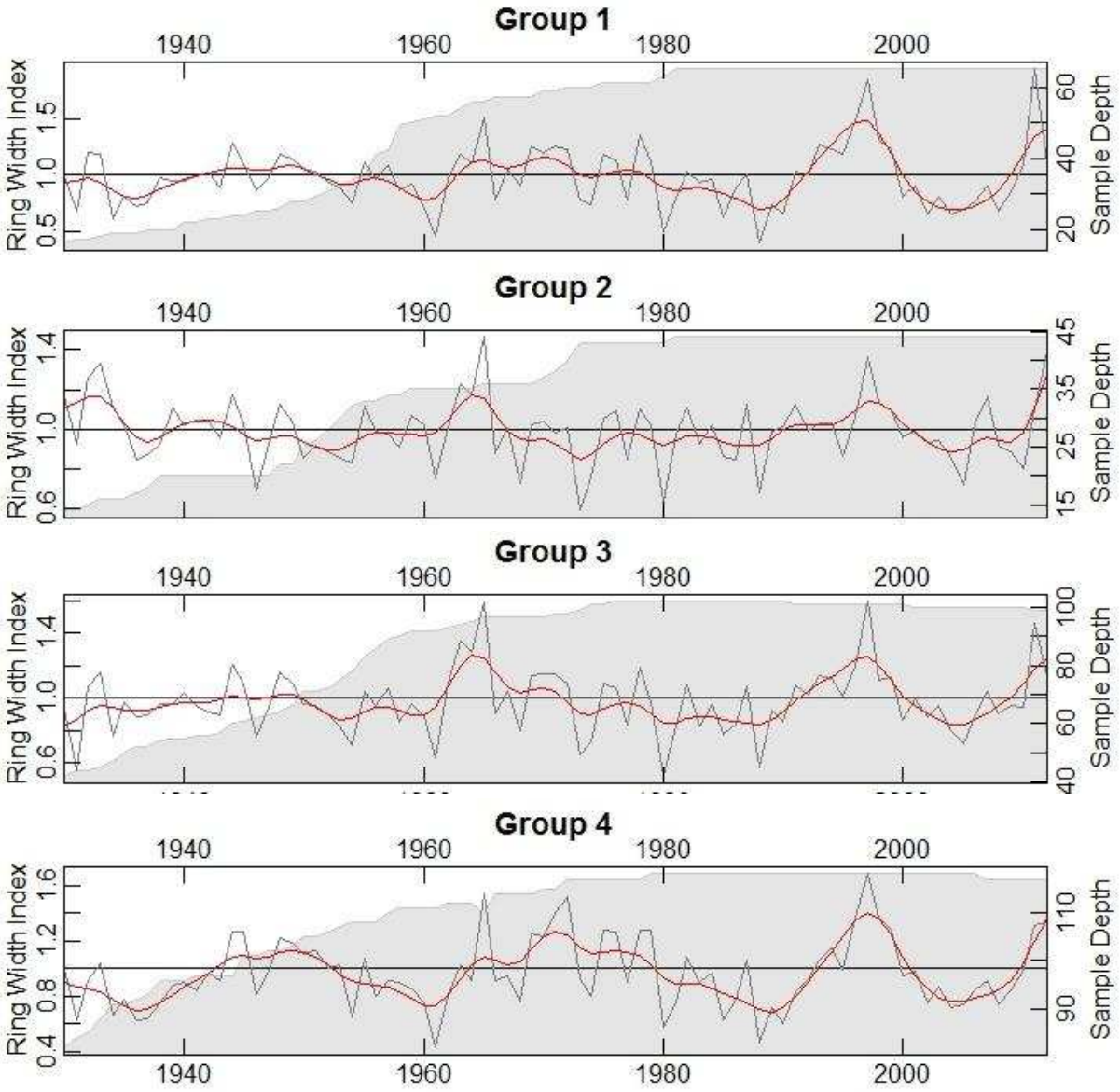

Figure 7.20. Average ring widths (unitless) for cores in the four groups created by cluster analysis. Annual (gray line) and 8-year spline (red) ring width index is displayed for each group. Number of cores samples in each year is the shaded gray polygon. Note that y-axes differ.

Table 7.9: Summary statistics for each group created in cluster analysis. Estab_yr = establishment year, growth.class.9 = relative growth rate (9 = fastest), ar1 = autocorrelation, elev = elevation, and dist_9901, dist_7677 and dist_4850 are distances to the river channel in 2001, 1977 and 1950, respectively.

Group 1

	vars	n	mean	sd	median	trimmed	mad	min	max	range	skew	kurtosis	se
Estab_yr	2	64	1939.53	26.35	1949.50	1942.12	17.05	1871.00	1979.00	108.00	-0.94	0.31	3.29
growth.class9	3	64	5.39	2.47	5.50	5.42	3.71	1.00	9.00	8.00	-0.15	-1.26	0.31
ar1	5	64	0.70	0.11	0.70	0.70	0.13	0.42	0.90	0.48	-0.38	-0.48	0.01
elev	6	64	3.04	0.76	3.24	3.08	0.80	1.36	4.25	2.89	-0.49	-0.92	0.10
dist_9901	7	64	376.37	367.51	203.52	331.83	229.90	5.84	1436.88	1431.04	0.97	0.04	45.94
dist_7677	8	64	327.36	324.21	176.89	293.05	196.61	14.28	956.80	942.52	0.82	-0.97	40.53
dist_4850	9	64	116.61	185.64	48.42	73.74	71.02	0.00	856.84	856.84	2.62	6.83	23.20

Group 2

	vars	n	mean	sd	median	trimmed	mad	min	max	range	skew	kurtosis	se
Estab_yr	2	43	1925.19	53.59	1944.00	1935.97	20.76	1748.00	1977.00	229.00	-1.99	3.52	8.17
growth.class9	3	43	5.12	2.48	5.00	5.14	2.97	1.00	9.00	8.00	-0.03	-1.22	0.38
ar1	5	43	0.74	0.13	0.75	0.75	0.15	0.40	0.93	0.53	-0.57	-0.36	0.02
elev	6	43	3.23	0.63	3.27	3.23	0.72	2.13	4.53	2.40	0.07	-0.94	0.10
dist_9901	7	43	240.05	247.67	155.70	196.69	150.51	25.87	884.89	859.03	1.42	0.75	37.77
dist_7677	8	43	210.50	233.52	130.64	161.43	119.28	15.45	861.28	845.83	1.83	2.26	35.61
dist_4850	9	43	152.92	208.34	65.45	108.93	97.03	0.00	831.10	831.10	1.87	3.05	31.77

Group 3

	vars	n	mean	sd	median	trimmed	mad	min	max	range	skew	kurtosis	se
Estab_yr	2	101	1919.88	42.34	1931.00	1926.42	31.13	1765.00	1974.00	209.00	-1.46	1.86	4.21
growth.class9	3	101	4.95	2.49	5.00	4.98	2.97	1.00	9.00	8.00	-0.11	-1.23	0.25
ar1	5	101	0.73	0.11	0.75	0.74	0.09	0.29	0.91	0.62	-0.80	1.36	0.01
elev	6	101	3.17	0.67	3.26	3.18	0.68	1.53	5.13	3.60	-0.10	-0.02	0.07
dist_9901	7	101	314.73	305.60	212.37	264.38	192.37	3.78	1182.83	1179.05	1.29	0.70	30.41
dist_7677	8	101	263.48	241.35	173.15	224.23	152.44	14.28	1161.08	1146.80	1.56	2.34	24.02
dist_4850	9	101	143.04	141.37	88.52	123.22	113.72	0.00	615.28	615.28	1.16	0.91	14.07

Group 4

	vars	n	mean	sd	median	trimmed	mad	min	max	range	skew	kurtosis	se
Estab_yr	2	120	1887.92	52.39	1890.00	1890.10	62.27	1765.00	1977.00	212.00	-0.37	-0.86	4.78
growth.class9	3	120	4.85	2.47	5.00	4.81	2.97	1.00	9.00	8.00	0.12	-1.08	0.23
ar1	5	120	0.71	0.11	0.71	0.71	0.12	0.41	0.91	0.50	-0.27	-0.29	0.01
elev	6	120	3.55	0.61	3.55	3.55	0.60	2.26	5.13	2.87	-0.08	-0.39	0.06
dist_9901	7	120	415.31	360.08	292.22	365.64	333.37	12.82	1436.88	1424.06	1.04	0.38	32.87
dist_7677	8	120	269.78	210.45	224.71	237.43	164.37	25.96	919.60	893.64	1.26	1.18	19.21
dist_4850	9	120	256.03	182.00	258.52	236.58	146.37	0.00	856.84	856.84	1.00	1.20	16.61

Table 7.10: Summary statistics for each *age class* (1=old, …, 4 = young). Autocorrelation values are in bold, which address Hypothesis 6. Estab_yr = establishment year, growth.class.9 = relative growth rate (9 = fastest), kmean4_Wx = the groups (Table 7.9), ar1 = autocorrelation, elev = elevation, and dist_9901, dist_7677 and dist_4850 are distances to the river channel in 2001, 1977 and 1950, respectively.

Class 1

	vars	n	mean	sd	median	trimmed	mad	min	max	range	skew	kurtosis	se
Estab_yr	2	70	1837.39	35.83	1837.00	1841.00	48.93	1748.00	1877.00	129.00	-0.57	-0.66	4.28
growth.class9	3	70	3.81	2.02	4.00	3.71	2.97	1.00	9.00	8.00	0.28	-0.71	0.24
kmean4_Wx	4	70	3.49	0.83	4.00	3.66	0.00	1.00	4.00	3.00	-1.53	1.46	0.10
ar1	5	70	**0.68**	0.10	0.69	0.68	0.13	0.41	0.89	0.47	-0.26	-0.65	0.01
elev	6	70	3.71	0.67	3.86	3.71	0.80	2.58	5.13	2.55	0.00	-0.90	0.08
dist_9901	7	70	514.04	445.38	404.29	463.38	412.67	3.78	1436.88	1433.10	0.76	-0.75	53.23
dist_7677	8	70	310.22	245.02	252.83	278.06	206.06	15.45	919.60	904.15	0.99	0.07	29.29
dist_4850	9	70	324.43	202.86	281.40	303.81	157.59	13.40	856.84	843.43	0.90	0.56	24.25

Class 2

	vars	n	mean	sd	median	trimmed	mad	min	max	range	skew	kurtosis	se
Estab_yr	2	73	1903.44	13.68	1905.00	1903.64	13.34	1878.00	1925.00	47.00	-0.23	-1.01	1.60
growth.class9	3	73	5.79	1.83	6.00	5.86	1.48	2.00	9.00	7.00	-0.37	-0.79	0.21
kmean4_Wx	4	73	3.03	1.09	3.00	3.15	1.48	1.00	4.00	3.00	-0.81	-0.71	0.13
ar1	5	73	**0.76**	0.10	0.77	0.77	0.12	0.57	0.91	0.34	-0.39	-0.92	0.01
elev	6	73	3.36	0.50	3.48	3.38	0.48	2.26	4.25	1.98	-0.43	-0.72	0.06
dist_9901	7	73	356.94	275.67	276.72	328.80	260.61	34.50	1182.83	1148.33	0.95	0.30	32.26
dist_7677	8	73	296.30	247.68	224.38	257.69	161.39	30.62	1161.08	1130.46	1.55	2.32	28.99
dist_4850	9	73	212.01	171.22	175.96	183.63	122.41	0.00	753.09	753.09	1.54	2.05	20.04

Class 3

	vars	n	mean	sd	median	trimmed	mad	min	max	range	skew	kurtosis	se
Estab_yr	2	66	1933.88	5.51	1933.00	1933.78	7.41	1926.00	1943.00	17.00	0.19	-1.24	0.68
growth.class9	3	66	6.30	2.28	7.00	6.48	2.97	1.00	9.00	8.00	-0.51	-0.84	0.28
kmean4_Wx	4	66	2.83	1.05	3.00	2.91	1.48	1.00	4.00	3.00	-0.54	-0.91	0.13
ar1	5	66	**0.73**	0.13	0.74	0.74	0.16	0.40	0.93	0.53	-0.48	-0.64	0.02
elev	6	66	3.16	0.72	3.14	3.18	0.86	1.53	4.51	2.98	-0.21	-0.79	0.09
dist_9901	7	66	320.39	278.26	238.62	287.48	231.29	25.87	1048.73	1022.86	0.97	-0.19	34.25
dist_7677	8	66	210.14	162.00	173.22	192.28	163.63	23.15	857.26	834.11	1.83	5.13	19.94
dist_4850	9	66	201.65	159.63	167.89	184.16	162.95	0.00	831.10	831.10	1.77	4.83	19.65

Class 4

	vars	n	mean	sd	median	trimmed	mad	min	max	range	skew	kurtosis	se
Estab_yr	2	70	1950.67	3.49	1951.00	1950.77	4.45	1944.00	1956.00	12.00	-0.21	-0.97	0.42
growth.class9	3	70	4.83	2.93	4.00	4.79	4.45	1.00	9.00	8.00	0.11	-1.62	0.35
kmean4_Wx	4	70	2.24	1.06	2.00	2.18	1.48	1.00	4.00	3.00	0.10	-1.37	0.13
ar1	5	70	**0.74**	0.10	0.74	0.74	0.09	0.41	0.93	0.52	-0.70	0.85	0.01
elev	6	70	2.96	0.73	3.24	2.99	0.87	1.36	4.06	2.70	-0.35	-1.07	0.09
dist_9901	7	70	334.44	305.65	210.21	305.03	233.20	5.84	923.50	917.66	0.67	-1.16	36.53
dist_7677	8	70	350.38	305.37	183.72	324.34	197.98	14.28	908.14	893.86	0.63	-1.26	36.50
dist_4850	9	70	64.38	99.65	21.32	40.01	31.61	0.00	422.77	422.77	2.43	5.41	11.91